SIGNATURES OF CHARGE NOISE AND ITS IMPACT ON EXCITON QUBITS

Vishal Purohit

A Thesis Submitted for the Degree of PhD
at the
University of St Andrews

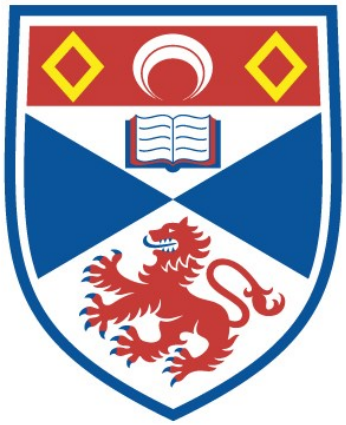

2016

Signatures of Charge Noise and its Impact on Exciton Qubits

by

Vishal Purohit

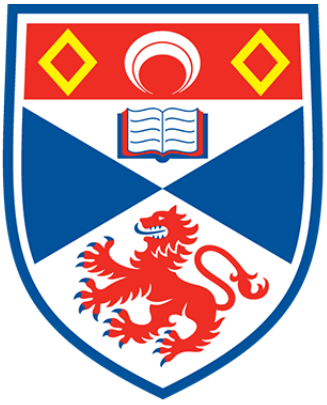

University of
St Andrews

A Thesis submitted for the degree of Doctor of Philosophy

School of Physics and Astronomy

May 3, 2016

Declarations

Candidate's declarations:

I, Vishal Purohit, hereby certify that this thesis, which is approximately 37,000 words in length, has been written by me, and that it is the record of work carried out by me, or principally by myself in collaboration with others as acknowledged, and that it has not been submitted in any previous application for a higher degree. I was admitted as a research student in September 2011 and as a candidate for the degree of Doctor of Philosophy in September 2011; the higher study for which this is a record was carried out in the University of St Andrews between 2011 and 2015.

Date: Signature of candidate:

Supervisor's declaration:

I hereby certify that the candidate has fulfilled the conditions of the Resolution and Regulations appropriate for the degree of Doctor of Philosophy in the University of St Andrews and that the candidate is qualified to submit this thesis in application for that degree.

Date: Signature of supervisor:

Permission for publication:

In submitting this thesis to the University of St Andrews I understand that I am giving permission for it to be made available for use in accordance with the regulations of the University Library for the time being in force, subject to any copyright vested in the work not being affected thereby. I also understand that the title and the abstract will be published, and that a copy of the work may be made and supplied to any bona fide library or research worker, that my thesis will be electronically accessible for personal or research use unless exempt by award of an embargo as requested below, and that the library has the right to migrate my thesis into new

electronic forms as required to ensure continued access to the thesis. I have obtained any third-party copyright permissions that may be required in order to allow such access and migration, or have requested the appropriate embargo below.

The following is an agreed request by candidate and supervisor regarding the publication of this thesis: Embargo on both printed and electronic copies for a period of six months on the following ground: publication of chapters 6 and 7 would preclude future publication in a peer-reviewed journal

Date: Signature of candidate:

Date: Signature of supervisor:

Abstract

The research contained within this thesis concerns the detection, identification and effect of charge noise on quantum dot systems.

In the first research chapter we study the cross correlation between pairs of exciton qubits subject to a common fluctuating charge environment, whose dynamics are solved using a transfer matrix approach. Our results show that we are able to discern features showing whether or not the charges interact with both quantum dots simultaneously i.e., form a correlated noise source. We find that qubits in a common charge environment display photon bunching, if both dots are driven on resonance or if the laser detunings are equal in both qubits and anitibunching if the laser detunings are in opposite directions.

In the second research chapter we study the auto-correlation function of a single optically driven exciton qubit interacting with an environment consisting of $1/f$ noise and a fluctuating charge. We again use the transfer matrix method and a sum of Lorentzian distributions to approximate $1/f$ noise. Our simulations show that signatures of $1/f$ noise do exist is photon correlation measurements. from such measurements we are also able to determine a minimum cut-off frequency of the $1/f$ noise, in the case that there is such a cut-off. In addition we also show that a $1/f$ and a single fluctuator can be distinguished using the auto-correlation.

In the final research chapter we study a pair of quantum dots, each with a low lying electron spin qubit and one higher lying level that can be selectively optically excited from one of the two spin states. Entanglement between the two spins can be achieved through path erasure. We look at the effect of a single fluctuating charge of the entanglement between these two 'L' shaped electronic structures.

Acknowledgements and publications

Acknowledgements

The are many people I need to thank and without whom, I couldn't have come this far. If you are reading this then, the chances are good that you are one of them and I would really like to take the opportunity to tell you how incredibly grateful I am for all the help and support that I've received during my PhD. Thank you. You are awesome, but you should already know that! What you might not know is how many people, in a myriad of ways, made this moment possible. To my supervisor, Brendon Lovett, thank you for all the help, guidance and encouragement you've given me over the years; I could not have asked for a better supervisor. I must also thank my collaborators, Bernd Braunecker and Brian Gerardot for the interesting physics we studied together and the insightful conversations that we had.

Thank you to the condensed matter doctoral training center (CM-DTC) for making me feel welcome from the outset and for always taking the time to make sure all of us students were happy. A particularly big thank you should go to Julie Massey and Christine Edwards, whom I bothered with almost continuously with administrative questions, but who always answered me with good cheer. I must thank Justyna Cwick, Alex Lamley and Kirsten Besemer for coffee, company and generally keeping me sane... well, reasonably. I would also like to thank Elliott Levi, for doing all of my washing up while I was stressing out with writing this thesis.

How can I write acknowledgements without thanking all of my family. Thank you all for your support at every step of the way, I couldn't have done this without you!

Publications

1. *Probing charge fluctuator correlations using quantum dot pairs* V. Purohit, B. Braunecker, and B. W. Lovett Phys. Rev. B 91, 245301 (2015)

Contents

CHAPTER 1

Motivations and thesis outline

COMPUTERS ARE now ubiquitous, inhabiting almost every electronic device available, from mobile phones to washing machines, pacemakers to ovens, clocks and even toilets. Every effort is being made to make computers smaller and more powerful, leading to the well-known Moore's law: 'The number of transistors incorporated in a chip will approximately double every 24 months'. This is a wonderful achievement, but there are doubts as to how long it can continue. Technological progress has been made in other areas and we have become able to control increasingly small systems to the point that engineering devices on the quantum scale is possible. Quantum mechanics is already being used in the electronics we use today, transistors in classical computers rely on quantum statistics. Some more exotic applications include quantum information processing, namely quantum cryptography systems are being used. One of the most anticipated technologies using quantum mechanics is the quantum computer. These quantum computers will require new hardware in the form of quantum bits (qubits) of which there have been many proposed ideas, the one that we will be focussing on in this thesis is the semiconductor quantum dot. This new technology promises, when applied to computers and at least for some classes of problems, to provide a significant speed up in relation to the number of qubits in the register than may be achieved with classical computers. There are currently few quantum algorithms devised to run on these quantum computers, and of those, few are particularly useful. Take for example the Deutsch-Josza algorithm [1], which is an algorithm for testing whether a register of qubits is in a constant or balanced state. That is to say, whether all the qubits in the register are the same, or if there are equal numbers of both. The practical applications of this algorithm are not numerous. On the other hand, the great power of the quantum algorithm is demonstrated in possibly the most famous example of it's kind: Shor's algorithm. It take incredibly large numbers and decomposes them into their

prime factors [2]. This has serious implications for security, since a large number of systems use RSA cryptosystems. The idea behind RSA is that this factorisation is incredibly difficult for classical computers to do. The second best known algorithm is Grover's search algorithm [3], which allows a search over an unsorted list to be done significantly faster than with a classical computer. The subject is still young and new and better algorithms can still be found. The reader may be excused for thinking that quantum computation is all about developing computers, but there is a more altruistic and scientific reason as well. In the same way that the development of the microscope allowed advances in Biology and Medicine by giving Biologists access to a region which is too small to see; the development of these quantum systems and the ability to control them allows us to be able to investigate in greater detail the counter-intuitive nature of quantum mechanics in the hope of expanding our knowledge of the universe we live in. Not only that, but being able to perform simulations of quantum systems on quantum systems will increase the rate at which quantum technologies grow. Currently we are trying to simulate quantum devices using classical computers, which is very slow.

The potential gains of being able to access the quantum regime are great, but there is a problem. The quantum properties that we wish to use are subject to degradation when they are allowed to interact with the environment. This process is known as decoherence. A key point in assessing the feasibility of any realisation of quantum computers is developing an understanding of how decoherence arises and affects the system. While it is true that a great deal of work has been done on decoherence in single qubits, less is known about how correlated noise across multiple qubits arises from different kinds of environment. Any long-range interaction that disturbs a common environment will cause correlated noise for closely spaced qubits. The example of such a common disturbance that this thesis is concerned with is that of fluctuating charges in the vicinity of quantum dots (QDs) [4–7] and this is an important theme in this thesis.

1.1 Thesis Outline

THE FOLLOWING work is broken into two parts. The first deals with background information that will allow the reader to more easily understand the work shown in the second as well as adding context. The second part of the thesis consists of three research chapters, which detail the work done during my PhD.

Part I: Background Chapters

Open and closed quantum systems

The first chapter in Part I sets out to discuss the modelling of quantum systems. We begin by defining the density operator or density matrix and discussing its properties, before showing how a system described by one may be evolved in time using a unitary time evolution operator. We go to say that not all systems may be time evolved with a unitary operator and go on to describe and detail the idea of an open quantum system and how it may be described by a master equation. The work shown in this thesis involve systems interacting with electromagnetic radiation and so we discuss and derive an optical master equation, which we use in all the research chapters. Once the optical master equation is outlined, we then apply it to a two level system, which is how we model quantum dots. A key aspect of an open system is that it suffers from decoherence, the irreversible loss of information. We describe two mechanisms of decoherence, namely population relaxation and pure dephasing. Many of the systems in the research chapters also involve coherent driving from lasers, which we describe and show how this gives rise to Rabi oscillations.

The conditional master equation

Continuing on from the ideas discussed in the chapter: open and closed quantum systems, we now consider the idea that we while the optical master equation describes the average result, we could derive a conditional master equation, which would describe the result for a single experiment.

Quantum dots

The work done in this thesis, while theoretical, assumes the use of semiconductor quantum dots as qubits. As such, in this chapter, we discuss what a quantum dot is, the properties that they display as well as the mechanisms by which they are created.

Part II: Research Chapters

Probing charge fluctuator correlation using pairs of quantum dot

The first of our research chapters in Part II, concerns the effect fluctuating charges on the statistics of the emitted photons i.e., how much the charges can be said to affect both qubits as opposed to having a system of charges that only affect one or the other. The aim is to find signatures of charge noise as a correlated source. We explain that the interaction between the charge and the qubits results in the Stark shift, before outlining a computational method for the time evolution of the density matrix, namely a transfer matrix [5]. We go on to also explain what photon statistics we are interested in and how we are able to calculate these using input-output theory and the quantum regression theorem. To show that the work is experimentally verifiable, we describe a possible experiment i.e. the Hanbury Brown-Twiss set up. The rest of the chapter is dedicated to the results and their discussion.

Probing $1/f$ correlations using quantum dots

The second research chapter considers a different noise source that is also found to affect quantum dot systems, namely $1/f$ noise. Like its preceding chapter, we hope to find signatures of noise and differentiate it from small numbers of charges that fluctuate in the fashion described in the first research chapter. We begin by explain what is meant by $1/f$ noise and the possible mechanisms that generate it. We then go on to discuss the paradoxical divergence of the spectral density and possible ways so resolve it, before discussing the model and results.

Entanglement in the face of correlated noise

In this final research chapter, we concern ourselves with noise sources that affect the entanglement between two 'L' shaped systems and how they impact the use of this kind of system for quantum computation. We begin by discussing what is meant by entanglement and how in can be generated via a technique known as path erasure. We go on to explain how this is the basis of measurement-based quantum computing by discussing the construction of graph states [8]. Due that the fact that the noise in the system will degrade the entangled states, we discuss measures of entanglement, to attempt to quantify it. We then introduce the model and discuss results.

Part I

Background Chapters

CHAPTER 2

Open and Closed Quantum Systems

All the work shown in this thesis involves excitons in quantum dots interacting with fluctuating charges and a electromagnetic field. In their simplest descriptions, these are systems interacting with an environment or reservoir, which tends to be a system large enough that its total energy remains largely unaffected by the system of interest, in fact for calculations we assume that this energy is constant. The dynamics of these system-environment interactions may be modelled with a master equation, which is a means by which the time evolution of a system may be calculated in terms of its density matrix. This is the method of choice for working with open quantum systems due to the inability of most open quantum systems to be time evolved using a unitary time evolution operator on the state.

2.1 The Density Matrix or Density Operator

To begin, since we shall formulate the time evolution of a system with its use, let us define and describe the density matrix. It is well understood that a system, whose preparation is known, may be described by a state vector. However, in many cases the initial preparation may not be known, in which case the system may be in one of many states, each with their associated probabilities. It also allows us describe entangled systems. Owing to this, we replace our state vector with the more general density matrix, which embodies all the possibilities. Mathematically, we write [9–12]:

$$\rho = \sum_i p_i |\Psi_i\rangle\langle\Psi_i|, \tag{2.1}$$

where p_i are the probabilities of each state $|\Psi_i\rangle$. We then need to define a basis set in which to measure and since we will be dealing with qubits, the basis set of choice here will be the computational basis, i.e. the set of states that the qubit may take

which we will define as $|0\rangle$ for the ground and $|1\rangle$ for the excited state for a two level system (TLS). Any pure state of the system may be written as a linear sum of these basis states, i.e. $|\Psi\rangle = \alpha|0\rangle + \beta|1\rangle$. The density matrix in terms of the basis states may then be constructed with the aid of the basis projectors $|\psi_i\rangle\langle\psi_i|$, where ψ_i covers the full basis set such that

$$\rho = \sum_{i,j} |\psi_i\rangle\langle\psi_i|\rho|\psi_j\rangle\langle\psi_j|. \tag{2.2}$$

When the indices $i = j$, the density operator elements are on the diagonal and represent the probabilities of the system being in each of the basis states given by $\langle\psi_i|\rho|\psi_i\rangle$ and $p_{(i,j)}$ are the coherences between states $|\psi_i\rangle$ and $|\psi_j\rangle$ given by $\langle\psi_i|\rho|\psi_j\rangle$. In order for the density matrix to describe physical systems it must be Hermitian, $\rho^\dagger = \rho$. This condition restricts the eigenvalues of the matrix and hence the probabilities of existing in each of the eigenstates to being real, which we know must be the case. Another property of the density matrix is that its trace is necessarily equal to one, $\mathrm{Tr}[\rho(t)] = 1$. The trace of a matrix is the sum of its diagonal values, which we know contain the probabilities associated with each state, which must necessarily sum to one. The density matrix is also described as being positive semi-definite, which is to say that the all eigenvalues are greater than or equal to zero. In other words, none of the probabilities may be negative.

2.2 Closed Quantum Systems

In order to better understand open quantum systems, it may be instructive to first see the dynamics of a system that is closed. More specifically, we shall be looking at the Liouville−Von Neumann equation. We know that the time evolution of a state vector may be described by the Schrödinger equation,

$$i\hbar\frac{d}{dt}|\psi\rangle = H|\psi\rangle, \tag{2.3}$$

where H is the Hamiltonian of the system. We shall use natural units for all calculations and set $\hbar = 1$.

Introducing explicit time dependencies, we can say that the state vector at time t may be determined by acting a unitary time evolution operator on the state vector at the initial time ($t = 0$). Therefore an equivalent form for the Schrödinger

equation in terms of the time evolution operator may be written as

$$|\psi(t)\rangle = U(t,t_0)\,|\psi(t_0)\rangle, \tag{2.4}$$

where $i\frac{\partial}{\partial t}U(t,t_0) = H(t)\,U(t,t_0)$ The solution, if the Hamiltonian is time independent, is exponential:

$$U(t,t_0) = e^{-iH(t-t_0)} \tag{2.5}$$

With the time evolution operator, we can show that the density matrix at some time t may be represented as

$$\rho(t) = \sum_{i,j} p_{(i,j)} U(t,t_0)\,|\psi_i(t_0)\rangle\langle\psi_j(t_0)\,|U^\dagger(t,t_0) \tag{2.6}$$

or equivalently and more succinctly as

$$\rho(t) = U(t,t_0)\,\rho(t_0)\,U^\dagger(t,t_0)\,. \tag{2.7}$$

Finally, differentiating with respect to time yields the Liouville−Von Neumann equation [9] for the time evolution of the density matrix

$$\frac{d}{dt}\rho(t) = -i\,[H(t)\,,\rho(t)]\,. \tag{2.8}$$

In general, we can have many systems that interact with each other, but for the purposes of pedagogy let this be limited to two. For a combined system of two such quantum objects, the two density matrices have a tensor product performed between them

$$\rho_S = \sum_{i,j,k,l} p_{(ijkl)} |\psi_{a,i}\psi_{b,j}\rangle\langle\psi_{a,k}\psi_{b,l}|, \tag{2.9}$$

where ρ_a and ρ_b are the two TLSs, ρ_S is the density matrix for the combined system. It has been alluded to that the basis set for a TLS may be written as $|0\rangle$ and $|1\rangle$, so the subscripts i,j,k,l may only take the values of 0 and 1. One may choose how this is shown in matrix form depending whether they choose the indices to read $1,0$ or $0,1$. Choosing $1,0$ gives the matrix representation of ρ_S

$$\rho_S = \left(\begin{array}{c|cccc} & \langle 1_a 1_b| & \langle 1_a 0_b| & \langle 0_a 1_b| & \langle 0_a 0_b| \\ \hline |1_a 1_b\rangle & p_{(1111)} & p_{(1110)} & p_{(1101)} & p_{(1100)} \\ |1_a 0_b\rangle & p_{(1011)} & p_{(1010)} & p_{(1001)} & p_{(1000)} \\ |0_a 1_b\rangle & p_{(0111)} & p_{(0110)} & p_{(0101)} & p_{(0100)} \\ |0_a 0_b\rangle & p_{(0011)} & p_{(0010)} & p_{(0001)} & p_{(0000)} \end{array}\right). \tag{2.10}$$

In practice, there are too many indices for the probabilities and it is easier to name them as a row and column

$$\rho_S = \left(\begin{array}{c|cccc} & \langle 1_a 1_b| & \langle 1_a 0_b| & \langle 0_a 1_b| & \langle 0_a 0_b| \\ \hline |1_a 1_b\rangle & p_{(11)} & p_{(12)} & p_{(13)} & p_{(14)} \\ |1_a 0_b\rangle & p_{(21)} & p_{(22)} & p_{(23)} & p_{(24)} \\ |0_a 1_b\rangle & p_{(31)} & p_{(32)} & p_{(33)} & p_{(34)} \\ |0_a 0_b\rangle & p_{(41)} & p_{(42)} & p_{(43)} & p_{(44)} \end{array}\right). \tag{2.11}$$

If we are only interested in one of the subsystems, we may retrieve its information by performing a partial trace over the other system. For example, if we wish to know about system a then we trace over system b,

$$\rho_a = \sum_i \langle \psi_{b,i}|\rho_S|\psi_{b,i}\rangle = \mathrm{Tr}_b[\rho_S] = \left(\begin{array}{cc} p_{(11)} + p_{(22)} & p_{(13)} + p_{(24)} \\ p_{(31)} + p_{(42)} & p_{(33)} + p_{(44)} \end{array}\right). \tag{2.12}$$

2.2.1 Interaction picture

The Hamiltonian of the overall system may be split into the component or free Hamiltonian (H_0), which contains the energies of the subsystems and is usually time independent, plus the interaction Hamiltonian (H_I)

$$H(t) = H_0 + H_I(t), \tag{2.13}$$

An operator $A(t)$ may be changed into the interaction picture via the relationship,

$$A_I(t) = U_0^\dagger(t, t_0) A(t) U_0(t, t_0), \tag{2.14}$$

where

$$U_0\left(t, t_{(0)}\right) \equiv e^{-iH_0(t-t_0)} \tag{2.15}$$

Alternatively, one may redefine the time evolution operator as:

$$U_I(t, t_0) \equiv {U^\dagger}_0(t, t_0)\, U(t, t_0) \tag{2.16}$$

Operating on the density matrix we can see that in the interaction picture it is defined as

$$\rho_I(t) = U_I(t, t_0)\rho(t_0)U_I^\dagger(t, t_0) \tag{2.17}$$

and the same relations hold under this change, so that the Liouville−Von Neumann equation is now

$$\frac{d}{dt}\rho_I(t) = -i\left[H_I(t), \rho_I(t)\right], \tag{2.18}$$

where $H_I(t)$ is in the interaction picture.

2.3 Open Quantum Systems

Now let us turn our attention to open quantum systems, which are similar to closed systems in that there is a susbsystem in which we interested and which we may access via the partial trace over the rest of the system or environment. It is true that the combined system may in fact be considered to be closed, however, it is in the nature of the environment that categorises it as open. The dynamics of the full system may in general be too complicated to study or in fact there may be elements, which are unknown. Thus it is only possible to study a reduced part of the system, namely the subsystem in contact with the environment. However, this has the consequence that while the combined system may be closed, one may not be able to use a unitary time evolution operator on the subsystem and that system and environment become correlated. This leads to an irreversible loss of information from the system and is known as decoherence. A new method is required then to evolve our system in time then, we use a master equation.

2.3.1 Quantum Master Equations

The following section is discussed in great detail in Breuer and Petruccione [9], whose treatment we shall follow. The outline of the problem thus far is that we have an open quantum system consisting of the environment and a subsystem that we are interested in studying. Their Hamiltonian is of the form,

$$H = H_s + H_b + H_I, \tag{2.19}$$

where H_s is the subsystem Hamiltonian, H_b is the bath or environment Hamiltonian and H_I is the interaction Hamiltonian. We are aiming to write a time local equation that shows the time evolution of the reduced system density matrix in terms of itself at an initial time,

$$\dot{\rho}_s(t) = \mathcal{L}\rho_s(t), \tag{2.20}$$

where $\mathcal{L}$ is a superoperator. Why we want this is that this is the basis of a dynamical semigroup. That is to say that this superoperator allows us to map from the space

of density matrices to itself. Simply put, this operation maps a density matrix to another at a future time t. It is a semigroup, because negative time elements are forbidden. The easiest way to proceed now is by using the interaction picture and our starting point shall be the Liouville−Von Neumann equation. To save confusion between using the subscript I for both the interaction picture and the interaction Hamiltonian, we will drop the subscript and assume all quantities from this point onwards are in the interaction picture.

$$\frac{d}{dt}\rho\left(t\right) = -i\left[H\left(t\right), \rho_S\left(t\right)\right]. \tag{2.21}$$

The solution of this equation of motion is given by the equation

$$\rho\left(t\right) = \rho\left(0\right) - i\int_0^t ds\left[H\left(s\right), \rho_S\left(s\right)\right]. \tag{2.22}$$

By substituting this solution back into the Liouville−Von Neumann equation and subsequently performing a partial trace over the environment, we arrive at an equation of motion for the reduced density matrix

$$\frac{d}{dt}\rho_s\left(t\right) = -\int_0^t ds \mathrm{Tr}_B\left[H\left(t\right), \left[H\left(s\right), \rho\left(s\right)\right]\right]. \tag{2.23}$$

For the above equation, it may be assumed that [9]

$$\mathrm{Tr}_B\left[H\left(t\right), \rho\left(0\right)\right] = 0. \tag{2.24}$$

This is currently an exact description of the system dynamics. The density matrix contains two times, t and s, although Eq. 2.22 may have the same commutator as Eq. 2.21 and so Eq. 2.22 may be substituted into Eq. 2.21 an infinite number of times. The problem is too complicated and so we shall be making three approximations known as the Born, Markov and Secular (also sometimes referred to as rotating wave) approximations to simplify matters. This equation still contains the density matrix for the overall system. To get rid of it, we must use the first of our approximations. The Born approximation.

The Born Approximation

The Born approximation is known as taking the weak coupling limit as it is assumed that the subsystem has very little effect on the environment. Thus, approximately, the environmental density matrix is not time dependent. This doesn't mean that the environment cannot be excited, but that the excitations decay quickly compared

to the time scales of the system dynamics, so we can say that it is constant. It also means that we can truncate the infinite series discussed in relation to Eq. 2.23. If the system-bath interaction is weak then we will have a convergent power series of Hamiltonians. It usually enough to keep the second order. We may write the overall system density matrix as a tensor product of the time dependent system matrix with the time independent environment matrix

$$\rho(t) \approx \rho_S(t) \otimes \rho_B, \tag{2.25}$$

which we may then substitute back into our differential equation.

$$\frac{d}{dt}\rho_s(t) = -\int_0^t ds \mathrm{Tr}_B \left[H(t), \left[H(s), \rho_S(s) \otimes \rho_B\right]\right]. \tag{2.26}$$

We are still left with a difficult-to-solve differential equation, which requires us to use our second approximation, the Markov approximation.

The Markov Approximation

In this regime, the time evolution of the system only depends on the current state of the system. That is to say that the path through which the system moved to arrive at the present moment has no bearing on the future condition of the system. Thus we can replace time dependent reduced density matrix and substitute it with a single value:

$$\frac{d}{dt}\rho_s(t) = -\int_0^t ds \mathrm{Tr}_B \left[H(t), \left[H(s), \rho_S(t) \otimes \rho_B\right]\right] \tag{2.27}$$

This equation is known as the Redfield equation and is local in time. However we require an equation that doesn't contain the initial time ($t = 0$). This constitutes the second part of the Markov approximation, which gets rid of the explicit dependence on $t = 0$, but making the equation time relative i.e. replacing s by $t - s$ and setting the upper limit of the integral to infinity. This is allowed so long as the integrand goes to zero quickly. Thus we have the Markovian quantum master equation

$$\frac{d}{dt}\rho_s(t) = -\int_0^\infty ds tr_B \left[H(t), \left[H(t-s), \rho_S(t) \otimes \rho_B\right]\right]. \tag{2.28}$$

The Markovian quantum master equation that we have just derived does not necessarily generate a semigroup and so we can't write it in Linblad form.

The Rotating Wave Approximation

Let us go back to the Schrödinger picture interaction Hamiltonian and rewrite it in the following form

$$H_I = \sum_\alpha A_\alpha \otimes B_\alpha, \tag{2.29}$$

where A and B are Hermitian and act on the subsystem and environment respectively. We can then decompose the interaction Hamiltonian into the eigenoperators of the subsystem. We can define the operators

$$A_\alpha(\omega) \equiv \sum_{\epsilon'-\epsilon=\omega} \Pi(\epsilon) A_\alpha \Pi(\epsilon'), \tag{2.30}$$

where ϵ and ϵ' are the eigenvalues and Π projects onto the eigenvalue space. The sum encompasses all of the eigenvalues and the projectors are separated by ω. It follows, directly from this that the following relations are true

$$\begin{aligned} [H_S, A_\alpha(\omega)] &= -\omega A_\alpha(\omega) \\ \left[H_S, A_\alpha^\dagger(\omega)\right] &= \omega A_\alpha^\dagger(\omega). \end{aligned} \tag{2.31}$$

Hence, by their form, these are known and eigenoperators of the subsystem Hamiltonian. Moving them into the interaction picture,

$$\begin{aligned} e^{iH_S t} A_\alpha(\omega) e^{-iH_S t} &= e^{-i\omega t} A_\alpha(\omega) \\ e^{iH_S t} A_\alpha^\dagger(\omega) e^{-iH_S t} &= e^{i\omega t} A_\alpha^\dagger(\omega). \end{aligned} \tag{2.32}$$

Since summing over all energies for A or $A^\dagger$ would give us the operator A, we can rewrite the equation in the form

$$H_I = \sum_{\alpha,\omega} A_\alpha(\omega) \otimes B_\alpha = \sum_{\alpha,\omega} A_\alpha^\dagger(\omega) \otimes B_\alpha^\dagger. \tag{2.33}$$

This allows us to write the interaction picture Hamiltonian as

$$H_I(t) = \sum_{\alpha,\omega} e^{-i\omega t} A_\alpha(\omega) \otimes B_\alpha(t) = \sum_{\alpha,\omega} e^{i\omega t} A_\alpha^\dagger(\omega) \otimes B_\alpha^\dagger(t), \tag{2.34}$$

where

$$B_\alpha^\dagger(t) = e^{iH_B t} B_\alpha e^{-iH_B t}. \tag{2.35}$$

Taking this Hamiltonian and substituting it into the Markovian quantum master equation (Eq. 2.28) we may obtain, after some lengthy algebra

$$\begin{aligned}\frac{d}{dt}\rho_S(t) &= \int_0^\infty ds\, tr_B\left[H_I(t-s)\,\rho_S(t)\,\rho_B H_I(t) - H_I(t)\,H_I(t-s)\,\rho_S(t)\,\rho_B\right] + h.c. \\ &= \sum_{\omega,\omega'}\sum_{\alpha,\beta} e^{i(\omega'-\omega)t}\Gamma_{\alpha\beta}(\omega)\left(A_\beta(\omega)\,\rho_S(t)\,A_\alpha^\dagger(\omega') - A_\alpha^\dagger(\omega')\,A_\beta(\omega)\,\rho_S(t)\right) + h.c.,\end{aligned} \tag{2.36}$$

where we have the one sided Fourier transforms of environmental correlation function

$$\Gamma_{\alpha\beta}(\omega) \equiv \int_0^\infty ds e^{i\omega s}\langle B_\alpha^\dagger(t)\,B_\beta(t-s)\rangle. \tag{2.37}$$

If the subsystem evolution time scale is much larger than that of the environment, then the terms where the frequencies ω and ω' are not equal are neglected. The rationale is that fast oscillations will average out over long time scales and won't affect system dynamics. This is the *rotating wave approximation* as leaves us with:

$$\frac{d}{dt}\rho_s(t) = \sum_{\omega}\sum_{\alpha,\beta}\Gamma_{\alpha\beta}(\omega)\left(A_\beta(\omega)\,\rho_S(t)\,A^\dagger{}_\alpha(\omega) - A^\dagger{}_\alpha(\omega)\,A_\beta(\omega)\,\rho_S(t)\right) + h.c.. \tag{2.38}$$

It is then possible to decompose the one sided Fourier transforms of the correlation functions into

$$\Gamma_{\alpha\beta}(\omega) = \frac{1}{2}\gamma_{\alpha\beta}(\omega) + iS_{\alpha\beta}(\omega), \tag{2.39}$$

where,

$$S_{\alpha\beta}(\omega) = \frac{1}{2i}\left(\Gamma_{\alpha\beta}(\omega) - \Gamma^*_{\beta\alpha}(\omega)\right). \tag{2.40}$$

If we define a Lamb shift Hamiltonian as

$$H_{LS} = \sum_{\omega}\sum_{\alpha,\beta} S_{\alpha\beta}(\omega)\,A_\alpha^\dagger(\omega)\,A_\beta(\omega), \tag{2.41}$$

then we have arrived at the interaction picture master equation,

$$\frac{d}{dt}\rho_S(t) = -i\left[H_{LS},\rho_S(t)\right] + D\left(\rho_S(t)\right), \tag{2.42}$$

where

$$D(\rho_S) = \sum_{\omega}\sum_{\alpha,\beta}\gamma_{\alpha\beta}(\omega)\left(A_\beta(\omega)\,\rho_S A_\alpha^\dagger(\omega) - \frac{1}{2}\{A_\alpha^\dagger(\omega)\,A_\beta(\omega)\,\rho_S\}\right). \tag{2.43}$$

If this equation is diagonalised, it will be in the Lindblad form.

2.4 The quantum optical master equation

In the previous section we derived the form of a quantum master equation, which is general, save the restrictions placed upon it by the approximations that we used. In this section we aim to show the dynamics of a system coupled with a thermal reservoir; that is to say a system that interacts with a quantized radiation field with a thermal distribution of modes. We will also reintroduce $\hbar$ as we continue to follow the procedure [9]. For the thermal reservoir, the density matrix will be as

$$\rho_B = \frac{1}{Z_B} e^{-\beta H_B} = \prod_{k,\lambda} \left(1 - e^{-\beta\hbar\omega_k}\right) e^{-\beta\hbar\omega_k b^{\dagger}{}_{\lambda}(k) b_{\lambda}(k)}, \tag{2.44}$$

where $\beta = \frac{1}{k_b T}$, Z_B is the partition function for the reservoir and $b^{\dagger}_{\lambda}(k), b_{\lambda}(k)$ are the creation and annihilation operators for light with polarisation (λ) and wavevector (k). The subsystem (ρ) will be in the form

$$\frac{d}{dt}\rho = \sum_{\omega,\omega'} \sum_{\alpha,\beta} e^{i(\omega'-\omega)t} \Gamma_{\alpha,\beta}(\omega) \left(A_{\beta}(\omega) \rho_S(t) A^{\dagger}_{\alpha}(\omega') - \{A^{\dagger}_{\alpha}(\omega') A_{\beta}(\omega), \rho_S(t)\} \right) + h.c. \tag{2.45}$$

where α, β run over the eigenenergies of the system and

$$\begin{aligned} \Gamma_{\alpha\beta}(\omega) &= \frac{1}{\hbar^2} \sum_{k,k'} \sum_{\lambda,\lambda'} \sqrt{\frac{2\pi\hbar\omega_k}{V}} \sqrt{\frac{2\pi\hbar\omega_{k'}}{V}} e^{\alpha}_{\lambda}(k) e^{\beta}_{\lambda'}(k') \\ &\times \int_0^{\infty} ds \langle b_{\lambda}(k) b^{\dagger}_{\lambda'}(k') \rangle e^{i(\omega_{k'}-\omega_k)t - i(\omega_{k'}-\omega)s} \\ &+ \langle b^{\dagger}_{\lambda}(k) b_{\lambda'}(k') \rangle e^{i(\omega_{k'}-\omega_k)t - i(\omega_{k'}-\omega)s} \\ &- \langle b_{\lambda}(k) b_{\lambda'}(k') \rangle e^{i(\omega_{k'}-\omega_k)t - i(\omega_{k'}-\omega)s} \\ &+ \langle b^{\dagger}_{\lambda}(k) b^{\dagger}_{\lambda'}(k') \rangle e^{i(\omega_{k'}-\omega_k)t - i(\omega_{k'}-\omega)s}. \end{aligned} \tag{2.46}$$

This is the one-sided Fourier transform of the electric field operator

$$\Gamma_{\alpha,\beta}(\omega) \equiv \frac{1}{\hbar^2} \int_0^{\infty} ds\ e^{i\omega s} \langle E_{\alpha}(t) E_{\beta}(t-s) \rangle, \tag{2.47}$$

where

$$E = i \sum_{k} \sum_{\lambda=1,2} \sqrt{\frac{2\pi\hbar\omega_k}{V}} \left(b_{\lambda}(k) - b^{\dagger}_{\lambda}(k) \right). \tag{2.48}$$

Using the relations:

$$\begin{aligned}\langle b_\lambda^\dagger(k)\, b_{\lambda'}(k')\rangle &= \langle b_\lambda^\dagger(k)\, b_{\lambda'}^\dagger(k')\rangle = 0\\ \langle b_\lambda(k)\, b_{\lambda'}(k')\rangle &= \delta_{kk'}\delta_{\lambda\lambda'}\left(1+N(\omega_k)\right)\\ \langle b_\lambda^\dagger(k)\, b_{\lambda'}(k')\rangle &= \delta_{kk'}\delta_{\lambda\lambda'}N(\omega_k)\end{aligned} \tag{2.49}$$

where,

$$N(\omega_k) = \frac{1}{e^{\beta\hbar\omega_k}-1} \tag{2.50}$$

We end up at the equation for the dissipator

$$\begin{aligned}D(\rho) &= \sum_{\omega>0}\frac{4\omega^3}{3\hbar c^3}\left(1+N(\omega)\right)\left(A_\beta(\omega)\,\rho_S A_\alpha^\dagger(\omega) - \frac{1}{2}\{A_\alpha^\dagger(\omega)\,A_\beta(\omega),\rho_S\}\right)\\ &+ \frac{4\omega^3}{3\hbar c^3}N(\omega)\left(A^\dagger{}_\beta(\omega)\,\rho_S A_\alpha(\omega) - \frac{1}{2}\{A_\alpha(\omega)\,A^\dagger{}_\beta(\omega),\rho_S\}\right)\end{aligned} \tag{2.51}$$

2.4.1 A Two Level System

A two level system is the simplest case of a quantum system and so it perfect as a tool to show pedagogically the use of the optical master equation. We shall denote the ground state as $|0\rangle$ and the excited state as $|1\rangle$, which in vector form is given by

$$|0\rangle = \begin{pmatrix}0\\1\end{pmatrix}, |1\rangle = \begin{pmatrix}1\\0\end{pmatrix} \tag{2.52}$$

It is easy to see that the projection operators in this case will be of the form

$$\sigma_+ = \begin{pmatrix}0&1\\0&0\end{pmatrix}, \sigma_- = \begin{pmatrix}0&0\\1&0\end{pmatrix}. \tag{2.53}$$

These projections operators are comprised of Pauli operators

$$\sigma_x = \begin{pmatrix}0&1\\1&0\end{pmatrix}, \sigma_y = \begin{pmatrix}0&-i\\i&0\end{pmatrix}, \sigma_z = \begin{pmatrix}1&0\\0&-1\end{pmatrix}, \tag{2.54}$$

which are combined as follows:

$$\sigma_+ = |\,1\rangle\langle 0\,| = \frac{1}{2}\left(\sigma_x + i\sigma_y\right)\ ,\ \sigma_- = |\,0\rangle\langle 1\,| = \frac{1}{2}\left(\sigma_x - i\sigma_y\right) \tag{2.55}$$

They are also the eigenoperators, as defined in section 2.3.1, of the system if the Hamiltonian is a function of σ_z alone and as such can be put straight into the

dissipator that we defined earlier in section 2.4. The Lamb shift term is often negligible compared to the dissipator and so is neglected to give

$$\begin{aligned}\frac{d}{dt}\rho(t) &= \gamma_0(N+1)\left(\sigma_-\rho(t)\sigma_+ - \frac{1}{2}\sigma_+\sigma_-\rho(t) - \frac{1}{2}\rho(t)\sigma_+\sigma_-\right) \\ &+ \gamma_0 N\left(\sigma_+\rho(t)\sigma_- - \frac{1}{2}\sigma_-\sigma_+\rho(t) - \frac{1}{2}\rho(t)\sigma_-\sigma_+\right),\end{aligned} \tag{2.56}$$

where γ_0 is the spontaneous decay rate of the TLS and N is the average occupation of the reservoir. In all subsequent sections we shall refer to this as the unconditional master equation.

2.5 Decoherence

THE PREVIOUS section shows mathematically how a master equation is constructed and it has been stated that there is a loss of information from the system, which is known as decoherence. In this section, we shall explore what is meant by the term as well as two mechanisms by which it may occur. It may be wise to first discuss what is meant by coherence before addressing how it is lost. In a technical sense, it is the characteristic of two basis states having constant phase difference. More simply put,it is degree to which two basis states are in superposition. A generalised pure state, where the coefficients may be complex, can be written as

$$\begin{aligned}|\Psi\rangle &= \left(\frac{1}{\sqrt{|\alpha|^2+|\beta|^2}}\right)\left(\alpha e^{i\theta_1}|0\rangle + \beta e^{i\theta_2}|1\rangle\right) \\ &= e^{i\theta_1}\left(\frac{1}{\sqrt{|\alpha|^2+|\beta|^2}}\right)\left(\alpha|0\rangle + \beta e^{i\Delta}|1\rangle\right),\end{aligned} \tag{2.57}$$

where θ_1 and θ_2 are the respective phases of each of the basis states and Δ is the difference between the two. We see that we can write the state as having a global phase and a phase difference between the two basis states. The global phase plays no part in any dynamics since it acts on everything so we need only worry about Δ. The density matrix is constructed to be

$$\rho = \left(\frac{1}{|\alpha|^2+|\beta|^2}\right)\begin{pmatrix} |\beta|^2 & \beta\alpha^* e^{i\Delta} \\ \alpha\beta^* e^{-i\Delta} & |\alpha|^2 \end{pmatrix}. \tag{2.58}$$

The important idea here is that a pure state as constructed is written as a linear superpostion of the basis states. A statistical mixture or mixed state cannot be

written in this way and the state is either $|\Psi_1\rangle = \left(\sqrt{\frac{|\alpha|^2}{|\alpha|^2+|\beta|^2}}\right) e^{i\theta_1}|0\rangle$ or $|\Psi_2\rangle = \left(\sqrt{\frac{|\beta|^2}{|\alpha|^2+|\beta|^2}}\right) e^{i\theta_2}|1\rangle$ which give the density matrix

$$\rho = \left(\frac{1}{|\alpha|^2+|\beta|^2}\right)\begin{pmatrix} |\beta|^2 & 0 \\ 0 & |\alpha|^2 \end{pmatrix}. \tag{2.59}$$

Decoherence then is the process by which we lose information about the phase, which reduces the superposition until the basis states are in a mixed state. There are two main forms of decoherence that we shall see in this thesis: population relaxation (T_1) and pure dephasing (T_2).

2.5.1 Population relaxation

One way to decrease the coherence between two states is through a loss of energy from the system, which can be seen intuitively by assigning the basis states physical energies. Let us define the excited state $|1\rangle$ as having an energy of ϵ. If we begin by having a the pure state described in Eq. 2.57, we know that the probability of the system being in the excited state is $|\beta|^2$. If the system is optically active and emits photons, then there is a chance that the system will decay from the excited stated to the ground state. If we monitor the system and we observe a photon emission of energy ϵ we know that the system must be in the ground state. The coherence between the ground and excited state must then be zero. Averaged over many observations, the coherence as well as the population of the excited state will diminish exponentially as function of time and the decay rate, defined as the average frequency of photon emission. To show this, let's take the example system of the optical master equation for a TLS as shown in Eq. 2.56. Our bath/environment has a thermal distribution of modes, so at room temperature for the visible frequencies we may set $N = 0$. This gives us the following set of equations

$$\begin{aligned} \dot{\rho_{11}} &= -\gamma\rho_{11}(t) \\ \dot{\rho_{12}} &= -\frac{\gamma}{2}\rho_{12}(t) \\ \dot{\rho_{21}} &= -\frac{\gamma}{2}\rho_{21}(t) \\ \dot{\rho_{22}} &= \gamma\rho_{22}(t). \end{aligned} \tag{2.60}$$

Given a general state of $\mid \psi\rangle = a \mid 1\rangle + b \mid 0\rangle$ for the initial conditions, we find the dynamics of the system follow

$$\begin{aligned} \rho_{11}(t) = a^2 e^{-\gamma t} \quad &, \quad \rho_{22}(t) = 1 - \left(1 - b^2\right) e^{-\gamma t} \\ \rho_{12}(t) = (ab) e^{-\frac{\gamma t}{2}} \quad &, \quad \rho_{21}(t) = (ba) e^{-\frac{\gamma t}{2}} \end{aligned} \tag{2.61}$$

If $a = b = \frac{1}{\sqrt{2}}$, we see the solution to these equations in Fig 2.1.

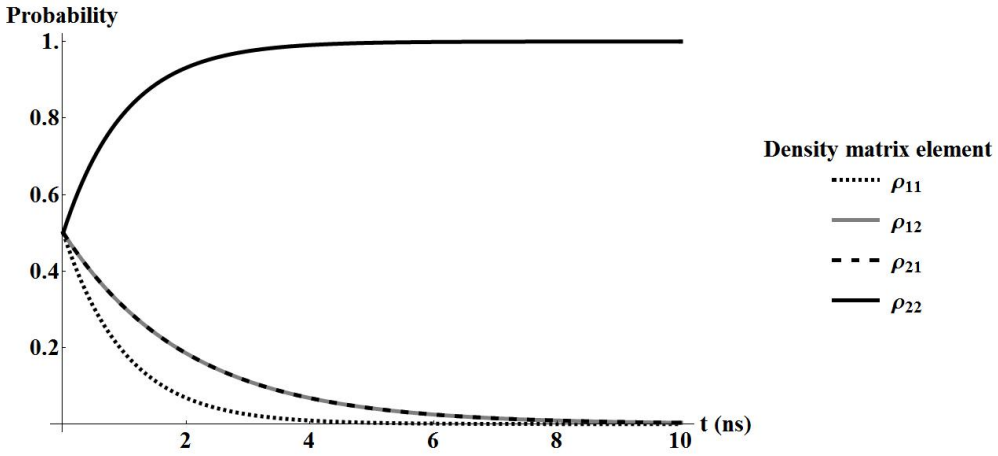

Figure 2.1: Dynamics of a TLS with a decays rate (γ) of 1 and initial conditions of a 50:50 superposition of ground and excited states.

2.5.2 Pure dephasing

Pure dephasing works by scrambling the phase information without affecting the probabilities of the ground and excited states. This is a time dependent process and works by perturbing the system energies and so altering the phase difference (Δ) between the states. If this perturbation is stochastic then the coherence between states will diminish to zero on a time scale dependent on the size and frequency of the perturbation. A periodic perturbation will cause a beating of the coherences. The current optical master equation with TLS does not show pure dephasing. To add this, we require an different dissipator. Let us allow the system to interact with a fluctuating charge that induces a Stark shift on the qubit dipole. That is to say, the charge being in the vicinity of the qubit causes a Coulomb interaction between the two and the energy levels of the excited and ground states to become wider separated. Assuming the charge is another quantum object and that it also has two levels, one for being close to the qubit and one being far away, the combined state is the tensor product of the two. If they are both equal superpositions, then they

can be represented as

$$(\mid 1_c\rangle + \mid 0_c\rangle) \otimes (\mid 1_q\rangle + \mid 0_q\rangle) = (\mid 1_c 1_q\rangle + \mid 1_c 0_q\rangle + \mid 0_c 1_q\rangle + \mid 0_c 0_q\rangle). \tag{2.62}$$

Using this order for the matrix diagonal, the interaction Hamiltonian may be written as

$$H = \begin{pmatrix} g & 0 & 0 & 0 \\ 0 & 0 & 0 & 0 \\ 0 & 0 & 0 & 0 \\ 0 & 0 & 0 & 0 \end{pmatrix}, \tag{2.63}$$

Where g is the additional energy given to the excited state of the qubit, when the charge is present. This Hamiltonian evolves via the Liouville−Von Neumann equation. Next we must define our dissipator. We know that the form of the equation must follow Eq. 2.56 and since we are treating the fluctuating charge as a TLS, we know that the operators involved are the tensor product of Pauli operators with the 2×2 identity matrix,

$$\sigma_i^c = \mathbb{1}_2 \otimes \sigma_i. \tag{2.64}$$

Defining the rate at which the charge fluctuates as γ_c, we arrive at

$$\begin{aligned} \frac{d}{dt}\rho(t) = -i[H, \rho(t)] \quad &+ \quad \gamma_c \left(\sigma_-^c \rho(t) \sigma_+^c - \frac{1}{2}\sigma_+^c \sigma_-^c \rho(t) - \frac{1}{2}\rho(t)\sigma_+^c \sigma_-^c \right) \\ &+ \quad \gamma_c \left(\sigma_+^c \rho(t) \sigma_-^c - \frac{1}{2}\sigma_-^c \sigma_+^c \rho(t) - \frac{1}{2}\rho(t)\sigma_-^c \sigma_+^c \right). \end{aligned} \tag{2.65}$$

If we give the system and initial state of

$$\rho(0) = \begin{pmatrix} 1/2 & 1/2 & 0 & 0 \\ 1/2 & 1/2 & 0 & 0 \\ 0 & 0 & 0 & 0 \\ 0 & 0 & 0 & 0 \end{pmatrix}, \tag{2.66}$$

then the system evolves as shown in Fig 2.2.

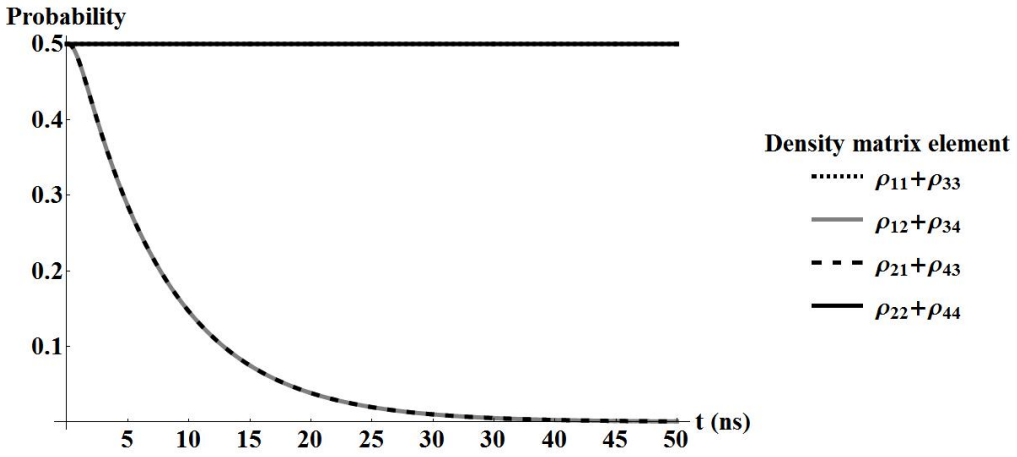

Figure 2.2: Dynamics of a TLS with a qubit decay rate (γ) of 0, charge flipping rate (γ_c) and initial conditions of a 50:50 superposition of ground and excited states.

2.6 Coherent Light: Rabi Oscillations

NOW THAT we have looked at the dynamics of two level systems interacting with a photon field, let us turn our attention to a two level system interacting with a classical light field. We shall define our two-level system to have an energy separation of ω and the laser coupling as $\lambda e^{-i\epsilon t}$. It is much easier to see the dynamics of the system if we transform into a rotating frame [12, 13]. The effective energy separation of the excited and ground states have changed from ω to a detuned value ν, which is a measure of how far off the frequency of the incoming light is from the energy separation of the two level system. Thus if the incident laser was on resonance, this would be zero.

$$H = \frac{1}{2}\begin{pmatrix} \nu & \lambda \\ \lambda & -\nu \end{pmatrix} \tag{2.67}$$

Ignoring the dissipator for the moment, meaning that we are not considering the photon dynamics, the equations governing the density matrix are as follows:

$$\dot{\rho}_{11}(t) = -\frac{1}{2}i\lambda[\rho_{12}(t) - \rho_{21}(t)] \tag{2.68}$$

$$\dot{\rho}_{22}(t) = \frac{1}{2}i\lambda[\rho_{12}(t) - \rho_{21}(t)] \tag{2.69}$$

$$\dot{\rho}_{12}(t) = -\frac{1}{2}[i\lambda[\rho_{11}(t) - \rho_{22}(t)] + 2\nu\rho_{12}(t)] \tag{2.70}$$

$$\dot{\rho}_{21}(t) = \frac{1}{2}[i\lambda[\rho_{11}(t) - \rho_{22}(t)] + 2\nu\rho_{21}(t)] \tag{2.71}$$

On solving these equations we see that the functions concerning the population probabilities are oscillatory and that this oscillation is at what is known as the Rabi frequency given by [14]

$$\Omega_{rabi} = \sqrt{\nu^2 + \lambda^2} \tag{2.72}$$

The different regimes may then be viewed; the on resonance case, in which we see complete oscillation of the populations and the coherence between the two levels of the system, being sinusoidal as shown in Figure 2.3.

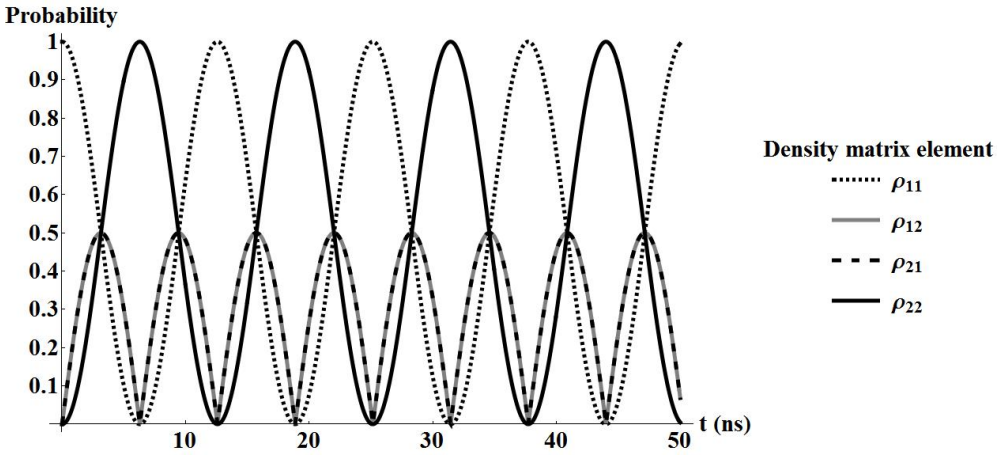

Figure 2.3: Complete Rabi oscillations for the on resonant case ($\Omega = 0.5$ GHz)

When the detuning is large it can be seen that the probabilities of the states don't cross and as the detuning increases to infinity, the probabilities remain constant recovering the no laser case. The threshold of crossing is when ν takes the same value as the field coupling λ. In this case the Rabi oscillations allow the probabilities of the excited and ground states to equal each other, but not cross as shown in Figure 2.4.

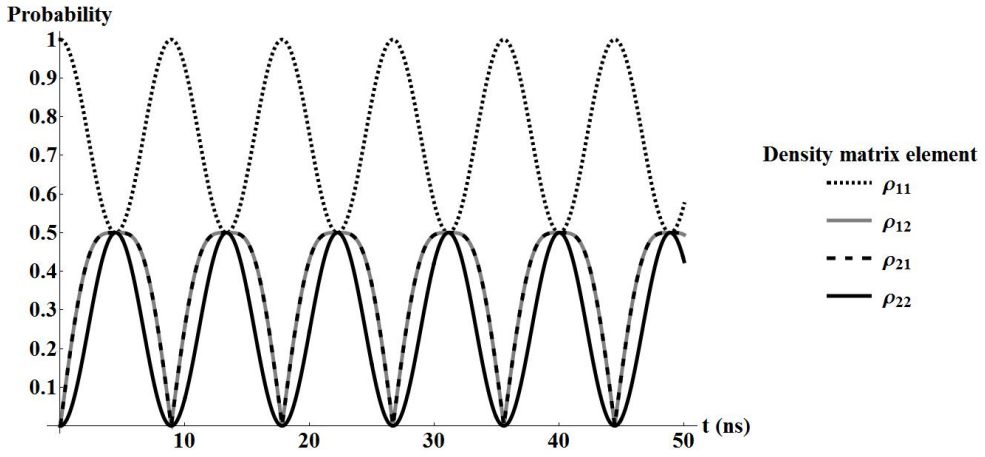

Figure 2.4: Threshold Rabi Oscillations, occurring when the detuning is equal to the field coupling ($\nu = \Omega = 0.5$)

Now let's reintroduce the dissipator. The equations for the population dynamics have increased in complexity, which will lead to some interesting results. We can compare this against the previous results by setting γ (the qubit decay rate) to zero, recovering the no dissipator case, and by setting the Rabi frequency to zero we recover the population dynamics associated with a two level system interacting with a photon field as shown in section 2.3.1. Starting then with the on resonant case, we see that the oscillations in the population probabilities diminish to a steady state value given by Figure 2.5 [9]:

$$\rho_{11}^{ss} = \frac{\Omega^2}{\gamma^2 + 2\Omega^2} \tag{2.73}$$

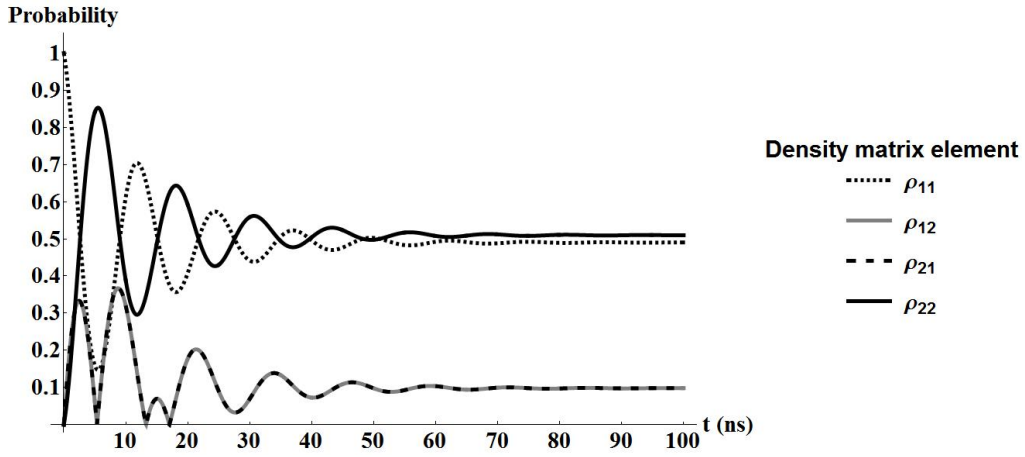

Figure 2.5: Decay of Rabi Oscillations for $\gamma = 0.1$ GHz $\Omega = 0.5$ GHz. The curves shown the absolute values of the density matrix elements.

The coherence, which in the case of no dissipation showed a sinusoidal profile, now also decays in fluctuations and settles to a steady state value determined by Eq. 2.67-2.69 [15]):

$$\rho_{12}^{ss} = \frac{i\Omega\gamma}{\gamma^2 + 2\Omega^2} \tag{2.74}$$

Turning on the detuning again we see that if we make it large, the detuning diminishes the extent to which the oscillations of excited and ground state probabilities reach. So for large detuning, the dynamics return to that obtained without the laser. This is only to be expected as the more detuned the laser, the weaker the effective coupling with the two-level system. Setting the decay rate ($\gamma = 0$), we can see the effect of the detuning on the Rabi oscillations, which is shown in Figure 2.6.

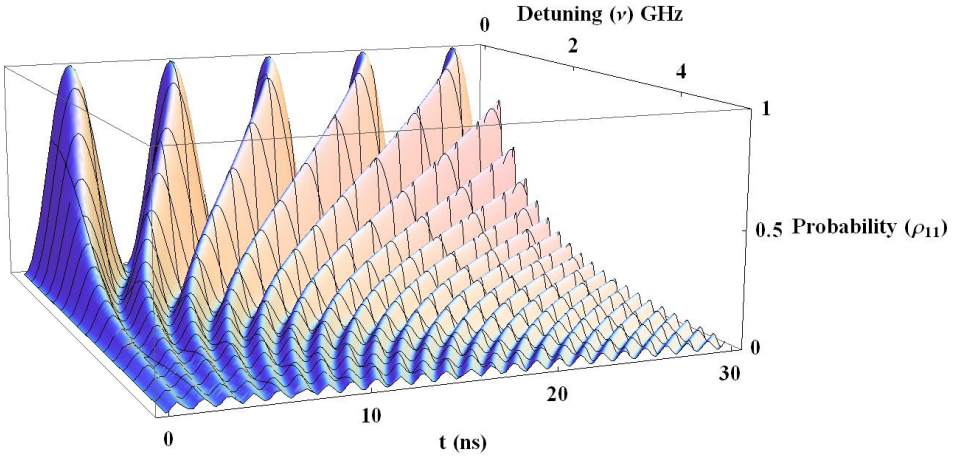

Figure 2.6: Rabi Oscillations of the excited state probability as a function of laser detuning, with the initial condition that the qubit was in the ground state

CHAPTER 3

Conditional Master Equation

THE PREVIOUS chapter shows what is also known as the unconditional master equation and is built on the principle of ensemble averages. It shows the average dynamics of a system and not what would be seen by an experimentalist performing a single experiment. This naturally requires that the experimentalist in question may in some way measure some observable and in doing so will alter the state of the system and so leads nicely to the idea of the monitored systems which are described by a conditional master equation. For a pedagogical approach to the subject, let us then take the example of a two level system, which is continuously monitored by a photo-detector. The initial system shall be in a superposition of the ground and excited states. With a monitored system, we may question what state our system really is in. That is to say, that the system may or may not be excited and cannot be conclusively proven to be in either state as the condition for it having been in the excited state may only be determined by virtue of a detected photon in our detector. Conversely the system being in the ground state may be ascertained with certainty only if no photon is ever detected. Thus, during a time interval, in which there has been no photon detection event, the probability of the system being in the ground state increases; naturally to a maximum of one at infinite time. At the moment that there is a detection event the wavefunction must necessarily collapse to being in the ground state with a probability of one as the excitation must be removed from the system in order to emit a photon. This is an idealised model, of course, and one may argue that the detector may not be 100% efficient or the this two level system cannot be perfectly isolated in order for there simply to be a decay process whilst completely ignoring any absorption processes, which are both valid concerns and will be dealt with in due course. It is from this simplified example, although it applies in general, that we may see that there are two possibilities for the evolution of the density matrix, no detection and detection. When the later occurs,

there will be a discontinuity in the wavefunction as it collapses. This is worked extensively in Kok and Lovett [12], from which we may follow. We may write our density matrix in the following form,

$$\rho\left(t+dt\right)=\rho_0\left(t+dt\right)\left(1-d\upsilon\right)+\rho_1\left(t+dt\right)d\upsilon, \tag{3.1}$$

where $d\upsilon$ is a stochastic variable which is indicative of a photon detection event and can take the values 0 or 1 for no detection event and a detection respectively i.e. it is Boolean [12]. The first term ρ_0 represents the evolution of the density matrix when there is no detection event and ρ_1 represents the density matrix when a detection event had occurred. Now it is necessary to construct the different density matrix paths that may be taken. As such we must define a *jump operator*, which when operating on the density matrix serves to project into the ground state. We may define such an operator as,

$$J^-\rho=\sigma_-\rho\sigma_+=\langle 1|\rho|1\rangle|0\rangle\langle 0|=\mathrm{Tr}\left[J^-\rho\right]|0\rangle\langle 0|. \tag{3.2}$$

The effect of this operator is to project an excited state into a ground state - i.e. the system jumps from one state to the other, an event which is signalled by the detection of an emitted photon. The trace term describes the probability of being in the excited state to begin with. The sigmas refer to the projection operators as outlined in section 2.4.1. At this point the reader may wish to ask why, since in general there may be both decay and absorption processes, there is no equivalent absorption-jump operator. This is because, the decay-jump operator projects into the ground state when the stochastic boolean variable is true (1), which means that the detector has registered a photon count. There is no analogous process for absorption; no way to detect whether or not the two level system has indeed absorbed a photon at all. This forms the basis of the decay path, but we must divide by the trace of the jump operator to obtain the density matrix in the ground state, whilst preserving its trace,

$$\rho\left(t+dt\right)=\rho_0\left(t+dt\right)\left(1-d\upsilon\right)+\frac{J^-\rho}{\mathrm{Tr}\left[J^-\rho\right]}d\upsilon \tag{3.3}$$

The expectation value of our stochastic Boolean variable, for a perfect detector, will simply be the decay rate (γ) multiplied by the probability of being in the excited state. This must naturally be multiplied by the detector efficiency (η), if the detector

is not perfect. Thus after many runs of the simulation we would get an average of

$$\zeta\left(d\upsilon\right)=\eta\gamma\mathrm{Tr}\left[J^{-}\rho\right]dt \tag{3.4}$$

Using eqns 3.3 and 3.4 and averaging over many (theoretically infinite) runs must recover the original unconditional master equation,

$$\rho\left(t+dt\right)=\rho\left(t\right)+\gamma\left(N+1\right)\left(J^{-}\rho-A^{-}\rho\right)dt+\gamma N\left(J^{+}\rho-A^{+}\rho\right)dt, \tag{3.5}$$

where the operators A^{-} and A^{+} are the terms $\left(-\frac{1}{2}\sigma_{+}\sigma_{-}\rho\left(t\right)-\frac{1}{2}\rho\left(t\right)\sigma_{+}\sigma_{-}\right)$ and $\left(-\frac{1}{2}\sigma_{-}\sigma_{+}\rho\left(t\right)-\frac{1}{2}\rho\left(t\right)\sigma_{-}\sigma_{+}\right)$ respectively. Equating eqns 3.3 and 3.5 and rearranging them gives a non-linear differential equation for the no detection event part of the conditional master equation,

$$\frac{d\rho_{0}}{dt}=\gamma\left(\eta\mathrm{Tr}\left[J^{-}\rho_{0}\right]\rho_{0}+\left(N+1-\eta\right)J^{-}\rho_{0}-\left(N+1\right)A^{-}\rho_{0}+N(J^{+}\rho_{0}-A^{+}\rho_{0})\right) \tag{3.6}$$

This equation can be simplified if a numerical solution is sought. Currently, the equation is second order and non-linear. However, we may re-cast it into a linear equation that does not preserve the trace. This means that the density matrix must be re-normalised at each step. This is done by replacing ρ_{0} with $\rho_{0}=f(t)\tilde{\rho}$. This yields,

$$\dot{f}\tilde{\rho}-\gamma f^{2}\eta\mathrm{Tr}[J^{-}\tilde{\rho}]\tilde{\rho}+f\dot{\tilde{\rho}}=f\gamma\left(\left(N+1-\eta\right)J\tilde{\rho}-\left(N+1\right)A^{-}\tilde{\rho}+N(J^{+}\tilde{\rho}-A^{+}\tilde{\rho})\right). \tag{3.7}$$

For this equation to be linear, the relation

$$\dot{f}=\gamma f^{2}\eta\mathrm{Tr}[J^{-}\tilde{\rho}] \tag{3.8}$$

must be true. This equation is significantly simplified with the knowledge that

$$\gamma\eta\mathrm{Tr}[J^{-}\tilde{\rho}]=-\mathrm{Tr}[\dot{\tilde{\rho}}]. \tag{3.9}$$

Substituting Eq. 3.9 into Eq. 3.8 gives

$$\dot{f}=-f^{2}\mathrm{Tr}[\dot{\tilde{\rho}}], \tag{3.10}$$

which on integrating yields

$$f(t)=\frac{1}{\mathrm{Tr}[\tilde{\rho}]} \tag{3.11}$$

3.0.1 Decay only

Until this point, the discussion of the conditional master equation has been completely general. However, as suggested earlier, and for pedagogical purposes, we take a simplified example where the only process that we are interested in is decay, so we may set N to zero. The model here is a single TLS and for added simplicity, let the initial state be mixed, i.e. no coherences. This gives us a pair of coupled equations,

$$\begin{aligned} \dot{\rho_{11}} &= \langle 1 \mid \dot{\rho} \mid 1 \rangle = \gamma \left(\eta \left(\rho_{11} \right)^2 - \rho_{11} \right) \\ \dot{\rho_{22}} &= \langle 0 \mid \dot{\rho} \mid 0 \rangle = \gamma \left(-\eta \left(\rho_{11} \right)^2 + \rho_{11} \right), \end{aligned} \tag{3.12}$$

where ρ_{11} and ρ_{22} are the excited and ground state probabilities respectively. Using the fact that the trace of the density matrix must necessarily equal one, we may readily solve them.

$$\rho_{11} = \frac{x}{x\eta + e^{\gamma t}(1 - x\eta)} \quad , \quad \rho_{22} = 1 - \rho_{11} \tag{3.13}$$

Where x ranges between 0 and 1 and is the probability of being in the excited state. A good check here is to set the detector efficiency to zero. This should recover the solution to the unconditional master equation. As can be readily seen, if η is set to zero, the probability of existing in the excited state diminishes as a simple exponential of the decay rate, which is what we expect. Another interesting regime to note is when the detector efficiency is 100% ($\eta = 1$) and the initial excited state probability is one. In this case, the solution to Eq. 3.13 is independent of time and is always equal to unity. The probability of the qubit existing in the excited state does not reduce with time. This is an expected result since if we are certain that the system is excited, the only way that the ground state may increase in probability is for a detection event to occur. In all other cases, the probability of the excited state will decay with time as shown below in Fig 3.1, where the initial state of each of the runs is solely excited, i.e.

$$\rho(0) = \begin{pmatrix} 1 & 0 \\ 0 & 0 \end{pmatrix}. \tag{3.14}$$

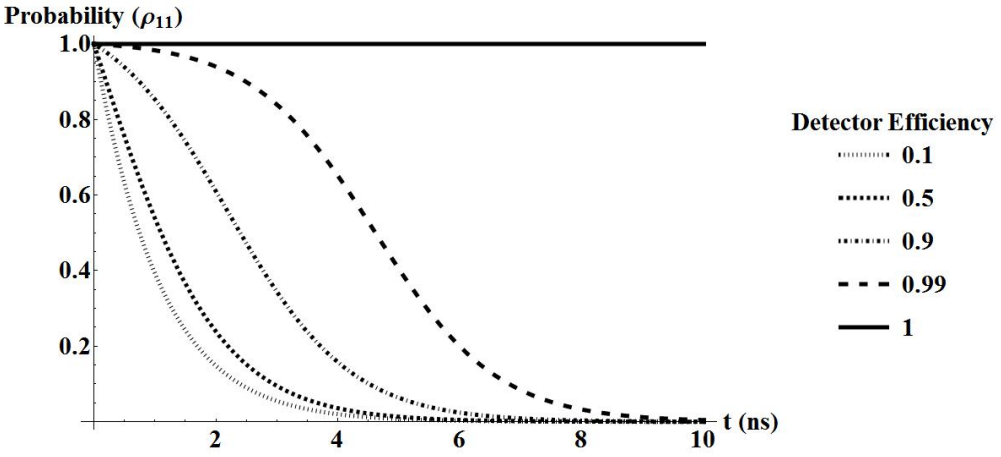

Figure 3.1: Solutions to the no-jump path of the conditional master equation with decay process only. The qubits all begin in the excited state with a probability of 1. The decay rate γ is set to 1 GHz.

If we reintroduce the jumping for a detector efficiency of 0.9, then we see what output we expect from the different trajectories as shown in Fig 3.2. There are 10 runs overlayed on one another. After an initial decay, each of the curves jump to a probability of zero, since a detection event would necessarily imply that the system is in the ground state. A detector efficiency of 0.9 was chosen here, because the graph looks pleasant, more so than $\eta = 1$, which would show a constant probability of one and be utterly featureless save for the vertical lines signifying jumps.

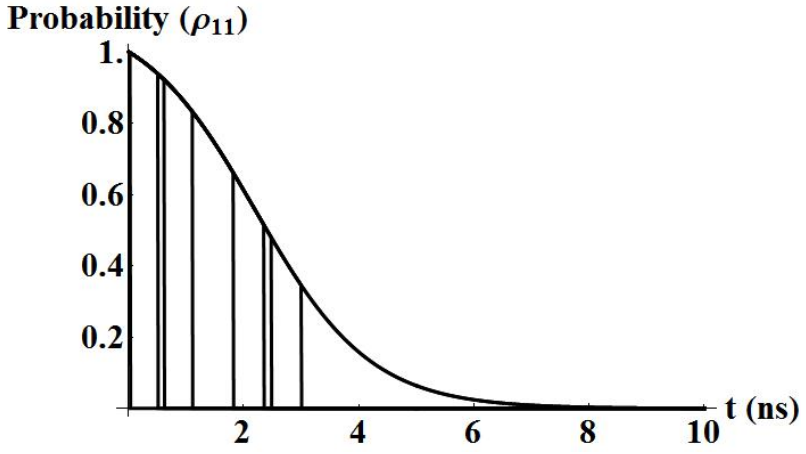

Figure 3.2: Solution to the conditional master equation with decay process only over 10 runs. The qubits all begin in the excited state with a probability of 1. The decay rate γ is set to 1 GHz and the detector efficiency is set to 0.9.The vertical lines show when the system in each trajectory has jumped.

It is stated in Eq. 3.6 that the conditional master equation must give the same solution as the unconditional when averaged over many runs and it is worth checking that this does indeed work, if for no other reason than to check the correctness of the code being run. The figures 3.3 - 3.5 below show the averages for 10, 50 and 1000 runs. It may be readily observed that the increase in the number of runs or trajectory markedly improves the agreement with the unconditional solution.

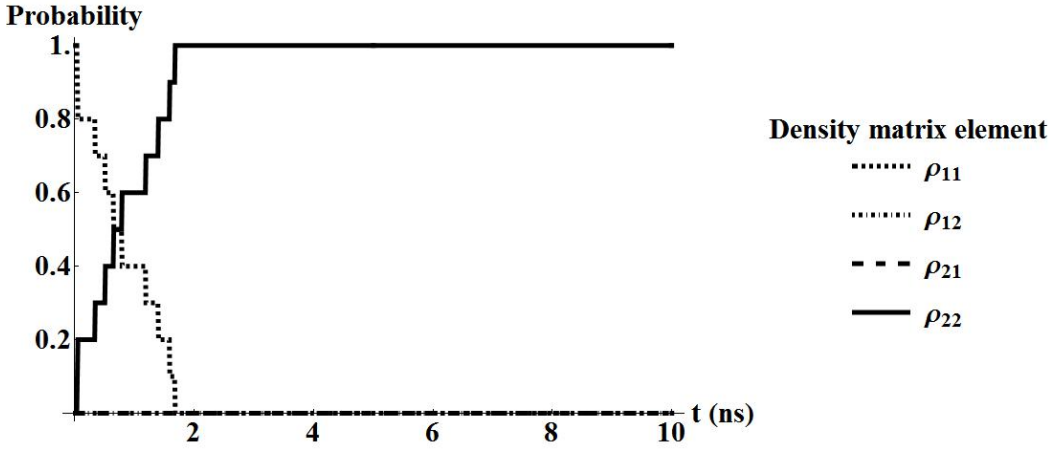

Figure 3.3: Solution to the conditional master equation with decay process only averaged over 10 runs. The qubits all begin in the excited state with a probability of 1. The decay rate γ is set to 1 GHz and the detector efficiency is set to 1. The curves shown are the absolute values of the density matrix elements.

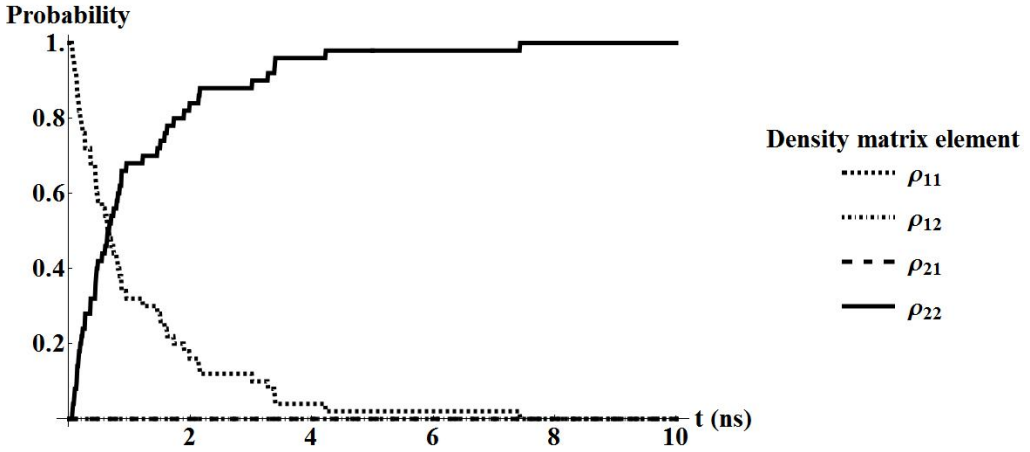

Figure 3.4: Solution to the conditional master equation with decay process only averaged over 50 runs. The qubits all begin in the excited state with a probability of 1. The decay rate γ is set to 1 GHz and the detector efficiency is set to 1. The curves shown are the absolute values of the density matrix elements.

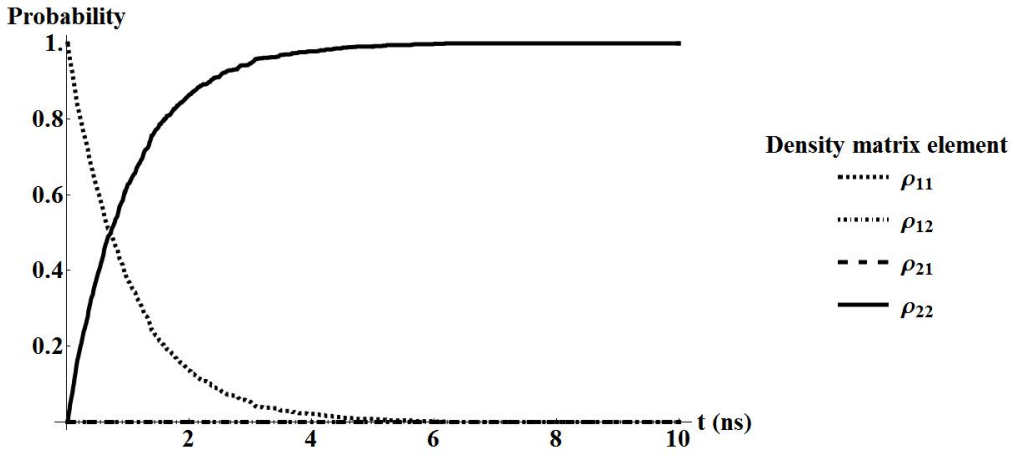

Figure 3.5: Solution to the conditional master equation with decay process only averaged over 1000 runs. The qubits all begin in the excited state with a probability of 1. The decay rate γ is set to 1 GHz and the detector efficiency is set to 1. The curves shown are the absolute values of the density matrix elements.

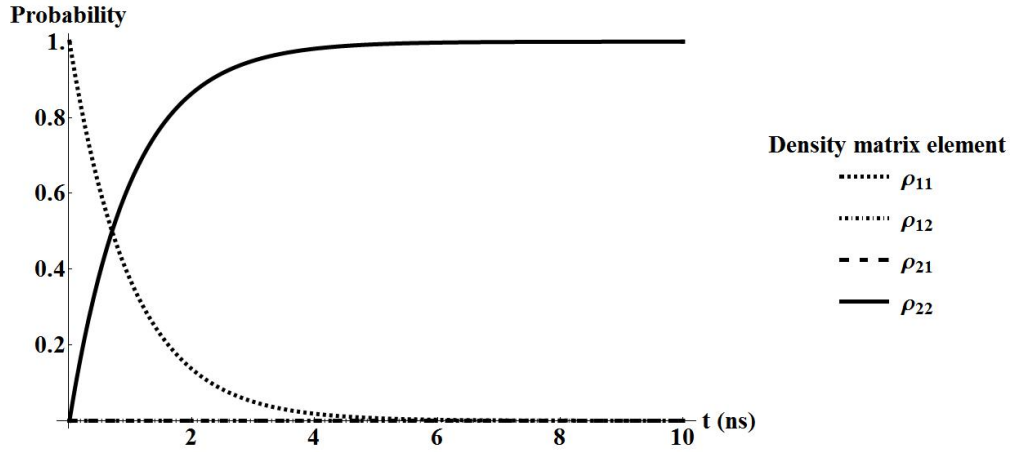

Figure 3.6: Solution to the conditional master equation with decay process only averaged over a single run. The qubit began in the excited state with a probability of 1. The decay rate γ is set to 1 GHz and the detector efficiency is set to 0 and hence equivalent to the unconditional master equations. The curves shown are the absolute values of the density matrix elements.

3.0.2 Decay and Absorption

After performing the same procedure as outlined earlier, but this time allowing N to be non-zero, we obtain the following set of coupled equations:

$$\begin{aligned} \dot{\rho_{11}} &= \langle 1|\dot{\rho}|1\rangle = \gamma\left((1+N)\,\eta\,(\rho_{11})^2 - (1+2N)\,\rho_{11} + N\right) \\ \dot{\rho_{22}} &= \langle 0|\dot{\rho}|0\rangle = \gamma\left(-(1+N)\,\eta\,(\rho_{11})^2 + (1+2N)\,\rho_{11} - N\right) \end{aligned} \tag{3.15}$$

These are first order non-linear differential equations of the Riccati form, which give the solutions

$$\rho_{11} = \frac{1 + 2N + \kappa \tan\left[\frac{\gamma t}{2}\kappa - \arctan\left(\frac{1+2N-2(1+N)x\eta}{\kappa}\right)\right]}{2\eta\,(1+N)}, \tag{3.16}$$

where $\kappa = \sqrt{-1 + 4N\,(1+N)\,(\eta - 1)}$. As with the decay only regime, we may plot the solution for the excited state as a function of the detector efficiency as can be seen in Fig 3.7.

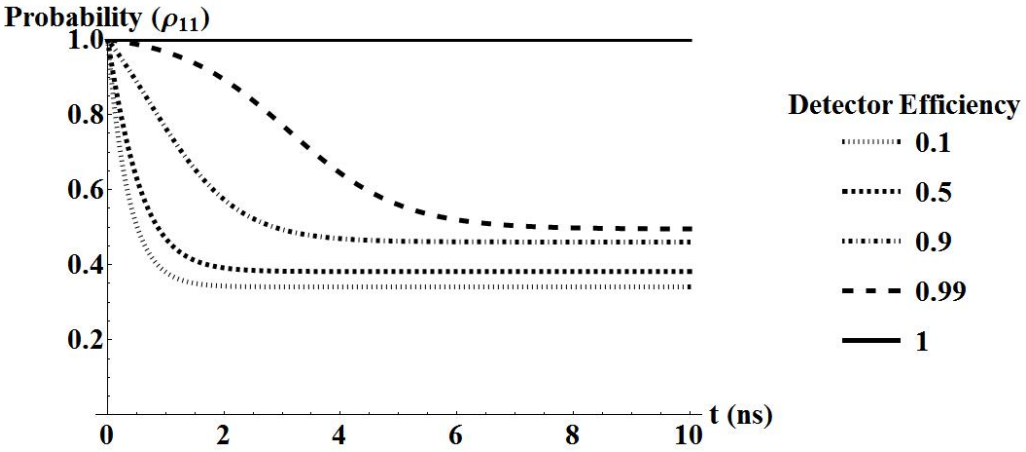

Figure 3.7: Solution to the no-jump part of the conditional master equation for absorption and decay processes. The qubits all begin in the excited state with a probability of 1. The decay rate γ is set to 1 GHz and N is set to 1.

Over 10 runs the conditional master equation solution looks as shown in Fig 3.8. We see that the solution begins in the excited state and remains there until the jump. After this point absorption process produces a mixed state, which moves towards a no-jump steady state of $\rho_{11}^{ss} = \frac{1}{3}$ with parameters $\eta = N = 1$.

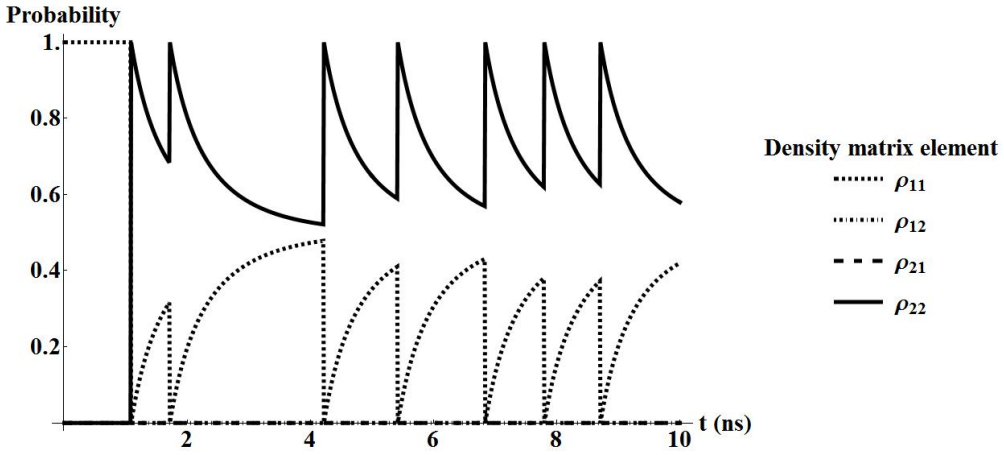

Figure 3.8: Solution to the conditional master equation with both absorption and decay process over a single run. The qubit began in the excited state with a probability of 1. The decay rate γ is set to 1 GHz and the detector efficiency is set to 1. The vertical lines show when the system in each trajectory has jumped. Note that after the curve jumps to zero, it then increases again due to the absorption process. The curves shown are the absolute values of the density matrix elements.

The averages for runs of 10, 50 and 1000 are shown in Figs 3.9-3.11 with the limit of zero detector efficiency shown in Fig 3.12.

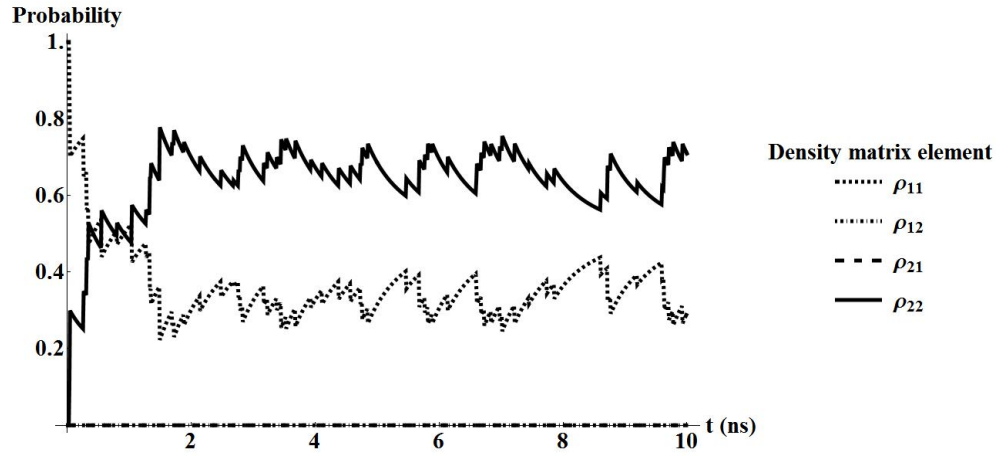

Figure 3.9: Solution to the conditional master equation both absorption and decay processes averaged over 10 runs. The qubits all begin in the excited state with a probability of 1. The decay rate γ is set to 1 GHz, the detector efficiency is set to 1 and N is set to 1. The curves shown are the absolute values of the density matrix elements.

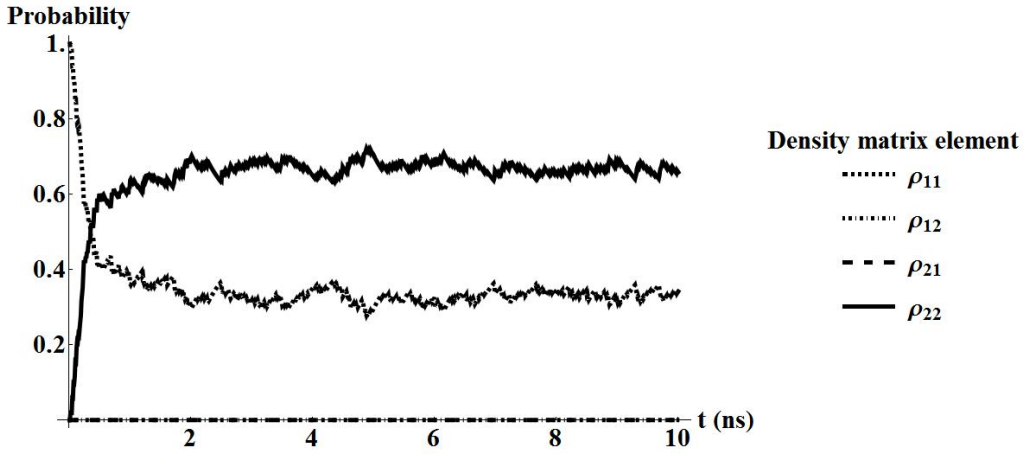

Figure 3.10: Solution to the conditional master equation both absorption and decay processes averaged over 50 runs. The qubits all begin in the excited state with a probability of 1. The decay rate γ is set to 1 GHz, the detector efficiency is set to 1 and N is set to 1. The curves shown are the absolute values of the density matrix elements.

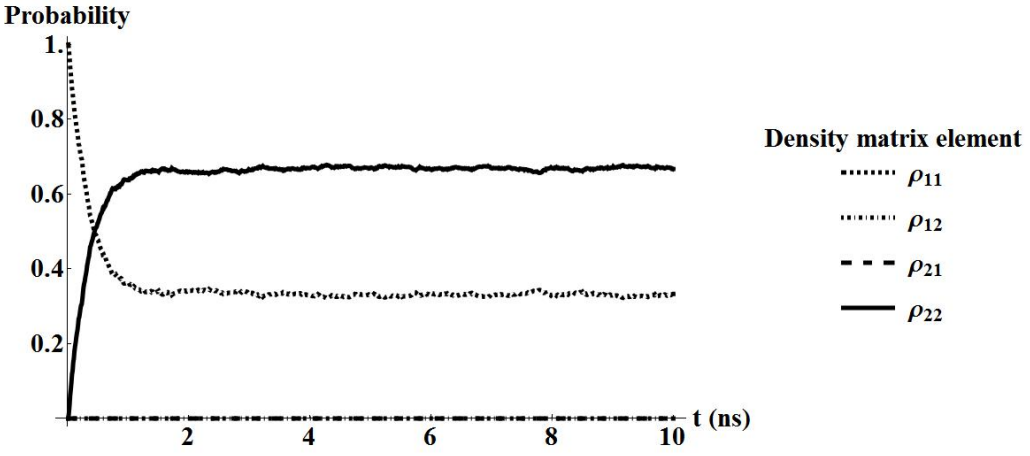

Figure 3.11: Solution to the conditional master equation both absorption and decay processes averaged over 1000 runs. The qubits all begin in the excited state with a probability of 1. The decay rate γ is set to 1 GHz, the detector efficiency is set to 1 and N is set to 1. The curves shown are the absolute values of the density matrix elements.

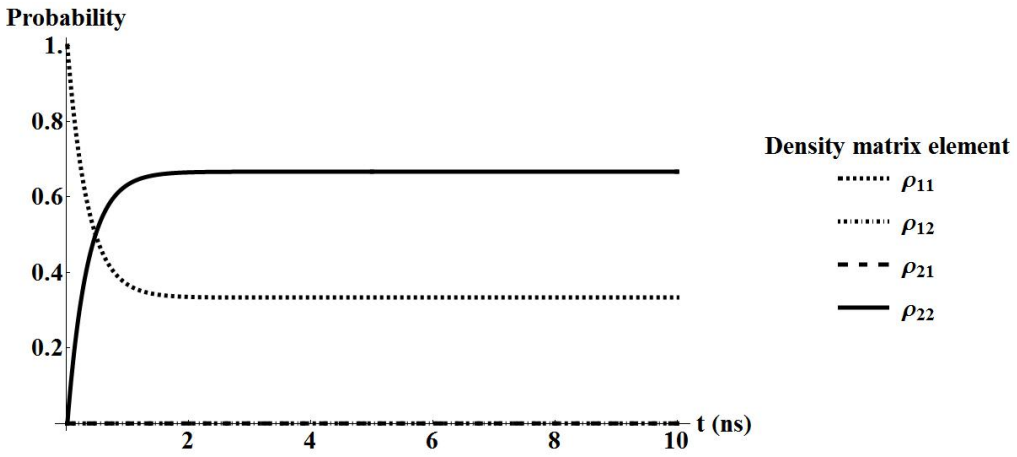

Figure 3.12: Solution to the conditional master equation with both absorption and decay processes averaged over a single run. The qubit began in the excited state with a probability of 1. The decay rate γ is set to 1 GHz, the detector efficiency is set to 0 and N is set to 1, which reduces to the unconditional master equation. The curves shown are the absolute values of the density matrix elements.

CHAPTER 4

Quantum Dots

To build a quantum computer we must have quantum bits, they must be physical objects that we can put into a physical computer. A very important question to answer is, how can we make them? There are in fact several ways that qubits may be taken out of the realms of hypothetical device into tangible device such as Nitrogen vacancies in diamond [16–18], superconducting flux qubits [19–21], photon polarisations [22–24] and donors in silicon [25, 26] to name but a few. The particular realisation that we shall be focussing on is the quantum dot. Quantum dots are semiconductor heterostructures that have confined electronic states in all three spatial dimensions. As a result they are called zero dimensional. When it is said that they are confined, it means that the size of the quantum dot is smaller than the de Broglie wavelength of the electrons within them. In general, quantum dots have complicated electronic systems, as shall be discussed, but there is experimental evidence that they can behave like atoms [27] in the sense that they have discrete energy levels and their eigenstates resemble those of a particle in a box [28, 29]. They are often referred to as 'artificial atoms' and display phenomena associated with atoms, for example Rabi oscillations [30–33]. Qubits may then be represented through a variety of different kinds of particles in QDs, including electron and hole spin or exciton states, which as we shall discuss in detail are bound electron-hole pairs [30, 34–38]. QD exciton qubits have large transition dipoles and interact strongly with an optical field [12, 39, 40], and therefore QDs make excellent sources of single photons making them a good choice for generating quantum entanglement as we shall discuss in chapter 7.

Quantum dots can absorb energy in the form of photons to promote an electron from the valence band to the conduction band. This leaves a hole behind in the conduction band. The electron and hole are bound together and form an exciton.

The complicated electronic structure of quantum dots means that there are many energy levels that the electron can be in. However, if we control the photon energies so that only the lowest of these energy levels is considered the presence or lack of the exciton may be approximated by a two level system design as described in section 2.4.1. Since atomic physics has been studied for a long time and much is understood about it, the quantum dot is a useful structure to build things. In addition to being good single photon sources, they can also be used as optical switches [41], and generate entangled photons [42, 43]. Whilst these properties are interesting, in order to be truly useful, we must be able to manipulate or control them. Before discussing how this may be achieved, let us discuss quantum dots and excitons in general.

4.1 Growth of self-assembled quantum dots

We begin this introduction on quantnum dots with a discussion about their growth. One growth mechanism is known as the Stranski-Krastanov technique or procedure [44, 45]. This process relies on heteroepitaxy, which is the technique of depositing layers of a material on a substrate of another. For use in quantum dots, pairs of materials include silicon-germanium (Si-Ge), indium arsenide-gallium arsenide (InAs-GaAs) and indium phosphide-gallium arsenide (InP-GaAs). It is of the utmost importance that the pairs of substrate and depositing material have dissimilar lattice constants, since were they to be too similar, the effects of the strain introduced in the crystal would not be enough to stop the creation of a film consisting of a single crystal. The strain in this type of growth is initially taken care of by biaxial compression of the deposited film, also known as the wetting layer, the initial layer of atoms grown on the substrate [46]. This being said, if the there is a sufficient lattice mismatch, the strain within the film will build with additional layers until it will become energetically favourable to form islands. These islands are known as self-assembled quantum dots and can range from a few to hundreds of nanometers[47]. The threshold above which the process of island forming is favourable is called the Stranski-Krastanov transition [48]. It has been observed in experiments of the heteroepitaxy of germanium on silicon as well as indium arsenide on gallium arsenide that this threshold is about three monolayers.

Since the dots are self-assembled, their properties such as size and shape follow a distribution rather that conform to some standard. The growth of dots with different sizes and shapes and strains will affect the excitation energies of the indi-

vidual dots. As a result, the photoluminescence of the many dots grown will show a broadened profile. Having grown many dots on a substrate, one may use a mask or aperture to reduce the numbers of dots able to emit photons to some detector. It has been seen that the smaller the aperture, the more discrete the photoluminescence spectrum becomes [33]. This distribution of properties is a problem since many quantum information applications require qubits to be indistinguishable as we will see in chapter 7 when we discuss measurement-based quantum computation. There has, however, been work done to create dots with emission distributions of about 1% [49] and develop some control over the growth locations of the dots, which can be achieved by patterning the substrates that the dots are grown on [49–52].

4.2 Physics of quantum dots

Now that we have introduced what a quantum dot is, we may now discuss some of the physics of quantum dots. A good place to start is the electronic structure, since that will be useful in determining their optical properties. There have been many methods, both analytical and empirical, developed to understand and predict the electronic structures of quantum dots, some of the most accurate of which are the pseudopotential [53] and DFT approaches [54]. The simplest is taking the dot to be a particle in a box. It is not very accurate, but in considering it we understand more about quantum dots as structures. Since a quantum dot is confined in all three spatial dimensions, i.e. it is a zero dimensional object, it would seem a good idea to treat the electrons and hole as a particle in a box, but since they are in a semiconductor, they will have effective masses according to the valence and conduction bands, the structure of which is shown in Fig. 4.1.

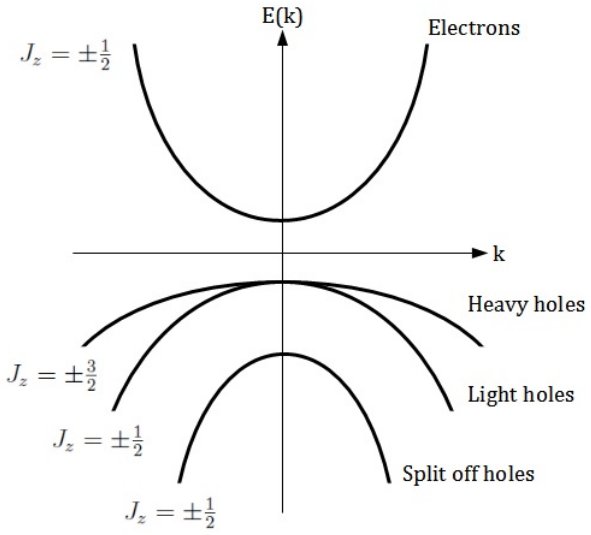

Figure 4.1: Schematic diagram of a semiconductor band structure.

4.2.1 Effective mass and envelope approximations (I)

Before discussing quantisation of electronic states in quantum dots, we first review the bulk properties of the semiconductors from which the dots are made. We start with effective mass approximation. This is the assumption that the effect of the potential produced by the crystal on the electron can be approximated by a free electron with an altered or effective mass [55–57]. This effective mass approximation is worked in great detail in Yu and Cardona [56] from which we shall follow. The initial aim is to show that the wave function can be approximated by the periodic part of the Bloch function and an envelope function. The example given by Yu and Cardona begins with a single particle wavefunction. The system set up is a substitutional phosphorous donor in silicon. The donor electron from the phosphorous travels through the semiconductor and is attracted to the phosphorous nucleus, so we must consider the crystal potential as well as the impurity potential. The Schrödinger equation for the donor electron is given by

$$(H_{bulk} + V(r))\psi(r) = E\psi(r), \tag{4.1}$$

where H_{bulk} is the single electron Hamiltonian for the bulk material, which takes into account the periodic lattice potential and $V(r)$ is the screened Coulomb potential, between the electron and donor nucleus. We know that without any screened impurity potential, the solution to the Schrödinger equation in a periodic potential is given by Bloch functions $\psi_{Bloch}(r) = u_{nk}(r)e^{ik\cdot r}$, where k is the wavevector and n

is the band index. We can expand the wavefunction in terms of Bloch or Wannier functions. Wannier functions are the Fourier transform of the Bloch functions and are localised around lattice points R [12, 58]. Expanding the wavefunction in terms of these Wannier functions we have

$$\psi(r) = \sum_i C(R_i) a(r - R_i), \tag{4.2}$$

where $C(R_i)$ are the envelope functions for lattice sites (R_i) and $a(r - R_i)$ are the Wannier functions. Performing the Fourier transform and converting these into their corresponding Bloch functions

$$\begin{aligned} \psi(r) &= \sum_i C(R_i) \sum_k e^{-ik\cdot R_i} \psi_{Bloch}(r) \\ &= \sum_i C(R_i) \sum_k e^{-ik\cdot(R_i - r)} u_k(r). \end{aligned} \tag{4.3}$$

We have assumed that the lattice points are discrete, but we can make them continuous, in which case the problem reduces to the hydrogen atom like situation, where the Bohr radius of the electron is

$$a^* = \left(\frac{\epsilon_0 h^2}{\pi e^2 m^*} \right), \tag{4.4}$$

where m^* is the effective mass of the conduction band. If the Bohr radius of the electron is very large in comparison to the lattice constant of the crystal then the sum over k in Eq. 4.2 can be restricted to near $k = 0$ [56]. The wavefunction can then be approximated by

$$\psi(r) = u_0(r) C(r). \tag{4.5}$$

Assuming that the band shape around $k = 0$ is parabolic, the energy association with H_{bulk} is

$$E_c(0) + \frac{\hbar^2 k^2}{2m^*}. \tag{4.6}$$

Inserting Eq. 4.6 and 4.5 into the Schrödinger equation and assuming that $V(r)$ is slowly varying over the length of a unit cell, we can get rid of the Bloch part of the wavefunction and so we are left with just the envelope function.

$$\left(\frac{\hbar^2}{2m^*} \nabla^2 + V(r) \right) C(r) = (E - E_c(0)) C(r), \tag{4.7}$$

which shows that the envelope functions are solutions to the single particle Schrödinger equation [59].

4.2.2 Excitons

When a QD is illuminated with light, it will absorb a photon and an electron will promoted from the valence band to the conduction band. Where the electron once was, is now a hole having a net positive charge when compared to its surroundings. This electron and hole, being oppositely charged, form a bound state, which is called an exciton. In general, there are many types of exciton and the energy spectrum can be complicated to calculate. In a bulk material, let us think of an ionic crystal, an ion may be excited by some means. This excitation may be transferred to other neighbouring ions and so the exciton, unlike the ions themselves are free to wander around the bulk. This type is called the Frenkel exciton [60, 61]. This is a very localised example of an exciton and exists on the scale of a unit cell. In the case of a semiconductor, the Coulomb attraction between the electron and hole may be screened somewhat and the pair are not so tightly bound. These are called Mott-Wannier excitons and they extend over many lattice sites. In general it is very difficult to solve the electronic structure of a quantum dot. Let us extend the analysis in section. 4.2.1 for single particles to a case where there are two particles.

4.2.3 Effective mass and envelope approximation (II)

Generalising the procedure that we saw in section 4.2.1 to an electron and hole, we define a wavefunction in terms of a combined excitonic envelope function and Wannier functions

$$\psi(r_e, r_h) = \sum_{R_e, R_h} C(R_e, R_h) a_{R_e}(r_e) a_{R_h}(r_h), \tag{4.8}$$

where the subscripts e and h describe electrons and holes respectively. This equation look slightly different to Eq. 4.2, because we have written the electron and holes as functions of their respective distances ($r_e = r_{electron} - R_i$, $r_h = r_{hole} - R_i$). We can form an analogous equation to Eq. 4.7 and put in an explicit form for $V(r)$

$$\left(\frac{\hbar^2}{2m_e^*} \nabla^2_{R_e} + \frac{\hbar^2}{2m_h^*} \nabla^2_{R_h} - \frac{e^2}{4\pi\epsilon |R_e - R_h|} \right) C(R_e, R_h) = E C(R_e, R_h). \tag{4.9}$$

Since the Coulomb term only in terms of the relative distance between the electron and hole, we can move into a centre of mass co-ordinate system

$$r = R_e - R_h \ , \ R = \frac{m_e R_e + m_h R_h}{m_e + m_h}, \tag{4.10}$$

where r is the relative distance between the electron and hole and R is the centre of mass vector. The envelope function will now be a function of r and R [56, 57]. We assume that the envelope function can be formulated to be a product of functions of R and r

$$\left(-\frac{\hbar^2}{2M}\nabla_R^2 - \frac{\hbar^2}{2\mu}\nabla_r^2 - \frac{e^2}{4\pi\epsilon r}\right) C(R)C(r) = (E_R + E_r)\, C(R)C(r), \tag{4.11}$$

where $M = m_e + m_h$ and $\frac{1}{\mu} = \frac{1}{m_e} + \frac{1}{m_h}$. We can then split up the equation into two parts

$$\begin{aligned}\left(-\frac{\hbar^2}{2M}\nabla_R^2\right) C(R) &= E_R C(R)\\ \left(-\frac{\hbar^2}{2\mu}\nabla_r^2 - \frac{e^2}{4\pi\epsilon r}\right) C(r) &= E_r C(r).\end{aligned} \tag{4.12}$$

The first of these equations describes a free particle

$$E_R = \frac{\hbar^2 K^2}{2M}, \tag{4.13}$$

where $K = k_e + k_h$. The second of the equations describes the hydrogen atom and so the total energy of the exciton is given by

$$E = E_{gap} + \frac{\hbar^2 K^2}{2M} - \frac{\mu e^4}{8h^2\epsilon^2}. \tag{4.14}$$

In direct band gap semiconductors the excitons form at $K = 0$ and so the energy equation, in this case, reduces to

$$E = E_{gap} - \frac{\mu e^4}{8h^2\epsilon^2}, \tag{4.15}$$

which very nicely is just the result for hydrogen atom with an effective mass and charge screening shown by a dielectric constant added to the band gap energy.

In a quantum dot the confinement of the electrons can be smaller than the Bohr radius that we found for Mott-Wannier excitons. This is called the strong confinement regime. In this regime the electrons and hole can be thought of as independent particles, but masses of the electron and the hole are the effective masses for the conduction (m_c) and valence (m_v) bands. They still interact with each other through the Coulomb interaction with a screening effect provided by the dielectric constant. A quantum dot is made of two materials with different band gaps and so you get

regions of confined states. Looking at Fig. 4.2, we see a cut through one of the spatial dimension and you would see the same thing if you cut though any of the others. Typically, the band gaps are bigger than the band offset,

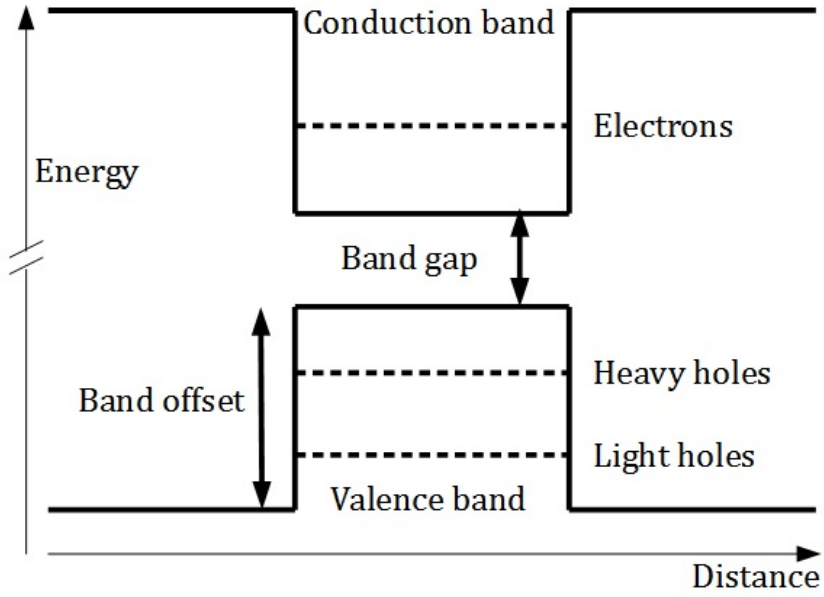

Figure 4.2: Schematic diagram of the energy profile of a confined quantum dot.

Now we can return to the idea of a particle in a box. Let us think of a box of side length L and using the uncertainty principle, we may calculate the minimum confinement energy of the electrons to be

$$E_{e,min} = \frac{9h^2}{8\pi m_c L^2}. \tag{4.16}$$

From solving Schrödinger's equation for a particle in a box, the discrete energy levels are given by

$$E_{e,n} = \frac{(n_x^2 + n_y^2 + n_z^2)h^2}{8m_c L^2} \ , \ E_{e,min} = \frac{3h^2}{8m_c L^2}|_{n_x,n_y,n_z=1}, \tag{4.17}$$

where n_x, n_y, n_z are integers, i.e., the principle quantum numbers in the three spacial dimensions and L as mentioned earlier is the size of the length box. The energy for holes is the same equation, but with the effective mass m_v. In addition to the particle energy, the electron sits above the band gap, which requires energy to achieve so

$$E_{e,min} = E_{gap} + \frac{3h^2}{8m_c L^2} \ , \ E_{h,min} = \frac{3h^2}{8m_v L^2}. \tag{4.18}$$

The two particles are also of opposite charges, so there is a Coulomb attraction $-E_c$.

The total energy of the exciton is given by

$$E_X = E_e + E_h + E_{gap} - E_c, \tag{4.19}$$

E_e and E_h are the particle energies, the minimum of which is given by Eq. 4.16. These will not be the same since they have different effective masses. The band gap energy is represented by E_{gap}. Finally, E_c represents the Coulomb interaction between the charged particles, which is negative since they are attracted to each other. The band structure in the strong confinement regime, now looks like that shown is Fig. 4.2.

The confinement of the system splits the heavy hole and light hole energies. This is due to the different curvatures of the two dispersions and their relation to the effective mass, $\frac{1}{m^*} = \frac{d^2E}{dk^2}$. As can be readily seen by the equation, the lower the curvature, the higher the effective mass and so heavy holes have a greater effective mass than lighter holes. The energy of confined particles is proportional to $\frac{1}{m^*}$, where m^* is the effective mass as shown in Eq. 4.2. This has the obvious consequence that heavy holes have a lower confinement energy than light holes. If we define the top of the valence band as having an energy of zero, then when an exciton is created, the electron in the conduction band will have a positive energy, the hole in the valence band will have a negative energy and the difference between them will be the energy of the absorbed photon. Since it takes less energy to confine a heavy hole than a light hole the energy gap between electron and hole will be smaller for a heavy hole than for a light hole, which is why heavy holes appear closer to the top of the valence band in Fig. 4.2.

4.2.4 Optical properties

When an exciton has formed in a quantum dot, it is by definition a pair of oppositely charged particles separated, but are still bound. If there is an overlap between the electron and hole wavefunctions, there is a transition dipole moment. This transition dipole moment is calculable from the equation

$$\boldsymbol{d} = \int_{space} d^3r \ \psi_e^*(r) \ r \ \psi_h(r), \tag{4.20}$$

where $\psi_{e,h}$ are the electron and hole wavefunctions [12]. Using the envelope approximation that we saw earlier in Eq. 4.5, we can re-write the equation as

$$\boldsymbol{d} = \int_{space} d^3r \ rC_e^*(r)u_e^*(r) \ r \ C_h^*(r)u_h(r), \tag{4.21}$$

where $u_{e,h}$ are the Bloch functions for the electron and hole and $C_{e,h}$ are envelope functions. Bloch functions are delocalised, but their Fourier transform, called Wannier functions are localised around lattice points. The wavefunction can be represented by these localised Wannier functions multiplied by an envelope function,

$$u_{k=0}(r) = \sum_{R_i} a(r - R_i), \tag{4.22}$$

which gives us

$$\boldsymbol{d} = \sum_i \int_{space} d^3r \; C_e^*(r - R_i) a_e^*(r - R_i) \; (r - R_i) \; C_h(r - R_i) a_h(r - R_i), \tag{4.23}$$

Since the Wannier functions are localised to within a unit cell, we can restrict the integral over them to just the unit cell. Since the envelope functions vary slowly [12], we may replace them with their average values

$$\boldsymbol{d} = \sum_i C_{i,e}^* C_{i,h} \int_{cell} d^3r \; a_e^*(r) \; r \; a_h(r). \tag{4.24}$$

Due to the periodicity of Bloch and Wannier functions the integral over each unit cell will be the same. The envelope functions, while approximately constant over each unit cell, may vary on larger scales and so we come to the expression [12]

$$\boldsymbol{d} = \int_{space} d^3r' \; C_e^*(r') C_h(r') \int_{cell} d^3r \; a_e^*(r) \; r \; a_h(r). \tag{4.25}$$

What this means is that the overlap integral of the envelope functions determines the dipole moment. The fact that quantum dots have such large transition dipole moments is due to this large overlap. The electrons of the conduction band have s-type orbital symmetry and so has angular momentum $J = \frac{1}{2}$, with $J_z = \pm\frac{1}{2}$. The valence band has p-type orbital symmetry and therefore has fourfold degeneracy. The orbital angular momentum is $L = \pm 1$ and the spin angular momentum is $s = \pm\frac{1}{2}$ so there are two bands $J = \frac{3}{2}$ for light and heavy holes and $J = \frac{1}{2}$ for spilt off holes. The split off holes are called so, because they are split off from the $J = \frac{3}{2}$ band, while the heavy and light holes become degenerate at $k = 0$. The difference between a heavy hole and a light hole is the J_z component of their angular momentum and their effective masses. Heavy holes have J_z component of their angular momentum $3/2$, $-3/2$ and light holes have $1/2$, $-1/2$. A photon can carry a spin of ± 1 if it is circularly polarised, so there are four possible transitions, σ_+ gives a spin of 1 and σ_- takes 1 away.

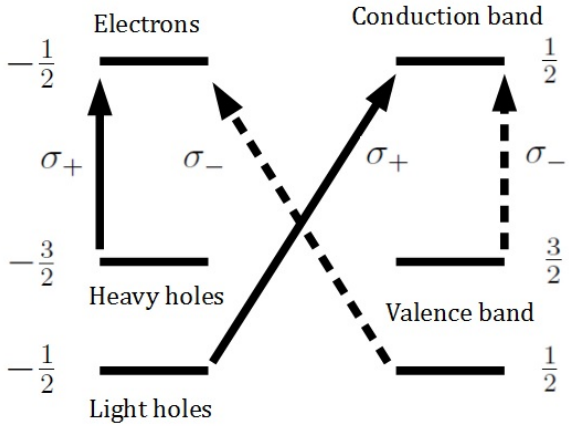

Figure 4.3: The direction of the polarised light add or take away a spin of 1 from the ground states unless there is heavy hole light hole mixing.

However, this is only valid in the case that there is no light hole heavy hole mixing [62]. If there is heavy hole light hole mixing, it means that the $\frac{3}{2}$ heavy hole mixes with the $-\frac{1}{2}$ light hole state and the $-\frac{3}{2}$ heavy hole mixes with the $\frac{1}{2}$ light hole state. As a result either direction of circularly polarised light could excite each of the ground states.

4.3 Controlling quantum dots

As already intimated, quantum dots interact with light and so lasers play a large part in manipulating the excitons used as qubits. One such way of using lasers is in resonance fluorescence experiments, where a probe laser resonantly excites the dot to create an exciton and once recombination of the electron and hole occurs, the emitted photons are detected. The problem for resonance fluorescence is having optical inputs and outputs, where it may become difficult to distinguish between the emitted photons and the laser photons. Schemes designed to help with this problem are to detect the signal along the same axis, but using opposite polarisations and a polarising filter [63] and measuring the photons at right angles to the laser probe. Using resonance fluorescence is good in the case where the dot is inside a cavity and has the added advantage that it combines the ability to manipulate the qubit as well as detecting the output for use in quantum computing [8, 16].

Early experiments on quantum dots used short laser pulses to optically excite electrons from the ground state creating a p-shell exciton. The resulting excitons were

short lived, relaxing from the p to s-shell in approximately 40 ps [49]. The recombination of electron and hole resulted in an emission of a photon that was lower in energy than that of the exciting laser by about 20 meV, which allowed the population of the p-shell to be known. This type of set up is not great for quantum information, since the relaxation time from the p to s bands is very fast. In addition, the p-shell is close to the energy of the electrons in the wetting layer and the hybridisation of the states results in faster decoherence [64].

Lasers inducing optical transitions in quantum dots are very useful since they not only form excitons, but once they are formed, the lasers can perform operations on them such as logical gates [65, 66], such as the CNOT [67] or CROT (controlled rotation) [65] have been demonstrated on exciton qubits. Exciton qubits have been made to show Rabi oscillations, which we have discussed in section 2.6. There are, however, other methods of control; for example, applying an electric field [33, 49]. The dot is pumped optically and the exciton is created, but the presence of the field forces the electron and hole to tunnel out of the dot and are detected as a photocurrent which is proportional to the exciton population. This approach works on the neutral exciton [68] as well as the biexciton and exciton-biexciton systems [49]. This is quite an effective method, since typically the detection of a photon due to recombination is limited by mismatches in refractive indices between semiconductor and air. This is about 2% in GaAs dots [49], though index matching structures can help with this. The tunnelling needed to detect the excitons has an adverse effect on the coherence time, about 300 ps [69], which is about half the radiative lifetime of the exciton measured at about 600 ps [70]. The detector efficiency and coherence time have also been found to be inversely proportional.

4.4 Gates

Since we mention logical gates we must say that it is not enough merely to have bits for a computer to work. There must be a way to manipulate those bits. This is done by logic gates, or quantum gates in our case. All quantum gates must be unitary since they must preserve the normalisation of the state. This is the only restriction on the gate, so any unitary matrix will be a quantum gate. Some quantum gates have a classical analogue and so they will be very useful for comparison. Let's look at the X gate since, it's classical analogue is the NOT gate, it swaps around the input value. We can represent the quantum NOT or X gate,

operation as a unitary matrix [71]

$$X \equiv \begin{pmatrix} 0 & 1 \\ 1 & 0 \end{pmatrix} \quad , \quad |\psi\rangle = \alpha|1\rangle + \beta|0\rangle \equiv \begin{pmatrix} \alpha \\ \beta \end{pmatrix}$$

$$X|\psi\rangle \equiv \begin{pmatrix} 0 & 1 \\ 1 & 0 \end{pmatrix} \begin{pmatrix} \alpha \\ \beta \end{pmatrix} = \begin{pmatrix} \beta \\ \alpha \end{pmatrix} \tag{4.26}$$

We can see from this that the basis states are transformed into their opposites. The Bloch sphere makes it easier to visualise what the X gate does. If the state were 0 then there would be a rotation by π around the X axis. The X gate performs an equivalent operation as a classical gate in this case, but let's not forget get it is a quantum operator and so can act on non-classical states. There are also gates that have no classical analogue. Two examples of these are the Z and Hadamard gates.

$$Z \equiv \begin{pmatrix} 1 & 0 \\ 0 & -1 \end{pmatrix} \tag{4.27}$$

$$H \equiv \frac{1}{\sqrt{2}} \begin{pmatrix} -1 & 1 \\ 1 & -1 \end{pmatrix} \tag{4.28}$$

The Z gate is a π rotation about the Z axis. This gate is off limits for a classical bit, which is locked to the Z-axis and so wouldn't do anything. To a quantum state, the Z gate leaves the $|0\rangle$ untouched, in our notation, but the $|1\rangle$ changes sign. The Hadamard is a very useful transformation and on the Bloch sphere is equivalent to a $\pi/2$ rotation about the Y-axis and then a π rotation about the X-axis. This is also equivalent to firstly rotating by π about the Z axis and subsequently rotating about the Y axis by $\pi/2$. Interestingly, performing the Hadamard transformation a second time recovers the original state.

These gate can be performed on quantum dot qubits, with the aid of lasers. Lasers, as we saw in section 2.6 give rise to Rabi oscillations, which rotate the qubit around the Bloch sphere. If we have a laser pulse of a duration that gives half a Rabi cycle, then we have performed a π rotation around the Bloch sphere and as a result have performed the X/NOT gate.

4.4.1 Multiple qubit gates

We can generalise these gates to multiple qubits. The classical two bit gates that we are used to such as AND, OR and their NOT counterparts, NAND and NOR,

take two inputs and give a single output. Two qubit gates have two inputs and two outputs. The type of gates that are relevant to us are called controlled gate and to explain them, let us define our terms. There are two types of input qubit, a control qubit and a target qubit. These correspond to the qubit that makes a decision and the one that is affected. In this way, if we begin with two inputs, then we are left with two outputs, but the target qubit has undergone some operation. As an example, let us consider the CNOT (controlled NOT) gate, which as we shall see is equivalent to a kind of classical XOR (exclusive OR) gate. The truth table for the CNOT gate with two qubits labelled C (control) and T (target) and the subscripts b (before) and a (after) is as follows

C_b	T_b	C_a	T_a
0	0	0	0
0	1	0	1
1	0	1	1
1	1	1	0

(4.29)

We see that the target qubit is flipped i.e. a NOT operation is performed on it, if and only if the control qubit is 1. Due to this fact, the only way to have an output of 1 in the target qubit is if the inputs are opposites. Thus the CNOT gate is the same as the classical XOR gate if the output is stored in the target bit. As mentioned earlier, we can represent this operation as a unitary matrix

$$U_{CNOT} \equiv \begin{pmatrix} 0 & 1 & 0 & 0 \\ 1 & 0 & 0 & 0 \\ 0 & 0 & 1 & 0 \\ 0 & 0 & 0 & 1 \end{pmatrix}, \tag{4.30}$$

or in the much more compact notation $|A, B\rangle \rightarrow |A, B \oplus A\rangle$, where $\oplus$ is a modulo two addition. We have mentioned that quantum gates are unitary. This means that they are reversible and since the gates shown so far have all been comprised of real elements, they are reversible by repetition of the gate. Classical gates like the normal XOR gate, where the result is not stored in the second bit, is not reversible since it is not possible to determine the states of the inputs from the output. Another important gate, which we will use later is the CPHASE (controlled phase) gate. This gate, as the name suggests, affects the phase of the target qubit. As a matrix,

it is described by

$$U_{CPHASE} \equiv \begin{pmatrix} e^{i\phi} & 0 & 0 & 0 \\ 0 & 1 & 0 & 0 \\ 0 & 0 & 1 & 0 \\ 0 & 0 & 0 & 1 \end{pmatrix}, \tag{4.31}$$

where ϕ is often set to π so that the $|11\rangle$ element flips sign.

Using gates like these to build algorithms is called the circuit model, and we can see this analogy as we have bee talking about classical logic gates as used of electrical circuits. This is not the only way algorithms can be build, however, as we shall see in Chapter 7.

This is the end of the background chapters. We have discuss open and closed quantum systems, from which we learnt much about the master equation formalism that can be used is the unconditional way to obtain averages and in the quantum jump formalism that allows us to model single experimental runs. This stands us in good stead since we shall use them throughout the research chapters. In addition we explored physical qubits with a focus of quantum dots. We learnt about their electronic structure, but also that while they may be complicated to model exactly, they can in fact be modelled as atoms and when considering low lying energy states, the complexity reduces to that of a two level system. Let us begin the research chapters.

Part II

Research Chapters

CHAPTER 5

Probing Charge Fluctuator Correlations Using Quantum Dot Pairs

5.1 Introduction

This is the first research chapter and as the title suggests, its aim to study fluctuating charges and correlations in photon statistics resulting from their presence. This is done with the aid of two quantum dots that are grown in such an environment. We shall assume that the dots are identical. The aim of this chapter is to show that the common, correlated, noise that is generated by charges fluctuating in the vicinity of two QDs can be detected by optically driving the QDs and then analysing the emitted photons. To this end, we shall determine the cross correlation function $g^{(2)}(\tau)$ of the emitted light and show that knowledge about the nature of the charge environment can be revealed; including how common it is to both qubits. It will be demonstrated that in some regimes it is possible to determine the number of charges and the rate of their fluctuation. For ease of reading and in order to provide context, let us recap some of the main points that we saw in Chapter 4, which will be of most use to us now. Quantum dots are semiconductors heterostructures, which by their nature, have a Fermi energy inside the band gap. When the temperature is relatively low, the gap can be small enough in doped samples that the conduction band may be thermally occupied. The crystal structure of any material is rarely perfect and vacancies or impurities in the structure of a semiconductor lead to local alterations to the band structure. As a result charges can become trapped in lower lying states [72]. This shall form the basis of our common environmental disturbance. Depending on the temperature, the charges in these traps will randomly hop into and out of them [73]. This leaves us with a system of traps that are either filled or not. As such they may then be modelled as two state fluctuators. In the vicinity of QD excitons, such fluctuators lead to random telegraph noise in the

exciton energy and thus, via the DC Stark shift, so too in the frequency of emitted photons; [5] see Figs. 5.1 and 5.2.

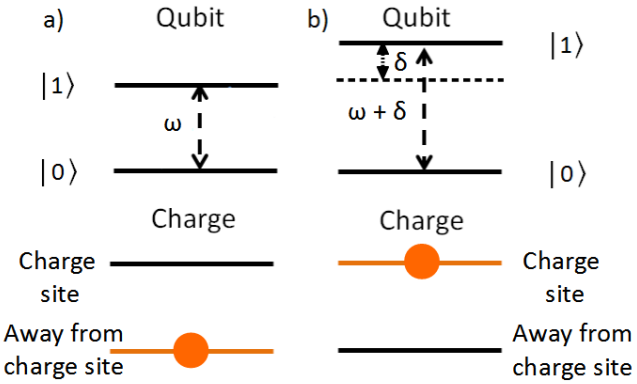

Figure 5.1: The qubit energy shift for an unoccupied (left) and charged (right) trap. The exciton creation energy is denoted by ω and the charge-qubit interaction strength is δ.

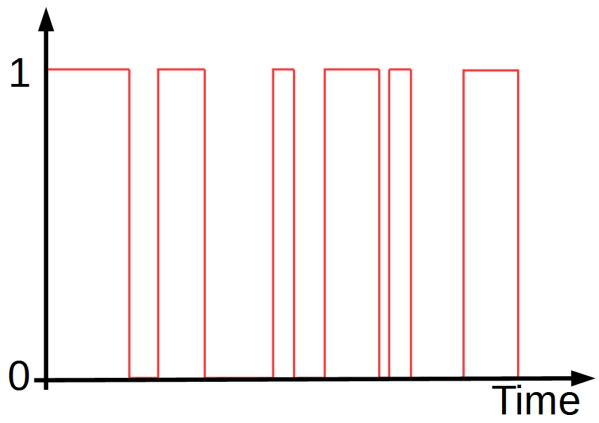

Figure 5.2: Demonstrative graph of telegraph noise. The fluctuating charge switches stochastically between states 1 (charged) and 0 (uncharged).

5.2 Model

We consider two driven and uncoupled QDs, that are modelled as two level systems with different energy spacings. As a result these emit photons of different frequencies, which can be measured by two time-resolving detectors. The

QDs are driven by lasers with different frequencies to match their respective resonances, though each has the ability to be detuned from this condition. In addition, these uncoupled QDs both interact with a common environment that takes the form of a limited number of charge fluctuators that will also be represented by two level systems; the situation is shown in Fig 5.3. The fluctuators will be treated as classical objects and as such there can be no coherence between the charged and uncharged states. The charges affect the qubits via the Coulomb interaction, inducing a DC Stark shift, which is explained in section 5.2.2. Any dielectric screening effects are neglected, since we are not interested in the absolute distances of the charges to the QDs. Including screening would merely require a renormalisation of the effective distance between qubits and fluctuators, which has no impact on the photon statistics.

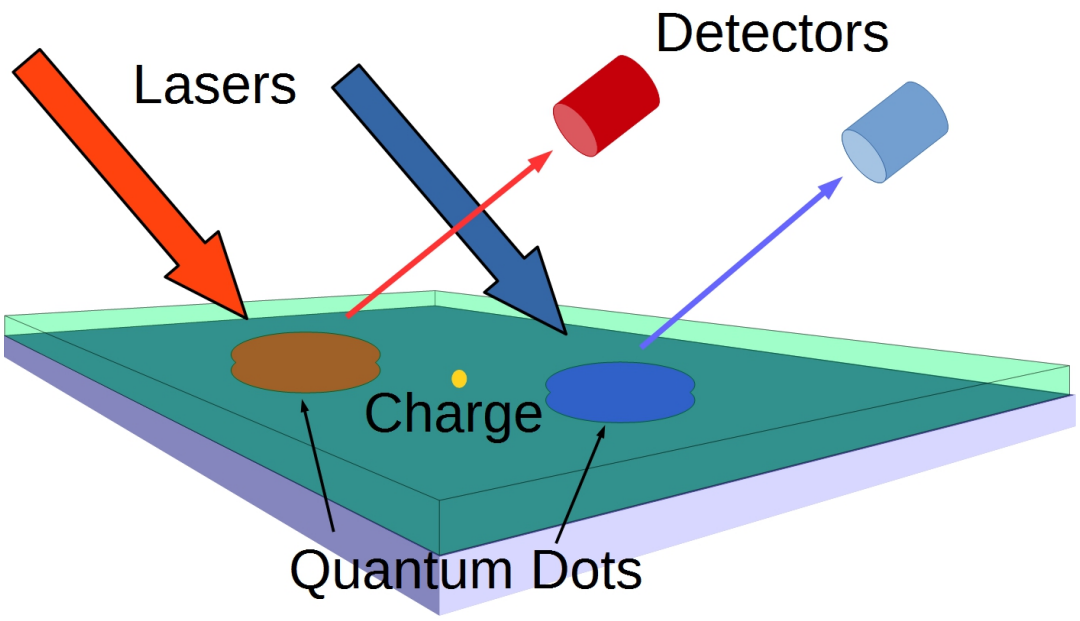

Figure 5.3: Diagram of the experimental set up. The two QDs are driven by lasers of different frequencies. The emitted photons are captured by the detectors, where the Hanbury Brown-Twiss style experiment is performed.

5.2.1 Qubits and Charge Hamiltonian

For the purposes of pedagogy, we present the Hamiltonian construction for the case of two QDs and a single charge, although it will be readily seen that through the processes outlined, extending to more complex situations requires little effort and is

quite obvious. Each QD i ($i \in \{1,2\}$) has a ground state $|0\rangle_i$ and excited state as $|1\rangle_i$, so that their uncoupled Hamiltonian may be written in terms of Pauli operators, utilising the same nomenclature as we would with spins, $\sigma_{z,i} = |1\rangle_i\langle 1| - |0\rangle_i\langle 0|$. The charge fluctuators are also two level systems, but they are classical, so they cannot have coherences. While a quantum two level system is represented as a two by two density matrix, a classical object has no coherences, so the off-diagonal matrix elements are unnecessary. A two-vector of classical populations (η_j) then describes the state of fluctuator j, with the first element giving the population in the ground (no-charge) state, and the second that in the excited (charged) state. We proceed by using the usual tensor product formulation of quantum mechanics for multi-partite systems, our overall description of our qubit-fluctuator state must then be a rectangular matrix. This corresponding to 2^N stacked square matrices, one for each of the classical states of N fluctuators. In the time between charge fluctuation events, each of the square density operators in the rectangular matrix act independently of the others and so each can be treated individually. For the case of two qubits and a single charge, which is described by a four by eight matrix, can be treated as two four by four matrices, each corresponding to one of the states of the charge.

With this in mind we define the uncoupled Hamiltonian of qubits and fluctuators as

$$H_{q+c} = \frac{1}{2}\omega_1\sigma_{z,1} + \frac{1}{2}\omega_2\sigma_{z,2} + \frac{1}{2}\xi_1\eta_1, \tag{5.1}$$

where we use

$$\begin{aligned} \sigma_{z,1} &= \begin{pmatrix} 1 \\ 1 \end{pmatrix} \otimes \mathbb{1}_2 \otimes \sigma_z, \\ \sigma_{z,2} &= \begin{pmatrix} 1 \\ 1 \end{pmatrix} \otimes \sigma_z \otimes \mathbb{1}_2, \\ \eta_1 &= \begin{pmatrix} 1 \\ -1 \end{pmatrix} \otimes \mathbb{1}_2 \otimes \mathbb{1}_2. \end{aligned} \tag{5.2}$$

The energy required to excite uncoupled QD i from ground to excited state is given by ω_i. The energy difference between the charge being at the trap site and the charge being elsewhere, which we assume to be at an infinite distance away is given by ξ. Each operator is now of rectangular matrix of dimension 4×8. As stated, coherent evolutions of the top and bottom square matrices of this object are treated individually and act on the top and bottom square matrices of the corresponding density operator respectively, following the usual rules of quantum mechanics. The

operator eigenstates corresponding to the different charge configurations can be found for each square component matrix. A charge flip would mean switching around these stacked matrices as we shall see in section 5.3.

5.2.2 Stark effect

A source that emits light does so at some characteristic frequency or frequencies, which is dependent on the particulars of its electronic configuration. Via the Coulomb interaction, this configuration may be perturbed by an electric field and in doing so, the frequency or frequencies of the emitted light is altered. This is known as the Stark effect and the change in frequencies is known as the Stark shift. In the context of this thesis, the stark shift of our quantum dots is achieved by the presence of a nearby charge. The degree to which this effect affects the system under study may be determined by perturbation theory. The interaction between the perturbing field and our system is described by,

$$V = -\mu F, \tag{5.3}$$

where F is the field due to the presence of the charge and μ is the dipole operator projected along the field direction. The perturbation is usually calculated to second order giving the equation

$$E = E_0 - \mu F + \alpha F^2, \tag{5.4}$$

where E_0 is the unperturbed energy gap, the term μ refers to the permanent dipole moment and α is the polarisability of the dots.

The position or distance of the charge in relation to the exciton determines the strength of the perturbing field and the sign of the charge determines the sign of the field. The field is one that is traditionally associated with a point charge. Modelled as a point charge, the field will decrease with an inverse quadratic dependence as the distance between the charge and dipole is increased. The values that the permanent dipole and polarisability take are variable and highly dependent on the shape and composition of the dot. For InGaAs, the polarisability $\frac{\alpha}{e}$ is between -10 and -300 nm^2/V, where e is the electronic charge. The permanent dipole $\frac{\mu}{e}$ can take both positive and negative values from -2.5 to 0.91 nm[74, 75]. Using values of 0.8 nm for the permanent dipole and -34 nm^2/V for the polarisability given in ref [75] and our default choice of charge interaction strength $\delta_{11} = \delta_{12} = 1$ GHz, we can calculate the distance the charge would need to be. Solving $h\delta + \mu F - \alpha F^2 = 0$ for F, where h is Plank's constant, we get two solutions -2.35×10^7 and -3.23×10^4 V/m. The field strength is given by $-e/4\pi\epsilon_r\epsilon_0 r^2$, where the relative permitivity for InGaAs

is between 13 and 14. Using 13 for the permitivity, we would need a charge at a distance of 2.171 nm or 58.545 nm. As the charge is brought closer to the qubits it detunes the qubits either towards or away from the laser frequency depending on the initial size and direction of detuning. For example, an interaction strength of 10 GHz, the distance the charge would have to be is 2.185 nm or 18.397 nm away. The stark shift, to second order, is made of two terms: the second of which deals with the polarisability of the dipole and is quadratic in nature. The value of the polarisability is so small in comparison to the permanent dipole that while the field is small the stark shift is dominated by the permanent dipole or linear term. At large fields, when the distance between the qubit and the charge falls below 2.1696×10^{-9}m, the quadratic term becomes greater in magnitude than the linear.

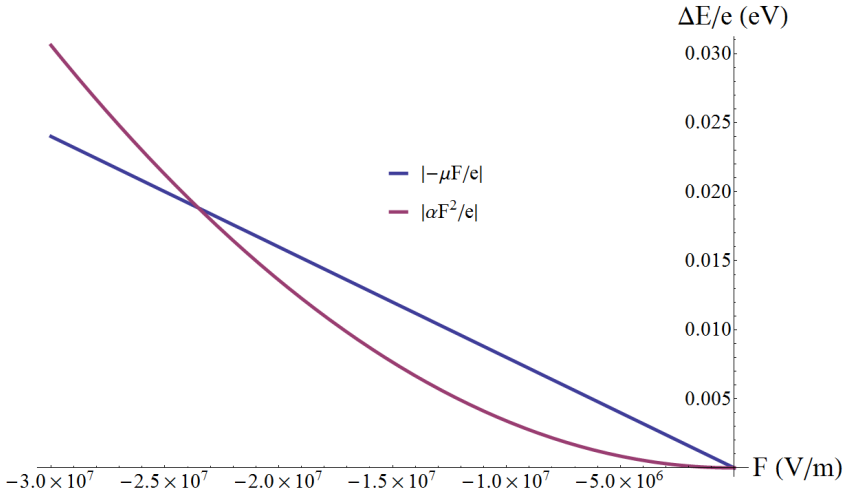

Figure 5.4: Magnitude of the permanent dipole and polarisability terms in the quantum confined stark shift equation.

In addition, the stark shift is given as the dot product of the dipole moment so a charge perpendicular to the dipole would have no effect on it. The polarisability is generally a tensor, but in the simplest case it is isotropic and so it is simply multiplied by the square of the field. This brings us onto the topic of geometries for the experimental set up. There are many possible geometries to choose from, but the one where the system is most simplified is if we have our two qubit dipoles separated from each other in the z-direction, with a charge in between them, also in the z-direction. This means that the $\cos\theta$ part of the dot products will always be equal to 1 and the theoretical treatment of different stark shifts can be presented by having the position of the charge trap be closer to one qubit than the other.

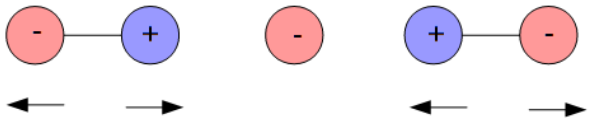

Figure 5.5: Dipoles in the z-direction with a charge in-between them

Of course we can have other geometries, such as the dipoles pointing in the z-direction whilst separated in the x-direction, which allows us the place the traps to be moved in both directions, but the calculation of the shifts become slightly more complicated as the vectorial nature of the system must be re-introduced.

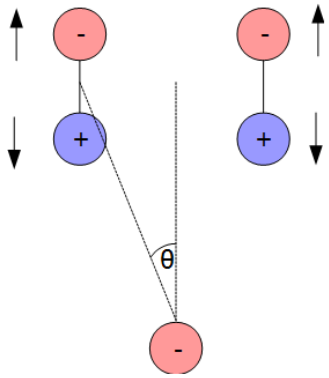

Figure 5.6: Dipoles in the x-direction with a charge in-between them

5.2.3 Interaction Hamiltonian

The qubit-bath interaction Hamiltonian, the bath being made of photons, is defined as:

$$H_{q,B} = \sum_{\mathbf{k}} \zeta_{1,\mathbf{k}}(a^{\dagger}_{\mathbf{k}}\sigma_{-,1} + a_{\mathbf{k}}\sigma_{+,1}) + \zeta_{2,\mathbf{k}}(a^{\dagger}_{\mathbf{k}}\sigma_{-,2} + a_{\mathbf{k}}\sigma_{+,2}), \tag{5.5}$$

where

$$\begin{aligned}
\sigma_{+,1} &= \begin{pmatrix} 1 & \\ & 1 \end{pmatrix} \otimes \mathbb{1}_2 \otimes \sigma_+, \\
\sigma_{+,2} &= \begin{pmatrix} 1 & \\ & 1 \end{pmatrix} \otimes \sigma_+ \otimes \mathbb{1}_2, \\
\sigma_{-,1} &= \begin{pmatrix} 1 & \\ & 1 \end{pmatrix} \otimes \mathbb{1}_2 \otimes \sigma_-, \\
\sigma_{-,2} &= \begin{pmatrix} 1 & \\ & 1 \end{pmatrix} \otimes \sigma_+ \otimes \mathbb{1}_2.
\end{aligned} \tag{5.6}$$

The interaction here describes the couplings between the QDs and the photonic bath, with coupling strengths $\zeta_{1,\mathbf{k}}$ or $\zeta_{2,\mathbf{k}}$, where $a_{\mathbf{k}}$ and $a^\dagger_{\mathbf{k}}$ are the annihilation and creation operators for the photon bath mode with wave vector $\mathbf{k}$. The QD raising and lowering operators in the interaction Hamiltonian are denoted by the σ_+ and σ_- Pauli matrices, which are constructed as $|1\rangle\langle 0|$ and $|0\rangle\langle 1|$ respectively. The effect of this part of the interaction with the system is taken into account by deriving a Born-Markov optical master equation.

We also account for a coupling between the qubits and the (classical) lasers. The qubit-laser Hamiltonian is

$$H_{q,l} = \Omega_1 \sigma_{x,1} \cos(\omega_{l1} t) + \Omega_2 \sigma_{x,2} \cos(\omega_{l2} t), \tag{5.7}$$

where Ω_i is the Rabi frequency of the ith QD and ω_{li} is the laser frequency of laser i which is assumed to drive only the ith QD with which it is closely resonant. Similarly to previous definitions:

$$\begin{aligned}
\sigma_{x,1} &= \begin{pmatrix} 1 & \\ & 1 \end{pmatrix} \otimes \mathbb{1}_2 \otimes \sigma_x, \\
\sigma_{x,2} &= \begin{pmatrix} 1 & \\ & 1 \end{pmatrix} \otimes \sigma_x \otimes \mathbb{1}_2.
\end{aligned} \tag{5.8}$$

The final interaction is between the qubits and charge:

$$H_{q,c} = \frac{\delta_{11}}{2} \mu_{11} + \frac{\delta_{12}}{2} \mu_{12}, \tag{5.9}$$

where

$$\begin{aligned} \mu_{11} &= \begin{pmatrix} 1 \\ 0 \end{pmatrix} \otimes \mathbb{1}_2 \otimes \sigma_z, \\ \mu_{12} &= \begin{pmatrix} 1 \\ 0 \end{pmatrix} \otimes \sigma_z \otimes \mathbb{1}_2. \end{aligned} \tag{5.10}$$

There are two terms, which show the interaction of the charge (labelled with the initial index 1, since we are considering only a single charge) with both of the QDs. In general the interaction is δ_{ji}, where the subscript denotes an interaction of charge j with QD i. The term describes a process in which the stationary charge at some well defined distance introduces a Coulomb potential that gives rise to a Stark shift of the excitonic states, thus creating a TLS with a larger energy spacing.

The qubit-laser Hamiltonian is still currently time dependent, but we can remove this by moving into a rotating frame and performing the rotating wave approximation (RWA). Some confusion may arise here, because we have already discussed the rotating wave approximation in section 2.3.1. In both cases we neglect the quickly oscillating terms. This is done by applying a unitary transformation to all parts of the Hamiltonian that involve the dots and the charges, i.e., all parts except $H_{q,B}$. From the time dependent Schrödinger equation, we get:

$$\begin{aligned} -i\hbar\partial_t(U^{-1} \mid \psi\rangle) &= -i\hbar(\partial_t U^{-1}) \mid \psi\rangle + U^{-1}H \mid \psi\rangle \\ &= HU^{-1} \mid \psi\rangle \end{aligned}$$

Therefore, the effective Hamiltonian becomes, after moving to the rotating frame

$$H_{\mathrm{rf}} = UHU^{-1} + U(i\hbar\partial_t U^{-1}). \tag{5.11}$$

The operator U^{-1} is

$$\begin{pmatrix} e^{\frac{1}{2}it(\omega_{l1}+\omega_{l2})} & 0 & 0 & 0 \\ 0 & e^{\frac{1}{2}it(\omega_{l2}-\omega_{l1})} & 0 & 0 \\ 0 & 0 & e^{\frac{1}{2}it(\omega_{l1}-\omega_{l2})} & 0 \\ 0 & 0 & 0 & e^{\frac{1}{2}it(-\omega_{l1}-\omega_{l2})} \end{pmatrix}. \tag{5.12}$$

It is worth noting that this is a 4×4 matrix. As stated previously, we can consider the two charge states as independent and as such, the 4×8 rectangular matrix can be thought of as two 4×4 matrices. This unitary transformation operates on each

of those two parts individually. After performing the rotating wave approximation, which removes rapidly oscillating terms, i.e. those with twice the frequency of ω_{l1} and ω_{l2}, and letting $\omega_i - \omega_{li} = \nu_i$, we get:

$$\begin{aligned} H'_S = \frac{1}{2}\left(\nu_1\sigma_{z,1} + \nu_2\sigma_{z,2} + \Omega_1\sigma_{x,1} + \Omega_2\sigma_{x,2}\right) \\ + \frac{1}{2}\left(\delta_{11}\mu_{12} + \delta_{12}\mu_{22} + \xi_1\eta_1\right). \end{aligned} \tag{5.13}$$

This is now our final system Hamiltonian, however we still need to define an operator in which a single charge fluctuates from occupied to unoccupied or *vice versa*, an operation executed by the operator σ_{xc}. In our rectangular density operator notation for a single charge this simply corresponds to swapping over the upper and lower square matrices. For more complex situations of more charge fluctuators, a similar reordering of the now multiple square matrices achieves the desired effect. The full and general Hamiltonian for a multiple qubit, multiple charge system using by same construction is given by

$$\begin{aligned} H &= \sum_i \frac{\omega_i}{2}\sigma_{z,i} + \sum_k \theta_{\mathbf{k}} a^\dagger_{\mathbf{k}} a_{\mathbf{k}} + \sum_j \frac{\xi_j}{2}\eta_j \\ &+ \sum_{\mathbf{k},i} \zeta_{i,\mathbf{k}}(a^\dagger_{\mathbf{k}}\sigma_{-,i} + a_{\mathbf{k}}\sigma_{+,i}) \\ &+ \sum_i \Omega_i \sigma_{x,i}\cos(\omega_{li}t) \\ &+ \sum_{i,j} \frac{\delta_{ji}}{2}\mu_{z,i}. \end{aligned} \tag{5.14}$$

5.3 Transfer Matrices

IN ORDER to proceed we treat the bath of photons as weakly coupled to the QDs and express the dynamics of the QDs - fluctuators system in terms of a density matrix, leading to the quantum optical master equation, [9]

$$\begin{aligned} \frac{d}{dt}\rho(t) &= -i[H_I, \rho(t)] \\ &+ \sum_i \gamma_i\left(N_i + 1\right)\Gamma\left[\sigma_{-,i}, \rho(t)\right] \\ &+ \sum_i \gamma_i N_i \Gamma\left[\sigma_{+,i}, \rho(t)\right] \end{aligned} \tag{5.15}$$

where H_I includes all but the Jaynes-Cummings and photon energy terms in Eq. 5.14, following a transformation into a frame rotating with the two laser frequencies and a rotating wave approximation:

$$\begin{aligned} H_I &= \sum_i \frac{\nu_i}{2}\sigma_{z,i} + \sum_j \frac{\xi_j}{2}\eta_j \\ &\quad + \sum_i \frac{\Omega_i}{2}\sigma_{x,i} + \sum_{i,j} \frac{\delta_{ji}}{2}\mu_{ji}, \end{aligned} \tag{5.16}$$

where $\nu_i \equiv \omega_i - \omega_{li}$ are the laser detunings. The dissipaters are given by

$$\Gamma\big[\hat{L}, \rho(t)\big] = \left(\hat{L}\rho(t)\hat{L}^\dagger - \frac{1}{2}\hat{L}^\dagger\hat{L}\rho(t) - \frac{1}{2}\rho(t)\hat{L}^\dagger\hat{L}\right). \tag{5.17}$$

The parameters in Eq. 5.15 are γ_i, which is the optical decay rate for the QD i and N_i, which is the Bose-Einstein occupation number of the photon bath taken at the transition frequencies of QD i.

Our calculation proceeds using a transfer matrix approach. This is performed by first writing Eq. 5.15 in the form

$$\dot{\rho}(t) = M\rho(t), \tag{5.18}$$

where M is the super-operator acting on the density operator ρ. Since we are solving the system numerically and for small time steps, we can write

$$\rho(t + \Delta t) = (1 + M\Delta t)\rho(t). \tag{5.19}$$

This tells us that the transfer matrix for a system that does not fluctuate, but has a constant charge bias, can be defined as $1 + M\Delta t$.

We can now introduce the fluctuating nature of the charge by using a Pauli-x operator, σ_{xc} (where the 'c' indicates that it operates on a charge) to flip the charge between its two states. Due to the fact that our two charge configurations are independent and therefore stacked into a rectangular matrix, when a charge fluctuates, we simply swap the density operators into a new order, reflecting the changed charge configuration. This takes the form of a σ_x, since

$$\sigma_x \begin{pmatrix} A \\ B \end{pmatrix} = \begin{pmatrix} B \\ A \end{pmatrix}, \tag{5.20}$$

where A and B refer to the square matrices pertaining to the different charge configurations. If the charges traps were quantum objects then we would require $(4n)\times(4n)$ elements to represent it - so we save a factor of n in the state description by doing this.

We then divide the time steps into two parts: we assume that there is a probability $P\Delta t$ within the time Δt that there is a change in the fluctuator's state, and a probability that there will be no change $1 - P\Delta t$. [5] In this paper, we will restrict the model to having the same rates for hopping onto and away from the trap sites correspondence to a temperature higher than the energy gap of the fluctuators. If Δt is small then higher order terms can be neglected and we find that the $(1+M\Delta t)$ term in Eq. 5.19 is modified to:

$$(1 - P\Delta t)(1 + M\Delta t) + P\Delta t\sigma_{xc} \approx 1 + (M - P + P\sigma_{xc})\Delta t. \tag{5.21}$$

Eq. 5.21 defines the transfer matrix for fluctuating charges and with this we can calculate the dynamics of the system.

5.4 Resonance Fluorescence and Photon Statistics

Let us turn our attention to photon statistics. To begin, we consider a simple system that does not have any charge fluctuations and attempt to derive the equations for the intensity correlation function $g^{(2)}(t, t+\tau)$, the intensity autocorrelation function.

$$g^{(2)}(t, t+\tau) \equiv \frac{\langle E^-(t)E^-(t+\tau)E^+(t+\tau)E^+(t)\rangle}{\langle E^-(t)E^+(t)\rangle\langle E^-(t, t+\tau)E^+(t, t+\tau)\rangle}, \tag{5.22}$$

As the definition suggests [15], this requires us to calculate the expectation of four photon operators or the semi-classical field operators in our case. We have dealt extensively with Master Equations, which focuses on the dynamics of the qubit rather than the photon field. However, the two are linked via the raising and lowering operator for the qubit such that a photon creation operator requires a qubit lowering operator to conserve energy. This is part of what is known as input-output theory.

Dealing with quantised fields, these field operators can be cast as the photonic

creation and annihilation operators

$$g^{(2)}(t, t+\tau) = \frac{\langle a^\dagger(t)a^\dagger(t+\tau)a(t+\tau)a(t)\rangle}{\langle a^\dagger(t)a(t)\rangle\langle a^\dagger(t+\tau)a(t+\tau)\rangle}. \tag{5.23}$$

In the case that $g^{(2)}(\tau) = 1$, the signal is random in time. The detection of an initial photon does not impact at all the detection of a second after a time (τ).

In the case that $g^{(2)}(\tau) > 1$, the signal is bunched. This means that there is a greater than random probability that if a photon is detected then a second is also likely in the time interval τ.

Lastly, in the case that $g^{(2)}(\tau) < 1$, the signal is anti-bunched. This means that if an initial photon is detected, there is a reduced probability that there will be a second will be detected after a time τ. The emission of a photon suppresses further emission. Of the three cases, this is the easiest to comprehend. In the example of a single emitter, let it be a TLS, there can only be a single excitation. If an emission event occurs, the system needs time to be re-excited and so, for small τ the system will display anti-bunching. All three cases of bunching, anti-bunching and neither bunching nor anti-bunching can be seen in Fig 5.7. After an initial detection, the system shows a negative correlation ($g^{(2)}(\tau) < 1$). The coherent driving of the lasers bring the correlation up to a maximum showing a positive correlation ($g^{(2)}(\tau) > 1$), which then steadily drops to no-correlation ($g^{(2)}(\tau) = 1$)

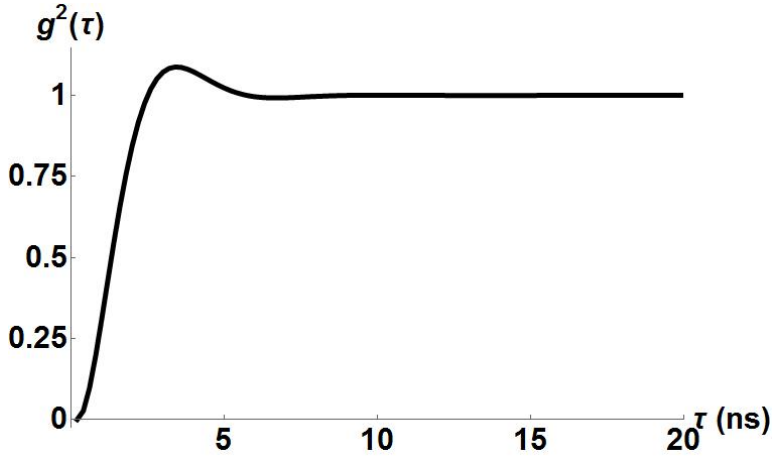

Figure 5.7: $g^{(2)}(\tau)$ showing an initially negatively correlated signal, which then becomes positive, before

5.4.1 Input-Output Theory

The external field operators are related to the system operators. The way that they are is described by input-output theory. The system operators and the photon operators interact via the Hamiltonian part,

$$H_I = \int_{-\infty}^{\infty} d\omega \;\; g(\omega)\left(a(\omega)\sigma_+ - a^\dagger(\omega)\sigma_-\right). \tag{5.24}$$

The following is mainly from Walls and Milburn's Quantum Optics [11], though I have restructured the steps somewhat to increase the ease of reading. The Heisenberg equation of motion for the field operator is given by,

$$\dot{a}(\omega) = -i\omega \; a(\omega) + g(\omega)\sigma_-. \tag{5.25}$$

For which the formal solution for the input time $t_0 < t$ and output time $t_1 > t$ are given by,

$$a(\omega) = e^{-i\omega(t-t_0)}a_0(\omega) + g(\omega)\int_{t_0}^{t} dt' e^{-i\omega(t-t')}\sigma_-(t') \tag{5.26}$$

and

$$a(\omega) = e^{-i\omega(t-t_1)}a_1(\omega) - g(\omega)\int_{t}^{t_1} dt' e^{-i\omega(t-t')}\sigma_-(t'). \tag{5.27}$$

The differential equation for the system operator follows as,

$$\frac{d}{dt}\sigma_- = -\frac{i}{\hbar}[H_S, \sigma_-] - \int_{-\infty}^{\infty} d\omega \;\; g(\omega)a(\omega). \tag{5.28}$$

For which we can then substitute our calculated expression for the field equation,

$$\frac{d}{dt}\sigma_- = -\frac{i}{\hbar}[H_S, \sigma_-] - \int_{-\infty}^{\infty} d\omega \;\; g(\omega)e^{-i\omega(t-t_0)}a_0(\omega) - \int_{-\infty}^{\infty} d\omega \;\; g^2(\omega)\int_{t_0}^{t} dt' e^{-i\omega(t-t')}\sigma_-(t')). \tag{5.29}$$

Now we can define an input field that has the same standard commutation relations as photonic creation and annihilation operators:

$$a_{in} = -\frac{1}{2\pi}\int_{-\infty}^{\infty} d\omega \;\; e^{-i\omega(t-t_0)}a_0(\omega). \tag{5.30}$$

Using the relation

$$\int_{-\infty}^{\infty} d\omega \;\; e^{-i\omega(t-t_0)} = 2\pi\delta(t-t'), \tag{5.31}$$

putting it into Eq. 5.29 and reversing the order of the integral in the last part of the equation

$$\int_{t_0}^{t} dt' \sigma_-(t') \int_{-\infty}^{\infty} d\omega \;\; g^2(\omega) e^{-i\omega(t-t')}, \tag{5.32}$$

where we now assume that $g(\omega)$ is independent of frequency over a large range of frequencies and define $g^2(\omega) = \frac{\gamma}{2\pi}$.

$$\gamma \int_{t_0}^{t} dt' \sigma_-(t') \delta(t-t') = \frac{\gamma}{2} \sigma_-(t). \tag{5.33}$$

Thus we can now write the whole equation for the system operator as

$$\frac{d}{dt}\sigma_- = -\frac{i}{\hbar}[H_S, \sigma_-] - \frac{\gamma}{2}\sigma_-(t) + \sqrt{\gamma} a_{in}(t). \tag{5.34}$$

We can do the same treatment for the output time case, defining an output operator in the same way as we did for the input,

$$\frac{d}{dt}\sigma_- = -\frac{i}{\hbar}[H_S, \sigma_-] + \frac{\gamma}{2}\sigma_-(t) - \sqrt{\gamma} a_{out}(t). \tag{5.35}$$

By equating Eqs. 5.34 and 5.35. It can be seen easily that a relation between the input and output fields involves only the system operator and the decay rate of the qubit,

$$a_{in} + a_{out} = \sqrt{\gamma}\sigma_-(t). \tag{5.36}$$

If the field is in the vacuum state and we have normal ordered correlations, the input field may be ignored. In this case the output field operator is equal to the system field operator multiplied by the square root of the decay rate.

Before proceeding, it may be wise to try to understand what $g^{(2)}(t, t+\tau)$ means physically. We see that there are four operators corresponding to the external field,

$$g^{(2)}(t, t+\tau) = \frac{\langle \sigma_+(t)\sigma_+(t+\tau)\sigma_-(t+\tau)\sigma_-(t)\rangle}{\langle \sigma_+(t)\sigma_-(t)\rangle \langle \sigma_+(t+\tau)\sigma_-(t+\tau)\rangle}. \tag{5.37}$$

Due to the cyclicity of the trace, we may rearrange the numerator to read

$$\mathrm{Tr}[\sigma_+(t+\tau)\sigma_-(t+\tau)\sigma_-(t)\rho\sigma_+(t)]. \tag{5.38}$$

We have seen before (Eq. 3.2) that $\sigma_-(t)\rho\sigma_+(t)$ is a jump operator. This tells us that a photon has been detected at time t. The same procedure can be done for the second set of operators, which tells about photons emitted at time $(t+\tau)$. Since

they are both used to calculate the expectation, Eq. 5.23 tells us information about the probability of measuring two photons separated by time (τ).

5.5 Calculating Intensity Correlations ($g^{(2)}(t, t+\tau)$)

From the dynamical equations of the system density matrix, we may obtain predictions of the statistics of emitted photon correlations. To this end we calculate the two-photon intensity correlation function

$$g^{(2)}(t, t+\tau) = \frac{\langle a_1^\dagger(t) a_2^\dagger(t+\tau) a_2(t+\tau) a_1(t)\rangle}{\langle a_1^\dagger(t) a_1(t)\rangle \langle a_2^\dagger(t+\tau) a_2(t+\tau)\rangle}. \tag{5.39}$$

The operators a_i and $a_i^\dagger$ refer to the photon field detected by a detector $i \in 1, 2$ (see Fig. 5.1). Each detector is responsive only to a range of frequencies around the resonant frequency of each QD, and for QDs that are sufficiently detuned from one another we expect that photons which activate detector i originate from QD i only. The QDs in a typical experimental set up would be quite closely spaced and so a Hanbury Brown-Twiss set up could be used [76] .

The cross-correlation in Eq. 5.39 is in terms of photon creation and annihilation operators, but we can relate these field operators to our system operators through input-output theory [11]. In general an output field is a sum of contributions from an input field and from the decay of the systems (QDs in our case) that decay optically: $a_{out}(t) = a_{in}(t) + \sqrt{\gamma_1}\sigma_{-,1}(t) + \sqrt{\gamma_2}\sigma_{-,2}(t)$. We presume a typical setup in which a_{in} is in the vacuum state, and so the output field is then the sum of two well frequency-resolved fields, which will be separately detected. We can then associate each detector field with a particular system operator:

$$a_i(t) = \sqrt{\gamma_i}\sigma_{-,i}(t). \tag{5.40}$$

This leads to an expression for $g^{(2)}$ which depends only on the QD system operators: [15]

$$g^{(2)}(t, t+\tau) = \frac{\langle \sigma_{+,1}(t)\sigma_{+,2}(t+\tau)\sigma_{-,2}(t+\tau)\sigma_{-,1}(t)\rangle}{\langle \sigma_{+,1}(t)\sigma_{-,1}(t)\rangle \langle \sigma_{+,2}(t+\tau)\sigma_{-,2}(t+\tau)\rangle}. \tag{5.41}$$

A general way of finding the two time correlation function from the master equation is to exploit the quantum regression theorem. [77]

5.5.1 Hanbury-Brown Twiss

While this chapter is theoretical in nature, is always a good idea to think about how such theory may be verified by experiment. Traditionally, we look to the Hanbury-Brown Twiss experiment, which is an extremely useful tool in collecting data about correlated photon sources. However, it does not measure $g^{(2)}(\tau)$, but rather a related quantity known as the waiting time. It is very difficult to time-resolve single photons so it becomes infeasible to perform an experiment where we note down all the times of detection. If this were possible, then $g^{(2)}(\tau)$ could be calculated directly from the measurements. Unlike $g^{(2)}(\tau)$, which measures the correlation between two photons separated by time τ, the waiting time measures the correlation between two consecutive photons, i.e., with no other photons in between. The related functions are both measures of correlation and are indeed proportional for times much smaller than the mean waiting time [78]. The $g^{(2)}(\tau)$ correlation function may be extracted from waiting time data and so this experiment may provide experimental verification of the results shown in this chapter.

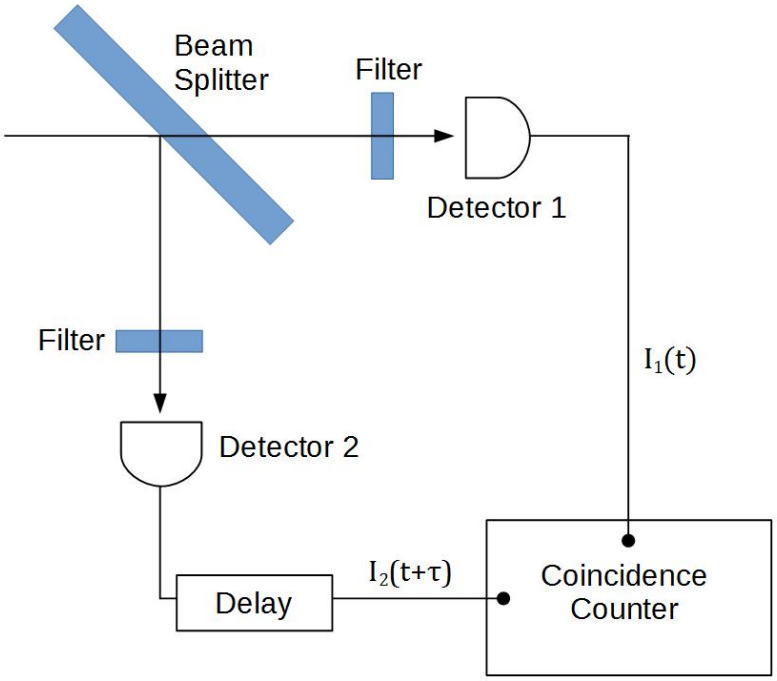

Figure 5.8: Hanbury-Brown Twiss experimental set up

In this experiment, the photons from the QDs are passed through a beam split-

ter so that there are two paths that each lead to a detector, before which filters and polarisers can be placed depending on what exactly the experiment requires. The detection of a photon in the first detector begins a timer, which is then stopped by a detection of a photon in the second detector [10]. The results are collected into a histogram to display the number of events as a function of time between detection events.

5.6 Calculating $g^2(\tau)$ Method I

We have discussed the for of the g^2 correlation function, but as of yet, we have not said how it can be solved. The correlation function has expectations are that are comprised of many operators, which can deal with using the quantum regression theorem. Let us set up a toy system to explain its use; a coherently driven single dot. The interaction Hamiltonian reads as

$$H = \frac{1}{2}\begin{pmatrix} 0 & -\Omega \\ -\Omega & 0 \end{pmatrix}. \tag{5.42}$$

Using the standard dissipator for the optical master equation (Eq. 2.56), we may obtain a closed set of operators,

$$\langle \dot{\sigma}_- \rangle = -\left(\frac{i\Omega}{2}\right)\langle \sigma_z \rangle - \left(\frac{\gamma}{2}\right)\langle \sigma_- \rangle, \tag{5.43}$$

$$\langle \dot{\sigma}_+ \rangle = \left(\frac{i\Omega}{2}\right)\langle \sigma_z \rangle - \left(\frac{\gamma}{2}\right)\langle \sigma_+ \rangle, \tag{5.44}$$

and

$$\langle \dot{\sigma}_z \rangle = i\Omega\langle \sigma_+ \rangle - i\Omega\langle \sigma_- \rangle - \gamma(\langle \sigma_z \rangle + 1). \tag{5.45}$$

We now have calculated the expectation for the operators, but we eventually want the expectation for four operators and different times. To do this, we require the use of the quantum regression theorem. This allows us to rewrite our closed set of equations in a reformulated form as [9],

$$\begin{pmatrix} \langle \dot{\sigma}_- \rangle \\ \langle \dot{\sigma}_+ \rangle \\ \langle \dot{\sigma}_z \rangle \end{pmatrix} = \begin{pmatrix} -\frac{\gamma}{2} & 0 & -\frac{i\Omega}{2} \\ 0 & \frac{\gamma}{2} & \frac{i\Omega}{2} \\ -i\Omega & i\Omega & -\gamma \end{pmatrix} \begin{pmatrix} \langle \sigma_- \rangle \\ \langle \sigma_+ \rangle \\ \langle \sigma_z \rangle \end{pmatrix} - \begin{pmatrix} 0 \\ 0 \\ \gamma \end{pmatrix}. \tag{5.46}$$

The specifics of the system don't really matter and all we wanted was to show that a closed set of equations would be in the form show in Eq. 5.46, which we shall

use later. Looking at the expression for the correlation function, we see that we can take the product of the raising and lowering operators and re-write them as $\sigma_+\sigma_- = \frac{1}{2}(\sigma_z + 1)$. This means that we can split the correlation function into two parts [15],

$$\begin{aligned} G^{(2)}(t, t+\tau) &= f(r)^2 \langle \sigma_+(t)\sigma_+(t+\tau)\sigma_-(t+\tau)\sigma_-(t)\rangle \\ &= f(r)^2 \langle \sigma_+(t) \left(\frac{1}{2}(\sigma_z(t+\tau)+1)\right) \sigma_-(t)\rangle. \\ &= f(r)^2 \frac{1}{2} \left[\langle \sigma_+(t)\sigma_-(t)\rangle + \langle \sigma_+(t)\sigma_z(t+\tau)\sigma_-(t)\rangle\right] \end{aligned} \tag{5.47}$$

In the long time limit ($t \to \infty$),

$$G^{(2)}_{ss}(\tau) = f(r)^2 \frac{1}{2} \left[\langle \sigma_+\sigma_-\rangle_{ss} + \langle \sigma_+(0)\sigma_z(\tau)\sigma_-(0)\rangle_{ss}\right]. \tag{5.48}$$

Let us then solve the two parts of this equation. The first part is trivial to solve,

$$\sigma_+\sigma_- = |1\rangle\langle 0|0\rangle\langle 1| = |1\rangle\langle 1| \therefore \langle \sigma_+\sigma_-\rangle_{ss} = \rho^{ss}_{11}. \tag{5.49}$$

We can then use the quantum regression theorem and Eq. 5.46 to calculate the second part of this.

5.6.1 Quantum regression

This theorem states that if one has a complete set of operators, such that the differential equations of the expectations may be described by a sum of those operators with corresponding pre-factors, then the expectation of two operators may be described using those same prefactors [15].

$$\langle \dot{s}\rangle_i = \sum_j M_{ij}\langle s\rangle_j \tag{5.50}$$

$$\frac{d}{d\tau}\langle A(t)s_i(t+\tau)\rangle = \sum_j M_{ij}\langle A(t)s_j(t+\tau)\rangle \tag{5.51}$$

In the following $s(t)$ represents a column vector comprised of full set of operators that completely defines a system, for example all the elements of the density matrix $\sum_{i,j} \mid i\rangle\langle j \mid$ or the set of operator that we found in Eq. 5.46. We may rewrite the equation as

$$\langle \dot{s}(\tau)\rangle = M\langle s(\tau)\rangle + b, \tag{5.52}$$

where s is a vector of σ_+,σ_- and σ_z, M is the co-efficient matrix and b is the vector on the end of Eq. 5.46. We can also write the equation

$$\frac{d}{d\tau}\left(\langle s(\tau)\rangle + M^{-1}b\right) = M\left(\langle s(\tau)\rangle + M^{-1}b\right), \tag{5.53}$$

to which the formal solution is

$$\langle s(\tau)\rangle = e^{M\tau}\left(\langle s(0)\rangle + M^{-1}b\right) - M^{-1}b, \tag{5.54}$$

Using s in place of the σ_z in Eq. 5.48 we obtain for the second term

$$\frac{d}{d\tau}\langle\sigma_+(0)s(\tau)\sigma_-(0)\rangle_{ss} = M\langle\sigma_+(0)s(\tau)\sigma_-(0)\rangle_{ss} + b\langle\sigma_+\sigma_-\rangle_{ss}. \tag{5.55}$$

The formal solution to the integral of this is

$$\langle\sigma_+(0)s(\tau)\sigma_-(0)\rangle_{ss} = e^{M\tau}\left(\langle\sigma_+s\sigma_-\rangle_{ss} + M^{-1}b\langle\sigma_+\sigma_-\rangle_{ss}\right) - M^{-1}b\langle\sigma_+\sigma_-\rangle_{ss}. \tag{5.56}$$

If we then put in some initial conditions into our vector s, i.e. $\sigma_+(0)$, $\sigma_-(0)$, $\sigma_z(0)$. We then have

$$\langle\sigma_+(0)\begin{pmatrix}\sigma_-(0)\\ \sigma_+(0)\\ \sigma_z(0)\end{pmatrix}\sigma_-(0)\rangle_{ss} = \begin{pmatrix}0\\ 0\\ -\langle\sigma_+(0)\sigma_-(0)\rangle_{ss}\end{pmatrix}, \tag{5.57}$$

since $\langle\sigma_+(0)\sigma_z(0)\sigma_-(0)\rangle = |1\rangle\langle 0|\left(|1\rangle\langle 1| - |0\rangle\langle 0|\right)|0\rangle\langle 1| = -|1\rangle\langle 1| = -\langle\sigma_+(0)\sigma_-(0)\rangle$. There is then a common factor of $\langle\sigma_+(0)\sigma_-(0)\rangle_{ss}$ in Eq. 5.56, which can be factored out.

$$\langle\sigma_+\sigma_-\rangle_{ss}\left(e^{M\tau}\left(-\hat{z} + M^{-1}b\right) - M^{-1}b\right), \tag{5.58}$$

where $\hat{z} = (0, 0, 1)$. If we initialise the system in the ground state, then $\langle\sigma_z(0)\rangle = -1$, so we can write

$$\langle\sigma_+\sigma_-\rangle_{ss}\left(e^{M\tau}\left(\langle s(0)\rangle + M^{-1}b\right) - M^{-1}b\right). \tag{5.59}$$

Looking at the form of Eq. 5.56 we see that the term in the bracket of the Eq. 5.58 is the formal solution to the integral of $\frac{d}{d\tau}\langle s(\tau)\rangle_{ss}$ Therefore, we can rewrite Eq. 5.48 as

$$G^{(2)}_{ss}(\tau) = f(r)^2\frac{1}{2}\langle\sigma_+\sigma_-\rangle_{ss}\left[1 + \langle s(\tau)\rangle\right]. \tag{5.60}$$

On substituting in σ_z as the specific case of $s(\tau)$, we find that the correlation function is the product of the steady state value of the excited state and the probability of

the excited state at time τ,

$$G^{(2)}_{ss}(\tau) = f(r)^2 \left[(\rho^{ss}_{11})\rho_{11}(\tau),\right]. \tag{5.61}$$

5.6.2 Calculating $g^2(\tau)$ Method II

We can user a simpler method if we assume that experimental measurements take place when the system has reached a steady state (ss) with density operator ρ_{ss}. In this case $g^{(2)}$ is only dependent on the delay time τ:

$$\begin{aligned} g^{(2)}(\tau) &= \frac{\langle\sigma_{+,1}(0)\sigma_{+,2}(\tau)\sigma_{-,2}(\tau)\sigma_{-,1}(0)\rangle_{ss}}{\langle\sigma_{+,1}\sigma_{-,1}\rangle_{ss}\langle\sigma_{+,2}\sigma_{-,2}\rangle_{ss}} \\ &= \frac{\mathrm{Tr}[\sigma_{+,1}(0)\sigma_{+,2}(\tau)\sigma_{-,2}(\tau)\sigma_{-,1}(0)\rho_{ss}]}{\langle\sigma_{+,1}\sigma_{-,1}\rangle_{ss}\langle\sigma_{+,2}\sigma_{-,2}\rangle_{ss}}. \end{aligned} \tag{5.62}$$

Owing to the cyclicity of the trace we can project the steady state density matrix into the ground state:

$$g^{(2)}(\tau) = \frac{\mathrm{Tr}[\sigma_{+,2}(\tau)\sigma_{-,2}(\tau)({}_1\langle 1|\rho_{ss}|1\rangle_1)|0\rangle_{11}\langle 0|]}{\langle\sigma_{+,1}\sigma_{-,1}\rangle_{ss}\langle\sigma_{+,2}\sigma_{-,2}\rangle_{ss}}, \tag{5.63}$$

where $|1\rangle_1$ and $|0\rangle_1$ represent the two basis state vectors for QD 1. We may now define a new density operator ρ_P, which is properly normalised and represents the steady state projected from the excited state of QD 1 to its ground state:

$$\rho_P = \frac{{}_1\langle 1|\rho_{ss}|1\rangle_1|0\rangle_{11}\langle 0|}{\langle\sigma_{+,1}\sigma_{-,1}\rangle_{ss}} = \frac{{}_1\langle 1|\rho_{ss}|1\rangle_1|0\rangle_{11}\langle 0|}{\mathrm{Tr}[{}_1\langle 1|\rho_{ss}|1\rangle_1|0\rangle_{11}\langle 0|]} \tag{5.64}$$

and write

$$g^{(2)}(\tau) = \frac{\mathrm{Tr}[\sigma_{+,2}(\tau)\sigma_{-,2}(\tau)\rho_P]}{\langle\sigma_{+,2}\sigma_{-,2}\rangle_{ss}} = \frac{\mathrm{Tr}[\sigma_{-,2}\rho_P(\tau)\sigma_{+,2}]}{\langle\sigma_{+,2}\sigma_{-,2}\rangle_{ss}}. \tag{5.65}$$

After a long enough period, $\rho_P(\tau)$ becomes ρ_{ss} and so $\lim_{\tau\to\infty}[g^{(2)}(\tau)] = 1$ as expected.

5.7 Results

In this section we present the $g^{(2)}(\tau)$ results across a variety of parameters and for a single fluctuator or two fluctuators.

5.7.1 One charge fluctuator

Let us begin with the case of a single fluctuator. To reiterate our aim, we seek to assess what kinds of photon cross correlation signatures may be obtained for different charge fluctuation rates and interaction strengths. There is a single charge fluctuator that affects each of the two qubits in the same way - i.e. $\delta_{11} = \delta_{12}$ in Eq. 5.14. We use QD parameters typical of InGaAs structures: Fixed throughout the paper will be the spontaneous decay rates ($\gamma_1 = \gamma_2 = 1$ GHz), and the Rabi frequencies ($\Omega_1 = \Omega_2 = 1$ GHz). Other parameters are varied for particular sets of results but their default values will be: Laser detuning $\nu_1 = \nu_2 = 0$, charge fluctuation rate is $P = 1$ MHz. Using values of 0.8 nm for the permanent dipole and -34 nm^2/V for the polarisability, [75] for our default choice of charge interaction strength $\delta_{11} = \delta_{12} = 1$ GHz, we would need a charge at a distance of 1.32 μm. As the charge is brought closer to the qubits it detunes the qubits either towards or away from the laser frequency depending on the initial size and direction of detuning.

In Fig 5.9, we show $g^{(2)}(\tau)$ as a function of $\delta_{11} = \delta_{12}$ between 0 and 10 GHz. This corresponds to effective detunings of between 0 and 6 μeV, which encompasses the photoluminescence range from resonance to effectively zero photon emission for InGaAs type QDs. [79] We can see that the greater the charge-qubit interaction, the greater the initial cross-correlation of the detected photons. This initial correlation then decays back to the no-correlation value of $g^{(2)} = 1$. For all values of the interaction strength this decay is on the 1 μs scale, which corresponds to the charge fluctuation rate. The explanation for this is straightforward: for a larger interaction, then either QD is only likely to emit when the charge trap is empty. If one QD emits, then since the noise is correlated, the other is likely to also emit – at least for over a timescale less than the charge fluctuation time. On the other hand, for a smaller interaction – less than the Rabi frequency Ω – then it is also possible for a QD to be excited when the charge trap is occupied: an so we expect no cross correlations for $\delta_{1i} \ll \Omega_i$.

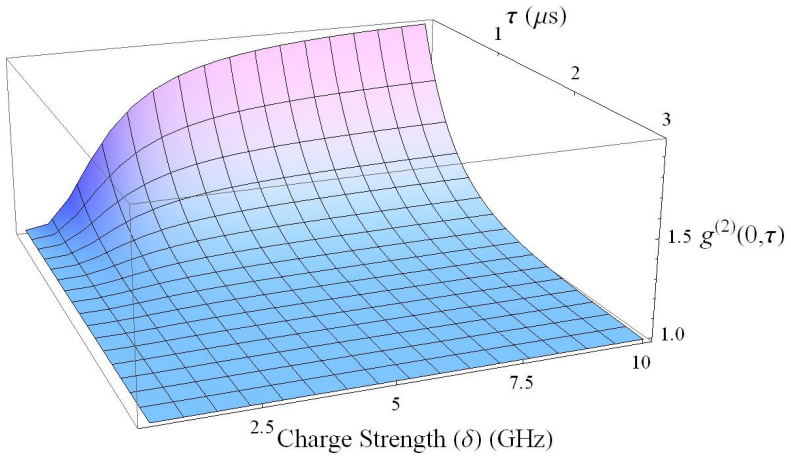

Figure 5.9: $g^{(2)}(\tau)$ cross-correlation for two qubits interacting with a single charge, where the charge-qubit interaction strength (δ_{ij}) is being varied. γ_i, the spontaneous decay rate of the qubits, is set to 1 GHz and determines the timescale of the return to uncorrelated photons.

We next keep the charge-qubit interaction constant, and in Fig. 5.10 look at how a changing fluctuation rate affects $g^{(2)}(\tau)$. When the fluctuation rate is smaller than the photon emission rate, we simply find that $g^{(2)}(\tau)$ decays on a timescale similar to that of the charge fluctuation rate. At the fastest fluctuation rates studied, however, there is a decrease in the initial value $g^{(2)}(0)$; this happens when the charge fluctuation rate exceeds the photon emission rate. In this regime, the experiment is no longer sensitive to the charge fluctuator.

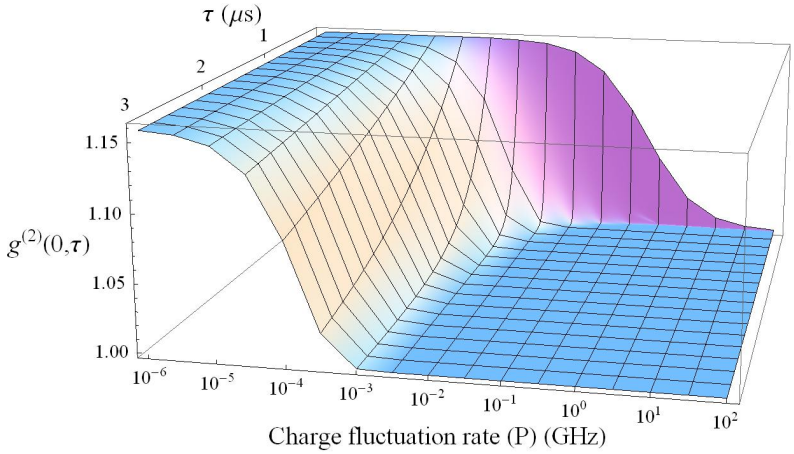

Figure 5.10: $g^{(2)}(\tau)$ cross-correlation for two qubits interacting with a single charge, where the fluctuation rate (P) of the charge is being varied. The values of P are given relative to γ_i (the spontaneous decay rate of the qubits).

Since the effect of a charge fluctuator is to shift the resonance frequency of the qubits away from that of the lasers, we can use laser detuning as a further probe of the fluctuator correlation dynamics. In Fig. 5.11 we illustrate a typical photoluminescence spectrum of two QDs. We know that if the two lasers are resonant with the two QDs then we expect to see correlated emitted photons as shown in Fig. 5.9. Imagine instead allowing both the lasers to be detuned from the QD resonance (see Fig. 5.11), by the same amount and in the same direction. Depending on the direction of the detuning, the effect of the charge will be to bring the QDs back into resonance or take them further from resonance. In this way, the emitted photons, regardless of the direction of detuning, will display a positive cross correlation.

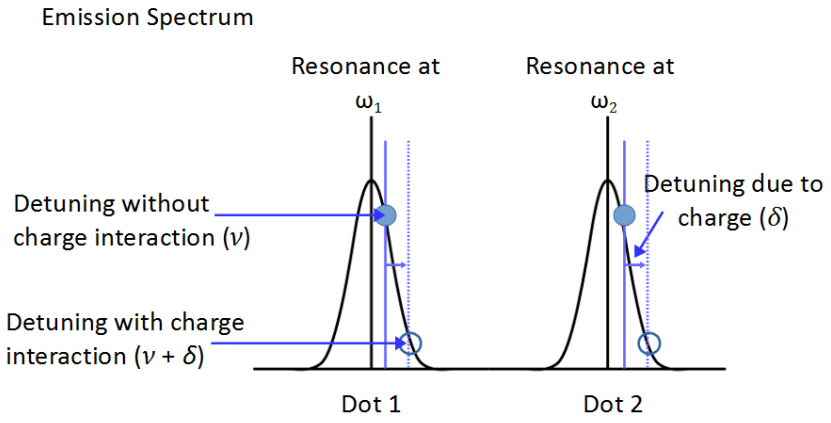

Figure 5.11: Schematic drawing of the shifting detuning caused by charge interactions when the lasers are detuned in the same direction.

On the other hand if the lasers are detuned in opposite directions, i.e. if one is blue shifted and the other red shifted with respect to the QD resonant frequencies, then charging the trap will shift one QD towards resonance and the other further away from it. This situation is shown in Fig 5.12. In this way the QD closer to resonance is more likely to emit a photon, while the other is less likely. We then expect a negative correlation between the emitted photons, for a large enough initial detuning.

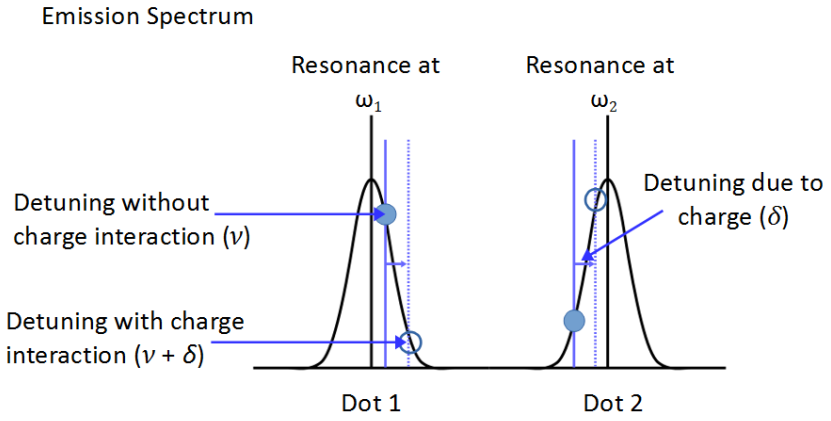

Figure 5.12: Schematic drawing of the shifting detuning caused by charge interactions when the lasers are detuned in opposite directions.

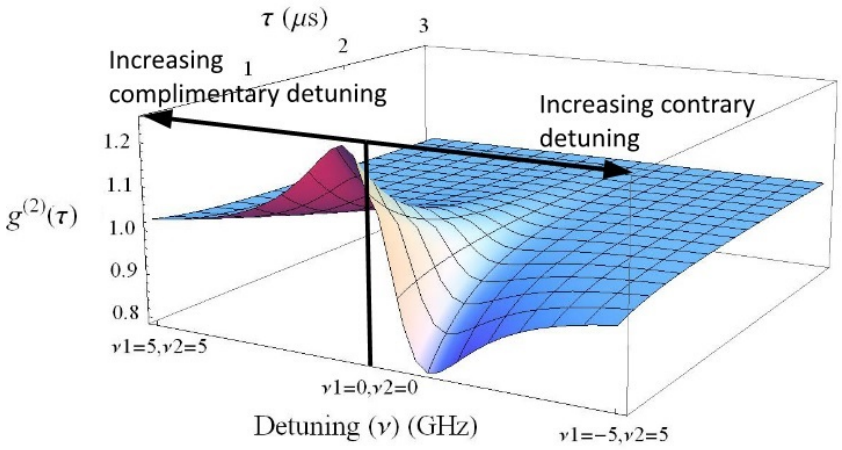

Figure 5.13: $g^{(2)}(\tau)$ cross-correlation for two qubits interacting with a single charge, where the laser detuning (ν_i) is being varied. On the left of the zero detuning line, detuning increases and is equal in magnitude and sign for both dots; on the right it increases with equal magnitude but opposite signs.

In Fig 5.13 we show the cross-correlation for both the detuning scenarios just described. As expected, we see positive correlation for same sense detuned, and negative for opposite sense – expect around $\nu = 0$, when the charge fluctuation moves both QDs away from resonance and we recover a positive cross-correlation.

5.7.2 More than one charge

Let us now introduce a second charge fluctuator into the model, and establish whether it is possible to distinguish multiple from single fluctuators by using cross

correlation measurements.

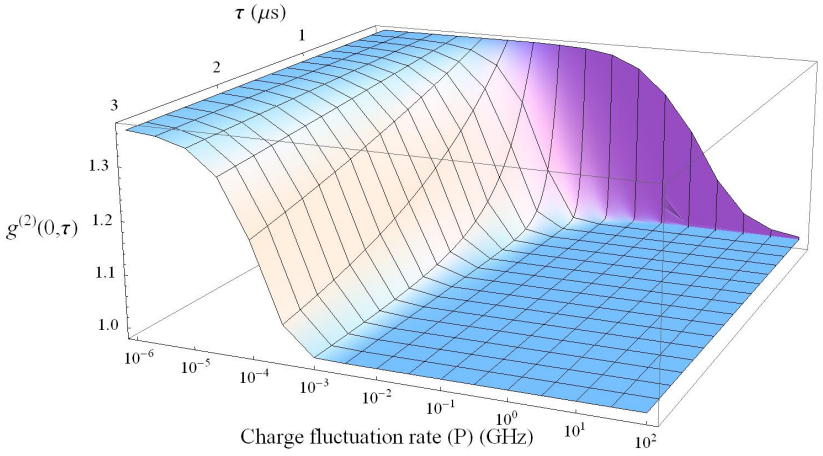

Figure 5.14: $g^{(2)}(\tau)$ cross-correlation for two qubits interacting with two charges, where the fluctuation rate (P_i) of the charges are being varied. The values of P are set equal to each other.

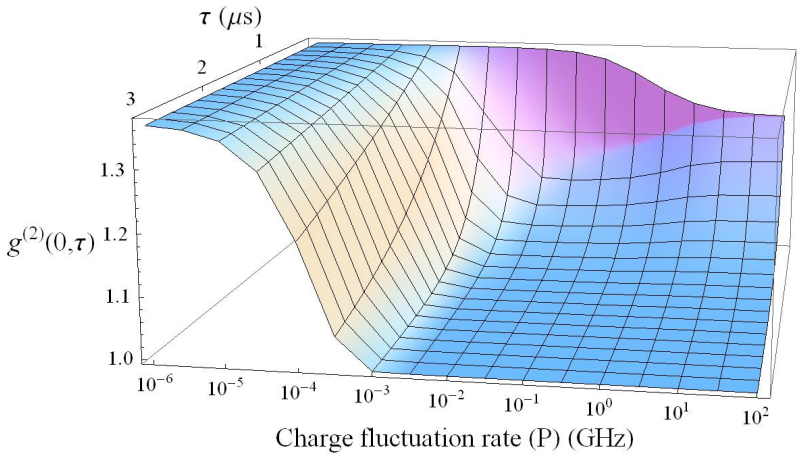

Figure 5.15: $g^{(2)}(\tau)$ cross-correlation for two qubits interacting with two charges, where the fluctuation rate (P_i) of one charge is being varied and the other held at 10^{-3} GHz.

Fig. 5.14 shows $g^{(2)}(\tau)$ as a function of (equal) fluctuation rates for the two charges. We can see immediately that $g^{(2)}(0)$ is larger in this case than for the single fluctuator case shown in Fig. 5.10. This is expected since the two fluctuators working together increase the total possible detuning of each QD; as we have seen in Fig. 5.9 this results in a higher initial cross-correlation. As the fluctuation rate increases, the decay of $g^{(2)}(\tau)$ happens at shorter times, similar to the single charge case.

It is unlikely, however, that the two charge traps will be fluctuating at exactly the same rate, so let us now look into how different rates of fluctuation affect the cross-correlation. In Fig. 5.15, we show the impact on $g^{(2)}(\tau)$ of altering one fluctuation rate while keeping the other fixed at 10^{-3} GHz. Comparing this figure with that for a single fluctuator shown in Fig. 5.10, we find that in certain cases it is possible to see a clear qualitative difference between the results for a single and two fluctuators. This is easier to discern by taking cuts through the plots for particular fluctuation rates, and using a log scale for the time; for the single and two fluctuator cases these are shown in Fig. 5.16(a) and Fig. 5.16(b). If the rates for the two fluctuators are significantly different then two plateaux can be seen in the curves, with two decay rates corresponding to two different fluctuation rates; this effect washes out once the faster fluctuation rate approaches that of the QD optical decay rate.

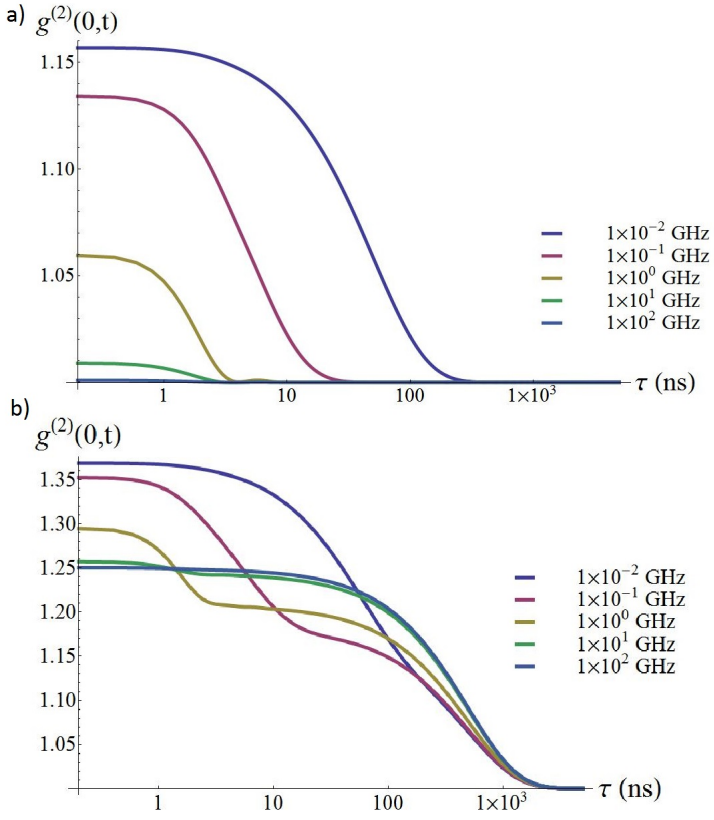

Figure 5.16: Log time plots for some representative frequencies of the data shown in Fig. 5.10 shown in a) and Fig. 5.15 shown in b).

As would be expected, when the fluctuation rates of the charges are very similar, no deviation from the single fluctuation curves can be distinguished: They do

not exhibit the plateaued structure that can be seen in Fig 5.16 b).

Finally, we look at varying the laser detunings for two qubits and two charges. In Fig 5.17 we show the cross correlation function for the same detuning parameters as in Fig. 5.13, in the case where the two fluctuation rates are not equal (1 GHz and 1 MHz). We also display various cuts through this 3D plot, for different values of the detuning, in Fig. 5.18. There is a clear contrast here with the surface shown in Fig. 5.13; the cuts in Fig. 5.18 show that the plateaued structure characteristic of two different rates survives as detuning is varied. At negative detuning the a negative correlation is observed, but with a clear long time plateau.

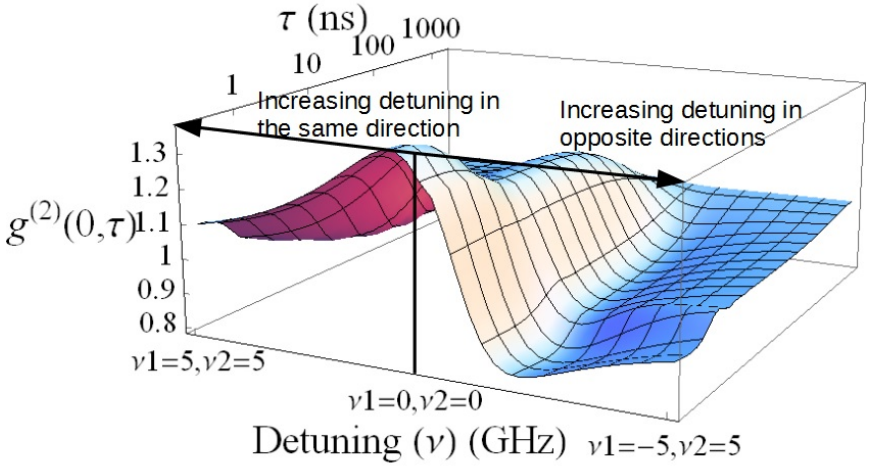

Figure 5.17: $g^{(2)}(\tau)$ cross-correlation for two qubits interacting with two charges, where the laser detuning (ν_i) is being varied. The two charges fluctuate with different rates of 1 MHz and 1 GHz.

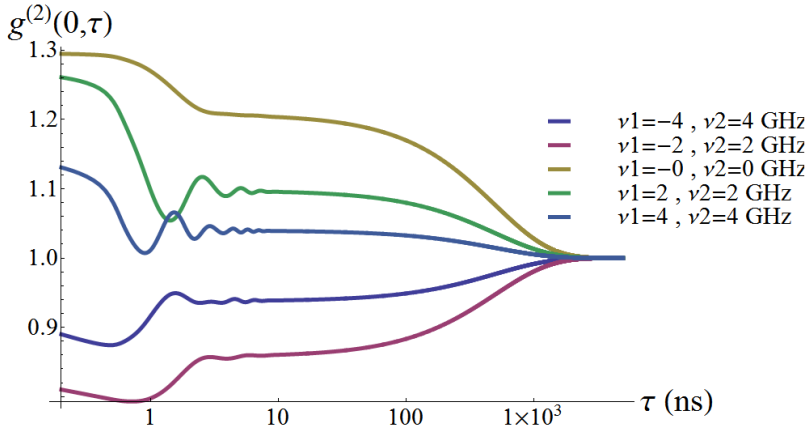

Figure 5.18: Cuts through Fig. 5.17, for five values of the detuning parameters.

The oscillatory behaviour here is a consequence of detuning. The magnitude of the oscillations is affected by various parameters, one of which, is the fluctuation rate of the charges. This behaviour is not seen in the single charge case, since the fluctuation rate is 1 MHz, which is small in comparison to the other parameters which are of the order of 1 GHz. We see in Fig. 5.19 and 5.20 that changing the charge fluctuation rate to 1 GHz allows the oscillations to be visible when the laser detunings are zero.

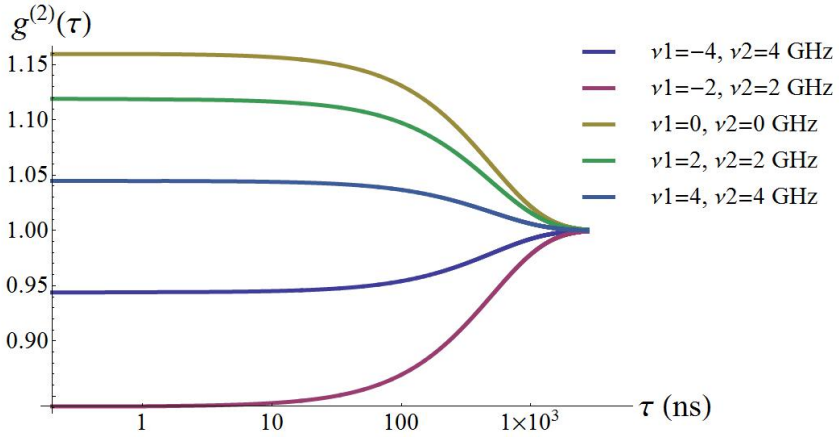

Figure 5.19: Cuts through Fig. 5.13, for five values of the detuning parameters. The charge fluctuation rate is 1MHz

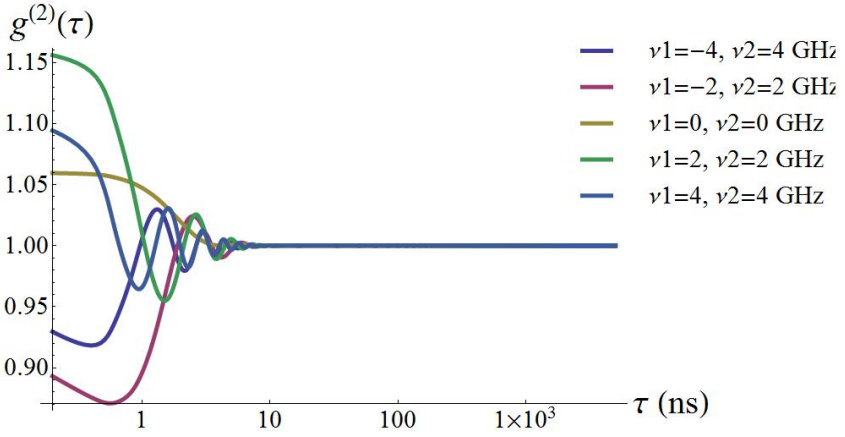

Figure 5.20: Five values of the detuning parameters with a a single charge at a fluctuation rate of 1 GHz.

The fluctuation rate of 1 GHz is the frequency at which these oscillations are most apparent as can be seen in Fig. 5.21 after which they diminish as does the $g^{(2)}(\tau)$ correlation, which we expect from Fig. 5.10. The charge fluctuation rate is not the only parameter to affect the magnitude of these oscillations. We have already seen in Fig. 5.20 that sweeping from complimentary to opposite detuning of the two lasers changes the frequency of the oscillations. We also see in Fig. 5.22 that making the decay rates of the qubits smaller means the oscillations continue for a longer time. As expected, the charge interaction strength also affects the the oscillations.

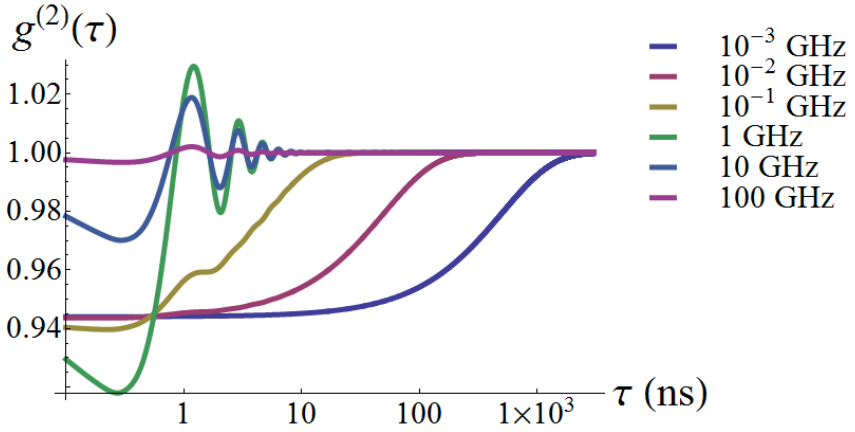

Figure 5.21: $g^{(2)}(\tau)$ cross-correlation for two qubits interacting with a single charges, where the laser detunings (ν_i) are in opposite directions at 4 GHz. The charge fluctuation rate (P) is swept from 1 MHz 100 GHz and both charge interaction strengths are set to 1 GHz.

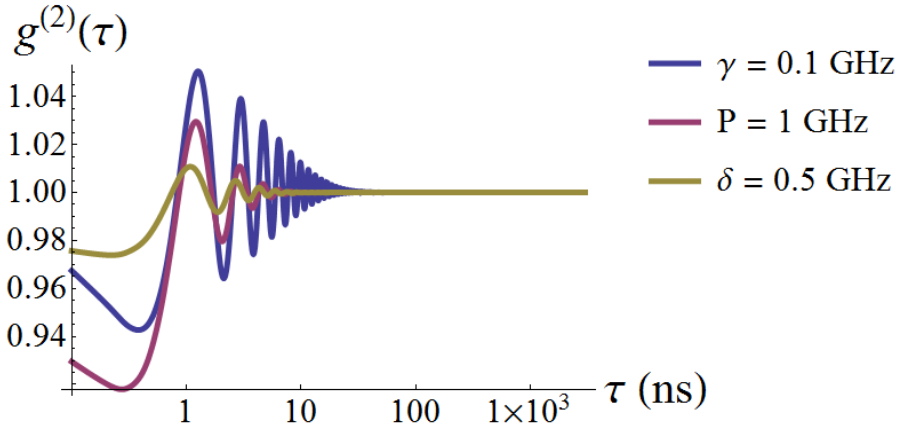

Figure 5.22: $g^{(2)}(\tau)$ cross-correlation for two qubits interacting with a single charges, where the laser detunings (ν_i) are in opposite directions at 4 GHz. Various parameters are altered from their standard values: ($\gamma_i = \delta_i = 1$ GHz, $P = 1$ MHz).

The main contributor to these oscillations is the detuning of the lasers. We saw in Figs. 5.18 and 5.20 that at zero laser detuning, there are little if any oscillations, which we see again in Fig. 5.23 while sweeping through the fluctuation rate.

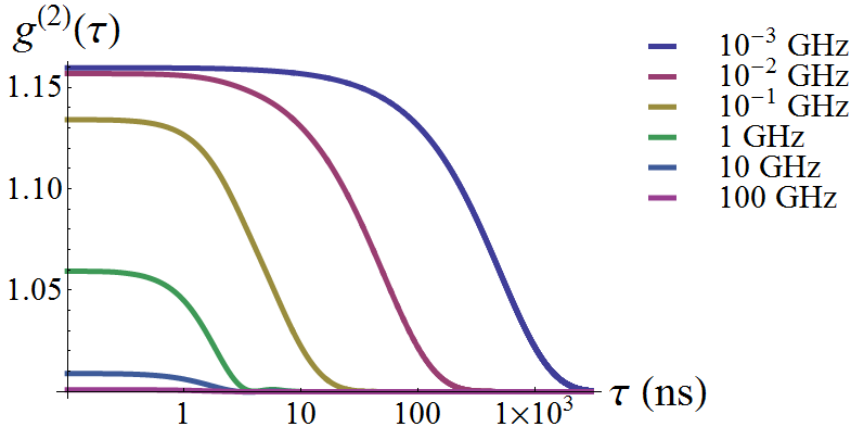

Figure 5.23: $g^{(2)}(\tau)$ cross-correlation for two qubits interacting with a single charges, where there are no laser detunings (ν_i). The charge fluctuation rate (P) is swept from 1 MHz to 100 GHz and both charge interaction strengths are set to 1 GHz.

5.8 Summary

In this first research chapter, we dealt with a system of two quantum dots interacting with one or two fluctuating charges. The aim of the research was to find signatures of common and correlated noise generated by fluctuating charges in the vicinity two quantum dots. This correlated noise should be able to be detected by

optically driving the dots and subsequently analysing the emitted photons. In this endeavour, we believe that we have succeeded in describing how a measurement can be used to determine information regarding the level of commonality of the interaction of a charge, which fluctuates between a charge trap and a site far away, with a two quantum dot system through the $g^{(2)}(\tau)$ correlation function.

We have demonstrated, with regards to a system consisting of one or two charge traps, that one may determine the frequency of fluctuation from the time dependence of the correlation function. In the case of two or possibly more charges, under the condition that the frequencies are quite different, one may also determine the number of charge traps as well as their individual fluctuation frequencies.

The work done in this research chapter has been theoretical, however, the nature of the simulations performed allow for the work to tested experimentally. We have performed a simulation that swept the detunings of the lasers, which drove the quantum dots and determined the correlation. This is an important simulation since the detunings of the driving lasers may are experimentally variable unlike the charge interaction strength, which is dependent on the locations of the charge traps. As such it is the only parameter that is accessible to the experimentalist. As a signature, we saw in Figs. 5.13 and 5.17 that as the detunings are swept in a complimentary way, the correlation is positive and when the detunings are swept in a contrary way, the correlation becomes negative. This change in sign is a very distinct signature that we believe should be easily verifiable. Indeed, the experiment itself is relatively simple and would not require on extremely fast detectors. The signatures are simple to spot and the experimental samples do not require any treatment other than to be optically driven, which should not cause undue difficulty. We believe that this will allow collective effects of noisy environments to be explored and would push quantum dots as useful probes of such systems.

Looking to the future or at least the next step in the continuation of the research done in this chapter, we must consider larger numbers of charges. Extrapolating from the work already done, if similar simulations are carried out, then the initial correlation displayed on $g^{(2)}(\tau)$ graphs will increase proportionally to the number charges, as we saw in Fig. 5.14. This is to be expected since the larger the number of charge traps and therefore charges interacting with the qubits equates to a larger charge interaction strength as we saw in Fig. 5.9. As alluded to at the start of this chapter, the increase in the number of charges should also be visible in a similar

way to Fig. 5.15, where the correlation is shown to display two plateaux, one for each fluctuation frequency, though this will only really be visible if the frequencies are quite distinct from one another.

In the next chapter we will consider a different type of noise, which has a $1/f$ spectral density. While the mechanism or indeed mechanisms giving rise to this type of noise are debated, it has been considered that it may be the result of many charge fluctuators. We will discuss this in further detail in the next chapter.

CHAPTER 6

Probing *1/f* Correlations Using Quantum Dots

6.1 Introduction

THIS CHAPTER is about $1/f$ noise and how it might be detected in an experimental measurement. As a phenomenon, $1/f$ noise is seen in large numbers of systems in different regimes. Examples of the wide range of systems exhibiting this type of noise include neuron dynamics, computer network and vehicular traffic and even in music and speech [80–83]. Although there is such a wealth of systems that display $1/f$ noise, a consensus concerning the mechanism or mechanisms generating it has not been reached. This type of noise is aptly called $1/f$, because the power spectral density is proportional to the reciprocal of the frequency that the noise displays.

The $1/f$ distribution can be approximated by summing Lorentzian functions, however, while this is mathematically true, it does not have any physical meaning in and of itself. One of the first models to be motivated by physical systems is the McWhorter model and is applied to charge fluctuations in semiconductors [73]. The model consists of having a large number of charge traps that would need to be located at various distances to a semiconductor-oxide layer interface. The electrons located at these traps are able to jump from them to the bulk of the semiconductor and back again. Under the assumption that the jump process is quantum tunnelling, the rates at which the electrons will jump decreases exponentially with increasing distance. The Fourier transform of this gives the Lorentzian function, which can then be summed. As a direct consequence, $1/f$ noise may only occur when the traps are located at a range of distances. Another aspect of $1/f$ noise is that it does not have a marked temperature dependence and since only electrons with energies similar to the Fermi level will fluctuate appreciably, this must mean that the traps

have a range of energies so that the number of traps able to capture charges remains roughly constant at different temperatures.

Dutta and Horn created a model along similar lines, a two site system between which charges fluctuate as shown in Figure 6.1. [73, 84] However, they argued that the traps may have a flat distribution of energies, if the transition rates between the states are allowed to vary as a function of temperature.

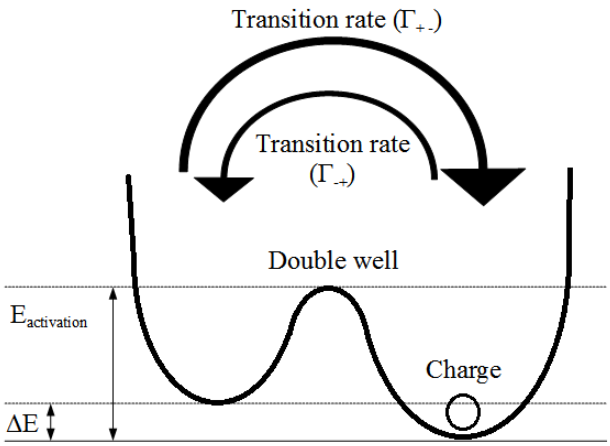

Figure 6.1: Double well with different energies and transition rates describing the Dutta-Horn model.

Another similar model in semiconductors is random telegraph noise (rtn). [73, 85] Once again, this system relies on bistable fluctuators, however, unlike the Dutta-Horn model it does not display a temperature dependent transition rate. As the name of the process suggests, the fluctuation between states occurs randomly in time. In order to generate $1/f$ noise there must be a series of rtn processes superposed. A model that combines rtn traps in this way is mathematically similar to the McWhorter model, though doesn't provide a physical explanation. Here, the concept of tunnelling between traps at distinct distances giving rise to different fluctuation rates that we saw in the McWhorter model has been replaced by simply stating that each of the fluctuators has a noise amplitude that flips between two distinct states.

In addition to theoretical work done on $1/f$ noise, there has also been a wealth of experiments performed. Intermittent emission of photons from quantum dots show a $1/f$ spectral density [86]. A model put forward to explain such a phenomenon has

been that QDs undergo Auger ionisation, ejecting an electron from the QD to the surrounding medium [87]. In the process, the dot becomes positively charged. Any further electron-hole pairs that are formed undergo non-radiative Auger relaxation, leaving the QD dark until the QD is neutralised [86, 88, 89]. This model does not reproduce the experimental results by itself, but several independent modifications have been made to it. One modification includes McWhoter-like charge traps [90] and others developed models with a fluctuating barrier height between the dot and the bulk trap site [88], both of which replicate the $1/f$ aspect of the intermittent emission that Pelton *et al.* measured. It has also been shown that fluctuations in resistance in metallic films [91, 92] and layers [93] have a $1/f$ dependence. In such systems a film is grown on a substrate with a various lattice spacings and it was found that the fluctuations can be orders of magnitude greater than in metals or semiconductors [92].

6.2 Divergence of the spectral density

While it may be the case that the microscopic model or indeed models of $1/f$ noise have not been entirely agreed upon, it is a phenomenon that undermines our ability to maintain coherence in qubits. It is made more curious by having a spectral density whose integral diverges, that is to say

$$\int_0^\infty \frac{df}{f} = \ln[\infty] - \ln[0], \tag{6.1}$$

which is not convergent. This in contradiction of Parseval's theorem, which states that if the integral of the square of the signal amplitude is finite then integral of the spectral density should also be finite [94]. Let us consider a signal amplitude $I(t)$, which is measured in a time interval $(0, t)$. The Fourier transform over this time interval is

$$\tilde{I}(\omega) = \int_0^t I(t')e^{-i\omega t'}dt'. \tag{6.2}$$

We define the spectral density as

$$S(\omega) = \frac{\tilde{I}(\omega)\tilde{I}^*(\omega)}{t}. \tag{6.3}$$

The integral over all frequencies is given by

$$\int_{-\infty}^{\infty} S(\omega)d\omega = \frac{1}{t}\int_{-\infty}^{\infty} d\omega \int_0^t dt_1 I(t_1)e^{-i\omega t_1}\int_0^t dt_2 I(t_2)e^{i\omega t_2} = \frac{2\pi}{t}\int_0^t I^2(t_1)dt_1, \tag{6.4}$$

using the identity $\int_{-\infty}^{\infty} e^{-i\omega(t_1-t_2)} = 2\pi\delta(t_2 - t_1)$. No matter the form of $I(t)$, the function $I^2(t)$ must necessarily be less than I^2_{max}, which is independent of time, so the integral on the right hand side of Eq. 6.4 can be evaluated to give

$$\int_{-\infty}^{\infty} S(\omega)d\omega \leq 2\pi I^2_{max} \tag{6.5}$$

We see that this statement is independent of the time interval and so the integral over the spectral density must always be finite, meaning that Eq. 6.5 and Eq. 6.1 are directly contradictory.

6.2.1 Resolving the paradox

While generally considered to be an outstanding problem, there have been many attempted explanations. The simplest way to rid ourselves of this paradox is to say that the $1/f$ dependence of the spectral density breaks down at low frequencies and that there is a low frequency cut-off at some characteristic frequency. However, many experiments that have assumed this intrinsic low frequency cut-off displayed by the system have, after lengthy experiments, shown that this is at least not necessarily true [95]. It has been suggested that since $1/f$ noise is a phenomenological process that the low frequency limit is actually set by the length of the experiment and therefore the spectral density is always integrable [94].

This leads us to pose a set of questions:

(i) What are the experimental signatures of $1/f$ noise?
(ii) Can the effects of $1/f$ noise be determined or distinguished when other noise sources are present?
(iii) How can $1/f$ noise be experimentally observed if there is a low cut-off frequency?
(iv) Can the cut-off frequency be determined?

6.3 Model

THE SYSTEM we will study consists of a single quantum dot (QD), which is modelled as a two level system, interacting with a laser, at the resonant frequency of the QD. The environment here consists of two types of noise, namely $1/f$ noise and individual charges fluctuating between charge sites located in the vicinity of the QD and far away sites. The individual fluctuating charges will be of the same type as we saw in chapter5 and will show random telegraph noise. We shall consider the charges to be classical in nature and therefore they may not have coherences. We

shall also have the condition that the far away sites for the individual charges are effectively at infinite distance from the dot and therefore cease their interaction. A generalised Hamiltonian for the system in question is described as

$$\begin{aligned} H &= \frac{\omega}{2}\sigma_z + \sum_j \frac{\epsilon_j}{2}\xi_j \\ &\quad + \sum_{\mathbf{k}} \zeta_{\mathbf{k}}(a^\dagger_{\mathbf{k}}\sigma_- + a_{\mathbf{k}}\sigma_+) \\ &\quad + \Omega\sigma_{x,}\cos(\omega_l t) \\ &\quad + \sum_j \frac{\delta_j}{2}\mu_j \\ &\quad + \frac{1}{2}\eta(t)\sigma_z. \end{aligned} \tag{6.6}$$

All expect the last term in the Hamiltonian is described in section 5.2 in great detail. To avoid repetition, we point the reader to that section should they wish to re-familiarise with the operator definitions. Even so a short description of the Hamiltonian will follow. In Eq. 6.6, the first term describes the energy levels ω of the QD and σ_z is the z-Pauli spin operator. The second term represents the energy levels ϵ_j of the classical charges and the ξ_j describe the classical states which the charges can take. As a classical variable we limit its values to 0 or 1. In other words, the charge at the trap site has an energy of ϵ and a far away charge has an energy of 0. The third term describes the interaction of the QD TLS with a photonic bath with wave vectors $\mathbf{k}$. This interaction is represented by creation and annihilation operators $a^\dagger_{\mathbf{k}}$ and $a_{\mathbf{k}}$, with a strength $\zeta_{\mathbf{k}}$. The fourth term represents the interaction of the QD and the laser, where ω_{li} is the laser frequency and Ω_i is the coupling to QD. The fifth term is the interaction δ_j between the jth charge and the QD, it equals 1 when the trap is occupied and zero otherwise. The last term represents the time-dependent interaction that leads to $1/f$ noise, where $\eta(t)$ represents the classical, random Gaussian noise. Eq. 6.6 shows a generalised system of dots and charges with $1/f$ noise. We shall, in this investigation, restrict ourselves to a single dot and charge. This situation is shown in Figure 6.2.

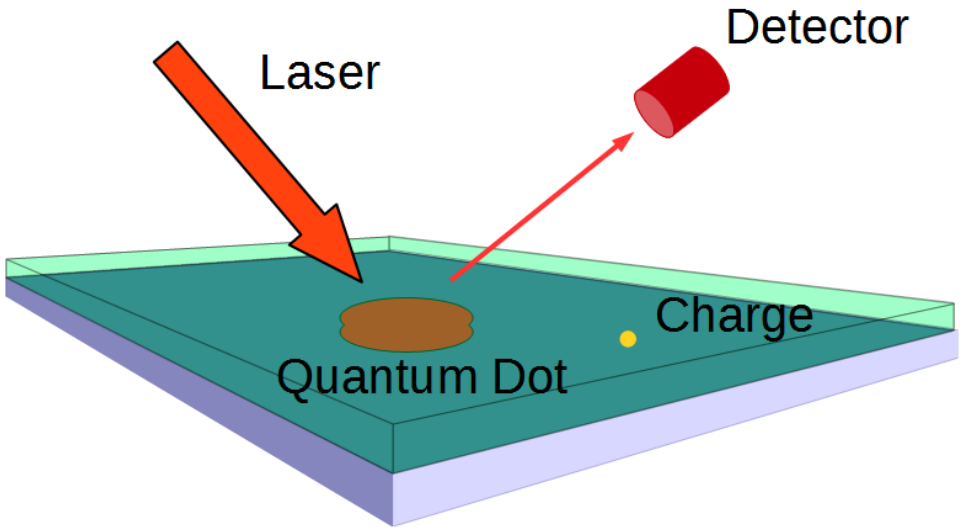

Figure 6.2: Diagram of the experimental set up. Here there is a single QD, driven by a laser at its resonant frequency and a detector. A single charge is also shown at a trap site and it displayes random telegraph noise. Since the mechanism for $1/f$ noise is not specified, we have not shown it on the diagram.

To calculate the dynamics of the system, we use a transfer matrix, which the reader will remember from section 5.21, is the Liouvillian super-operator in matrix form:

$$\dot{\rho}(t) = M\rho(t), \tag{6.7}$$

where M is the super-operator acting on the density operator ρ. The system is to be solved numerically and so for small time steps, we can write

$$\rho(t + \Delta t) = (1 + M\Delta t)\rho(t). \tag{6.8}$$

We shall treat the fluctuating charges as classical objects in the same way that we did in Chapter 5 (section 5.3) and so Eq. 6.8 described a transfer matrix for a system that does not fluctuate, but has a constant charge bias. This transfer matrix is defined as $1 + M\Delta t$. in order to include the fluctuating charges we are required to add in a σ_x term that takes us from the charge-near to the charge-far away cases. For details of how this is achieved, please see section 5.3 (Eq. 5.20).

Since there are two types of noise, at some time (t), the density matrix is constructed from two parts. We have already discussed the part coming from the fluctuating charges and so we must now go on to talk about the $1/f$ noise. For this we must

go back to the Von-Neumann equation (Eq. 2.10). We saw in section 2.3, that the Born approximation allowed us to truncate the series at a recursion depth of two, however, we can't do this for $1/f$ noise. The $1/f$ term is time dependent and correlated at long times. The interaction Hamiltonian for random Gaussian classical noise is $H_I = \frac{1}{2}\eta(t)\sigma_z$ [96]. It is assumed that the noise ($\eta(t)$) is unbiased and so has an average of $\bar{\eta} = 0$. The infinitely recursive Von-Neumann equation is then integrated to give the density matrix at time (t)

$$\begin{aligned}\rho(t) - \rho_0 &= \sum_{n=1}^{\infty} (-i)^n \int_0^t \int_0^{t_1} \dots \int_0^{t_{n-1}} dt_1 dt_2 \dots dt_n \\ &\quad \overline{\eta(t_1)\eta(t_2)\dots\eta(t_n)} \left[\frac{1}{2}\sigma_z, \left[\frac{1}{2}\sigma_z, \dots \left[\frac{1}{2}\sigma_z, \rho\right] \dots\right]\right], \end{aligned} \tag{6.9}$$

where $\overline{\eta(t_1)\eta(t_2)\dots\eta(t_n)}$ is the multi time correlation of the noise. Using Eq. 6.9, we can decompose the multi-time correlation function using Wick's theorem into two-time correlations. The n-fold commutator of σ_z and ρ can be evaluated quite easily since we know that $\sigma_z^2 = 1$ and that n is even.

$$\begin{aligned}\Lambda_1 &= \left[\tfrac{1}{2}\sigma_z, \rho\right] = \frac{1}{2}\left(\sigma_z\rho - \rho\sigma_z\right) \\ \Lambda_2 &= \left[\tfrac{1}{2}\sigma_z, \Lambda_1\right] = \frac{1}{2}\left(\rho - \sigma_z\rho\sigma_z\right) \\ \Lambda_3 &= \left[\tfrac{1}{2}\sigma_z, \Lambda_2\right] = \frac{1}{2}\left(\sigma_z\rho - \rho\sigma_z\right) \\ \Lambda_4 &= \left[\tfrac{1}{2}\sigma_z, \Lambda_3\right] = \frac{1}{2}\left(\rho - \sigma_z\rho\sigma_z\right), \end{aligned} \tag{6.10}$$

which shows that all even commutations given the same result.

$$\begin{aligned}\rho(t) - \rho_0 &= \sum_{n=2\ (evens)}^{\infty} (-i)^n \int_0^t \int_0^{t_1} \dots \int_0^{t_{n-1}} dt_1 dt_2 \dots dt_n \\ &\quad \overline{\eta(t_1)\eta(t_2)} \dots \overline{\eta(t_{n-1})\eta(t_n)} \left[\frac{1}{2}\left(\rho - \sigma_z\rho\sigma_z\right)\right]. \end{aligned} \tag{6.11}$$

There are $\frac{n!}{2^{\frac{n}{2}}(n/2)!}$ permutations of these two-time correlations. The integral is difficult to solve in this form, but we can re-write it with new limits and a combinatoric factor and since the limits of the integration can be made the same, we can simplify

the expression to

$$\rho(t) - \rho_0 = \sum_{n=2\ (evens)}^{\infty} (-i)^n \int_0^t \int_0^t dt_1 dt_2 \frac{1}{2^{\frac{n}{2}}(n/2)!} \left(\overline{\eta(t_1)\eta(t_2)}\right)^{n/2} \left[\frac{1}{2}\left(\rho - \sigma_z \rho \sigma_z\right)\right]. \tag{6.12}$$

For a single qubit, $\rho = \alpha^2|1\rangle\langle 1| + \beta\alpha|0\rangle\langle 1| + \alpha\beta|1\rangle\langle 0| + \beta^2|0\rangle\langle 0|$ and we have defined $\sigma_z = |1\rangle\langle 1| - |0\rangle\langle 0|$, which allows us to evaluate the term in the square bracket as

$$\frac{1}{2}\left(\rho - \sigma_z \rho \sigma_z\right) = \beta\alpha|0\rangle\langle 1| + \alpha\beta|1\rangle\langle 0|, \tag{6.13}$$

which are the coherences. The sum in Eq. 6.12 is the definition of the exponential function and so we obtain

$$\rho(t) - \rho_0 = e^{-\Gamma(t)t}\left(\beta\alpha|0\rangle\langle 1| + \alpha\beta|1\rangle\langle 0|\right), \tag{6.14}$$

where

$$\Gamma(t) = \frac{1}{2t}\int_0^t \int_0^t \overline{\eta(t_1)\eta(t_2)} dt_1 dt_2. \tag{6.15}$$

Determining the noise correlation begins by looking to the spectral density, which we know to be $1/f$ and which we will approximate by summing Lorentzian distributions of different widths (γ_k) [97]. The widths γ_k describe the frequencies of fluctuations in the noise correlation. The noise associated with a single width or frequency (γ) shall denoted using the symbol $\xi(t)$. The spectral density for a single frequency is then given by

$$S(f) = \frac{\beta^2/\gamma_k}{1 + \left(\pi f/\gamma_k\right)^2}, \tag{6.16}$$

where f is the centre of the Lorentzian, γ is the correlation frequency and β is the noise amplitude. Applying a Fourier transform to the spectral density gives us the two time noise correlation function,

$$\int_{-\infty}^{\infty} df \frac{\beta^2/\gamma_k}{1 + \left(\pi f/\gamma_k\right)^2} e^{i2\pi f t} = \beta^2 e^{2\gamma_k|t|} = \overline{\xi_{\gamma_k}(t)\xi_{\gamma_k}(0)}. \tag{6.17}$$

A nice consistency check is to see if the Lorentzians do indeed reproduce a $1/f$ function. If we allow the noise amplitude to be dependent on the correlation frequency we then have

$$\beta^2(\gamma_k) = \frac{2\Delta^2}{\gamma_k}, \tag{6.18}$$

where Δ^2 is a constant. We can integrate the spectral density (Eq. 6.17) over (γ_k) to give [97, 98]

$$S(f) = \int_{f_l}^{f_h} d\gamma_k \frac{2\Delta^2/\gamma_k^2}{1+(\pi f/\gamma_k)^2} = \frac{2\Delta^2}{\pi f}\left[\arctan\left(\frac{\gamma_h}{\pi f}\right) - \arctan\left(\frac{\gamma_l}{\pi f}\right)\right] \simeq \frac{A}{f}, \quad f_l \ll \pi f \ll f_h, \tag{6.19}$$

where f_l and f_h are the low and high limits between which the Lorentzians approximate a $1/f$ distribution. Remembering that the noise correlations are comprised of a sum of those for individual frequencies

$$\overline{\eta(t_1)\eta(t_2)} = \left(\sum_{k=1}^{M} \frac{1}{\gamma_k}\Delta^2 e^{2\gamma_k|t_1-t_2|}\right) / \left(\sum_{k=f_l}^{f_h} \frac{1}{\gamma_k}\right), \tag{6.20}$$

where since we have altered the form of β to have a weighting of $\frac{1}{\gamma_k}$, we must divide the equation by the sum of the weightings. We can now evaluate Eq. 6.15 to give

$$\frac{1}{2t}\int_0^t \int_0^t \Delta^2 e^{2\gamma_k|t_1-t_2|} dt_1 dt_2 \;=\; \Delta^2\left(\frac{2\gamma_k t - 1 + e^{-2\gamma_k t}}{4\left(\gamma_k\right)^2 t}\right) \tag{6.21}$$

This gives the result for the dissipative term arise from $1/f$ noise, $\Gamma(t)$, being,

$$\Gamma(t) = \Delta^2\left(\sum_{k=f_l}^{f_h} \frac{1}{\gamma_k}\frac{2\gamma_k t - 1 + e^{-2\gamma_k t}}{4\left(\gamma_k\right)^2 t}\right) / \left(\sum_{k=1}^{M} \frac{1}{\gamma_k}\right). \tag{6.22}$$

Taking the continuum limit yields,

$$\Gamma(t) = \frac{\Delta^2\left(\int_{f_l}^{f_h} \frac{1}{\gamma}\frac{2\gamma t-1+e^{-2\gamma t}}{4(\gamma)^2 t} d\gamma\right)}{\left(\int_{f_l}^{f_h} \frac{1}{\gamma} d\gamma\right)}. \tag{6.23}$$

6.3.1 Properties of $1/f$ dephasing

Now that we have our expression for $\Gamma(t)$, we must develop a master equation that can describe both this noise as the random telegraph noise that we described earlier. We assume here that the $1/f$ noise is an independent process and as a result commutes with the random telegraph noise dephasing processes, which means that we can simply add it to the other dephasing terms. We have, from Eq. 6.14, for the density matrix at time t is given by

$$\rho(t) = e^{-\Gamma(t)t}\frac{1}{2}\left(\rho - \sigma_z\rho(t)\sigma_z\right), \tag{6.24}$$

but we can find its time derivative

$$\begin{aligned}\frac{d}{dt}\rho(t) &= \left(-\Gamma(t) - t\frac{d}{dt}\Gamma(t)\right) e^{-\Gamma(t)t}\frac{1}{2}\left(\rho(0) - \sigma_z\rho(0)\sigma_z\right) \\ &= \left(-\Gamma(t) - t\frac{d}{dt}\Gamma(t)\right)\frac{1}{2}\left(\rho(t) - \sigma_z\rho(t)\sigma_z\right) \qquad (6.25) \\ &= \Gamma_D(t)\frac{1}{2}\left(\rho(t) - \sigma_z\rho(t)\sigma_z\right), \qquad (6.26)\end{aligned}$$

Where $\frac{1}{2}\left(\rho - \sigma_z\rho\sigma_z\right)$ is in the form of a Linblad dissipator and $\Gamma_D(t)$ can be calculated from Eq. 6.23 as

$$\Gamma_D(t) = -\frac{\Delta^2\left[2f_hf_lt\left[\mathrm{Ei}(-2f_ht) - \mathrm{Ei}(-2f_lt)\right] - f_he^{-2f_lt} + f_l\left(e^{-2f_ht} - 1\right) + f_h\right]}{2f_hf_l\ln\left(\frac{f_h}{f_l}\right)} \qquad (6.27)$$

where $\mathrm{Ei}(x)$ is the exponential integral function, defined as

$$\mathrm{Ei}(x) = \int_{-x}^{\infty} dt\frac{e^{-t}}{t}. \qquad (6.28)$$

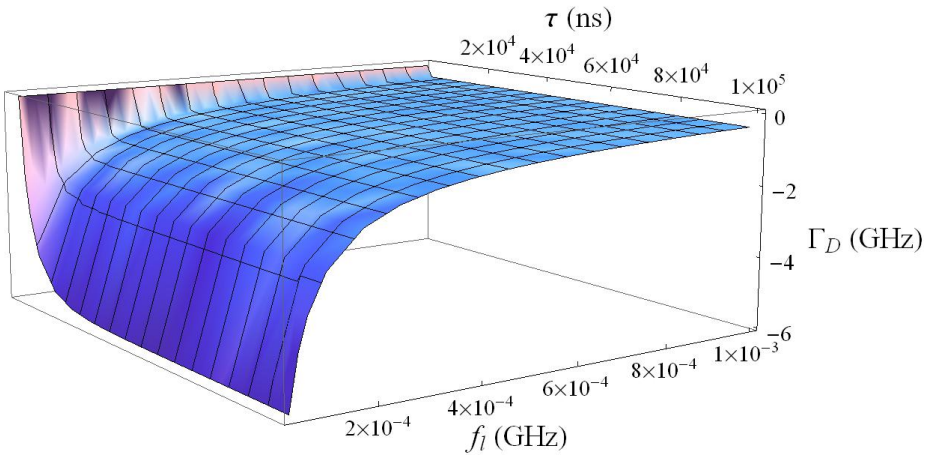

Figure 6.3: Dephasing rate Γ_D as a function of minimum frequency (f_l). The noise strength Δ^2 is fixed at 0.01 GHz and the f_h is fixed at 1 THz.

The dephasing rate $\Gamma_D(t)$ as a function of the minimum frequency (f_l) and time is displayed in Fig. 6.3. It can easily be seen from this figure, that the minimum frequency decreases, the dephasing rate rapidly increases. Taking the limit of minimum frequency going to zero, we are left with a dephasing rate that is linear in

time and independent of the maximum frequency. It is in fact controlled solely by the Δ^2 noise strength,

$$\lim_{f_l \to 0}(-\Gamma(t) - t\frac{d}{dt}\Gamma(t)) = -t\Delta^2. \tag{6.29}$$

6.3.2 Effect of infinite dephasing

Eq. 6.29 has the important consequence that as time goes to infinity, the dephasing rate also goes to infinity. Fig 6.4 shows the dynamics of such as system with initial conditions of

$$\rho(0) = \frac{1}{2}\sum_{i,j \in (0,1)} |i\rangle\langle j| \tag{6.30}$$

where the $\Delta^2 = 0.01$ GHz, where there is no decay rate or laser driving. The coherence should simply decrease.

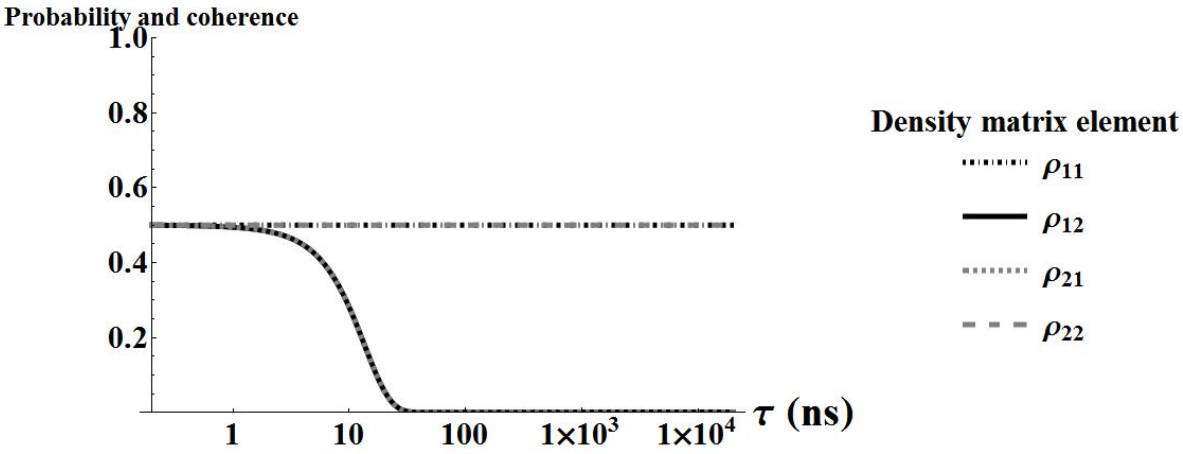

Figure 6.4: Dynamics of a single two level system prepared in a 50:50 superposition of ground and excited state, subject to $1/f$ noise. The noise parameter $\Delta^2 = 0.01$ GHz and the qubit decay rate (γ_i) and Rabi frequencies (Ω_i) are set to zero. There is no RTN.

As expected, the dephasing process causes the coherence between excited and ground states to decrease to zero. Let us investigate the effect of the noise strength Δ^2 in this regime.

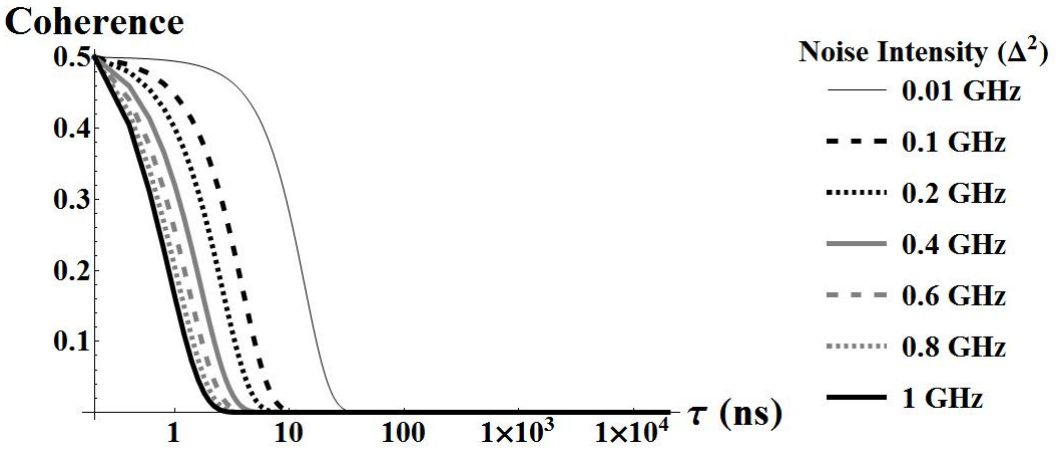

Figure 6.5: Dynamics of a single two level system prepared in a 50:50 superposition of ground and excited state, subject to $1/f$ noise. The noise parameter Δ^2 being varied and the qubit decay rate (γ_i) and Rabi frequencies (Ω_i) are set to zero. There is no RTN.

We see that the noise strength, in this regime sets the time scale on which the decay of the coherences occur, although this time scale does not seem to be simply inversely proportional to the noise strength.

An interesting result in this infinite dephasing regime is that with the introduction a loss mechanism (spontaneous decay) and coherent driving the steady state will always be the dot in its ground state. Fig 6.6 shows the dynamics of a system with a spontaneous decay rate and Rabi frequency of 1 GHz with a Δ^2 parameter of 0.01 GHz.

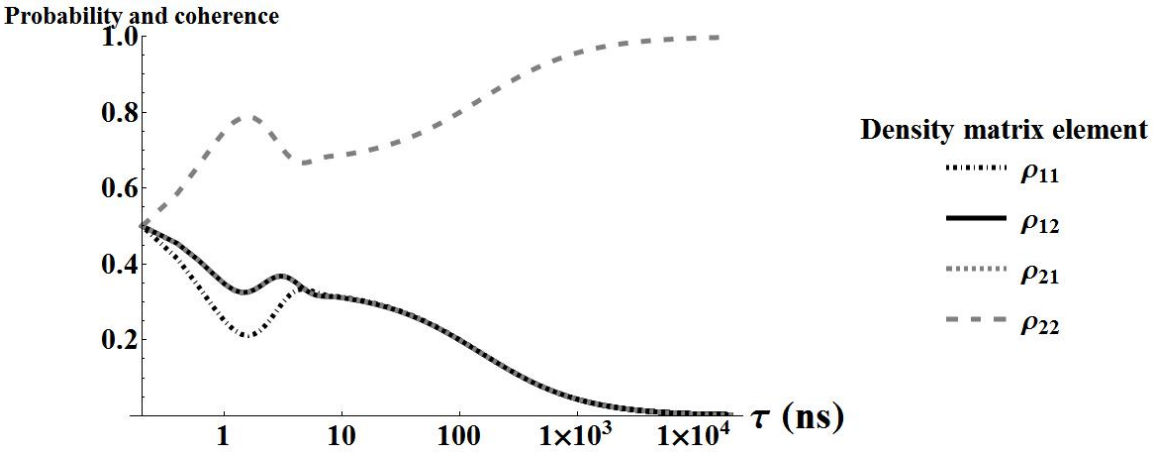

Figure 6.6: Dynamics of a single two level system prepared in a 50:50 superposition of ground and excited state, subject to $1/f$ noise and coherent driving. The noise parameter Δ^2 is fixed at 0.01 GHz and the qubit decay rate (γ_i) and Rabi frequencies (Ω_i) are set to 1 GHz. There is no RTN.

This is in comparison to the dynamics with no $1/f$ noise, as shown in Fig 6.7.

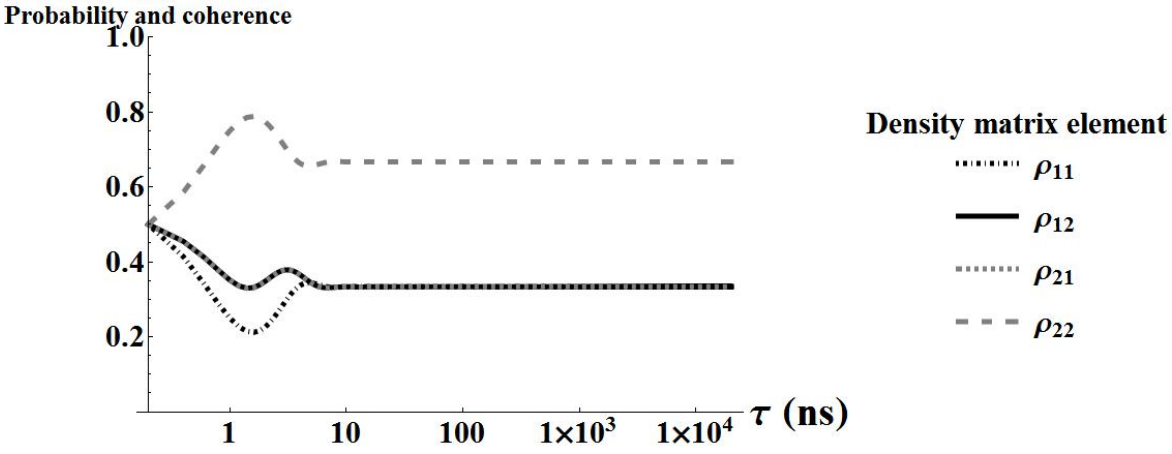

Figure 6.7: Dynamics of a single two level system prepared in a 50:50 superposition of ground and excited state, subject to no $1/f$ noise and coherent driving. qubit decay rate (γ_i) and Rabi frequencies (Ω_i) are set to 1 GHz. There is no RTN.

This regime does has the ground state as a steady state, which is not good news when we consider that the $g^{(2)}(\tau)$ correlation function that we have been using has got the excited state probability as denominator, so the correlation will always be infinite. We shall return to this thought in section 6.4.1, but for now, let us consider the finite regime.

6.4 Results

THE DECOHERENCE caused by $1/f$ noise, in the finite regime, is described by three parameters, namely, f_l, f_h and Δ^2. In some papers the minimum and maximum frequencies are set to the resolution of detection or arbitrarily [79, 97, 98]. However, these should be set depending on the material under investigation, if indeed there are cut-off frequencies [94, 95]. In this chapter we hope to show how measurements of correlation functions can be used to extract information about these quantities. We begin then by considering the case of a single quantum dot subject to $1/f$ noise. The quantum dot parameters are typical for InGaAs structures, where the spontaneous decay rate (γ) and Rabi frequency (Ω) will be fixed at 1 GHz. The laser will be fixed to resonance with the quantum dot.

In Fig 6.8, we show $g^2(\tau)$ as a function of f_l. Beginning with the profile of the curves, we see that in all cases there is an initial rise in the auto-correlation to a peak on the order of 5ns, after which it drops off. We see that as the low frequency limit is decreased, the peak of the auto-correlation of the detected photons increases non-linearly, which then all decrease to the no correlation value of $g^{(2)}(0,\tau) = 1$. We see that the time scale of the correlation decay, i.e., the time at which $g^{(2)}(0,\tau)$ becomes close to unity, is inversely proportional to f_l. The explanation for this is fairly straight-forward: frequency and time share and inverse relationship, so the scale of the minimum frequency determines the maximum time scale. However, the minimum frequency determines the time scale of the correlation decay, because the density of states scales proportionally as $1/f$. We have allowed the frequency to be a continuous variable, however it is instructive to imagine this as a limit of a discrete spectrum. Taking the time noise correlation we can perform a discrete Fourier transform, which allows us to represent the correlation as a set of equally spaced frequencies. This lets us think of $1/f$ noise in terms of numbers of fluctuators, fluctuating at a particular frequencies. The lower the frequency, the greater the number of fluctuators and since the minimum frequency is by definition the lowest noise frequency, it determines the longest timescale present in the correlation decay.

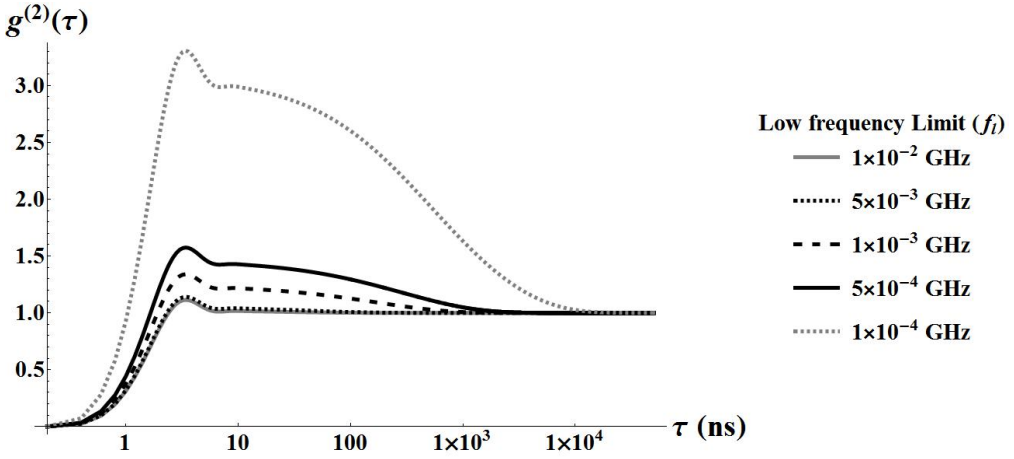

Figure 6.8: Graph showing $g^{(2)}(\tau)$ auto-correlation for different values of f_l. The spontaneous decay rate of the qubit as well as the Rabi frequency is set to 1 GHz, f_h is set to 10^3 GHz and the noise strength Δ^2 is set to 0.01 GHz.

Another feature of the figure is the magnitude of $g^{(2)}(\tau)$ as a function of f_l. As the frequency is lowered, the height of the curves increases. The lowering of the minimum frequency in addition to controlling the correlation decay time scale, also increases the rate of decoherence generally. The decoherence rate ($\Gamma_D(t)$) for $1/f$ noise is time dependent, but it does reach a steady state determined by,

$$\Gamma_{ss} = \frac{\Delta^2 \left(f_h - f_l\right)}{2 f_h f_l \ \ln\left(\frac{f_h}{f_l}\right)}. \tag{6.31}$$

As Eq. 6.31 shows, by lowering the minimum frequency, the steady state decoherence rate increases. This means that the steady state of the qubit density matrix will approach the ground state as the minimum frequency tends to zero.

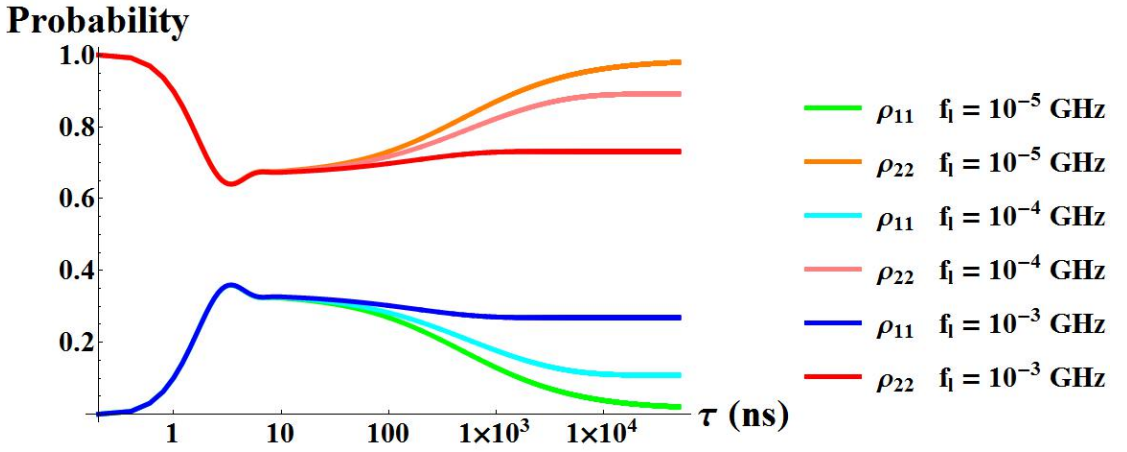

Figure 6.9: Graph showing the excited and ground state probabilities of the quantum dot as a function of f_l. The spontaneous qubit decay rate (γ_i) and Rabi frequencies (Ω_i) are set to 1 GHz, f_h is set to 10^3 GHz and the noise strength Δ^2 is set to 0.01 GHz.

Plotted in Fig 6.9 are the density matrix dynamics for a qubit subject to $1/f$ noise and it shows f_l being varied. Highlighted in the graph are the relative heights of the steady state for different f_l and the peak at roughly 5 ns. As the minimum frequency is lowered, the difference between the peak and the steady state is made greater. For this graph, when comparing features we will take the solid curves as the reference curves. The steady states in Fig 6.9 have absolute values, but these are normalised in the correlation calculations such that the steady states rest at 1 as shown in Fig 6.8. As a natural consequence, the peak is elevated relative to the steady state. We also note that the curves deviate from one another at 10 ns. The time at which this occurs is controlled by the noise strength Δ^2. The larger the amplitude, the earlier the peak arrives as shown in Fig. 6.10. The figure also raises the question of having a zero minimum frequency. As f_l gets smaller, the $g^{(2)}(\tau)$ peak gets larger. This trend makes the peak reach infinity as f_l goes to zero. Mathematically, as f_l tends to zero, the Lindblad term in the master equation dissipator attributed to the $1/f$ noise tends to $-t\Delta^2$. This means that at infinite time, the decoherence is infinite and the density matrix of the quantum dot must necessarily end in the ground state. A quantum dot in the ground state cannot emit photon and so $g^{(2)}(\tau)$ becomes infinite. Interestingly, the decoherence loses its dependence on the maximum frequency in this regime, though when we consider that the density of states for each frequency goes as $1/f$ it is easy to see that when the minimum frequency is very low, the higher frequencies are much less effective.

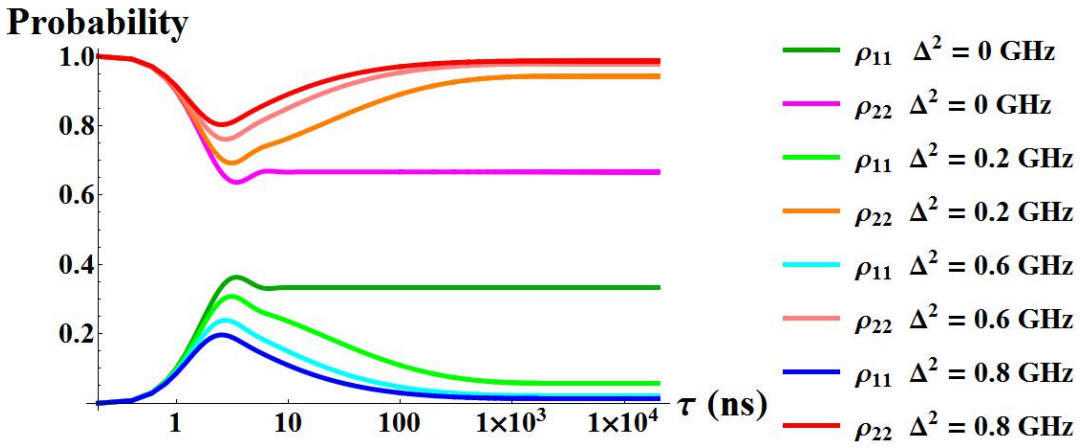

Figure 6.10: Graph showing the excited and ground state probabilities of the quantum dot as a function of time for varying Δ^2. The spontaneous decay rate of the qubit as well as the Rabi frequency is set to 1 GHz, f_h is set to 10^3 GHz and f_l is set to 10^{-3} GHz

The next parameter to investigate is the maximum frequency (f_h) to see how it affects the auto-correlation. Shown in Fig 6.11 is the $g^{(2)}(t)$ auto-correlation as a function of (τ) where the maximum frequency (f_h) is swept between the values of 10 MHz and 1 THz. The minimum frequency (f_l) is set to 1 MHz, the noise amplitude Δ^2 is set to 0.01 GHz.

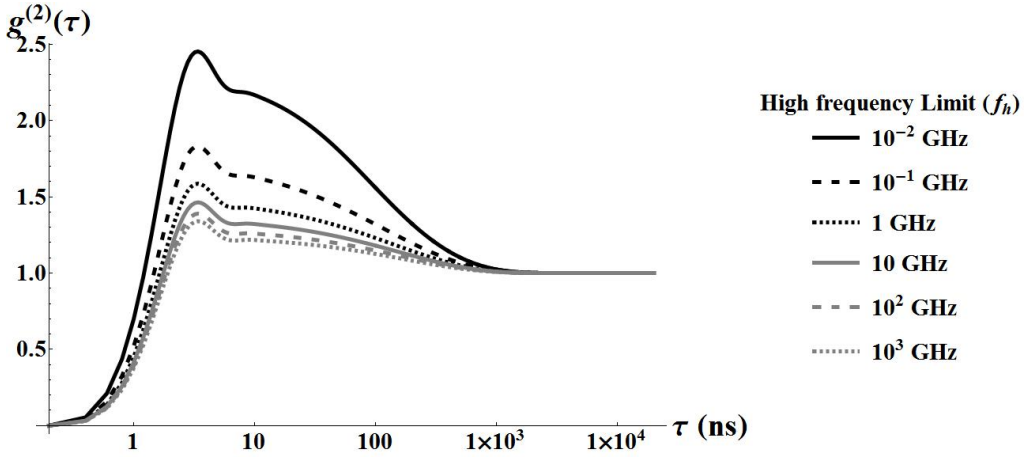

Figure 6.11: Graph showing $g^{(2)}(\tau)$ auto-correlation for different values of f_h. The spontaneous decay rate of the qubit as well as the Rabi frequency is set to 1 GHz, f_l is set to 1 MHz and the noise strength Δ^2 is set to 0.01 GHz.

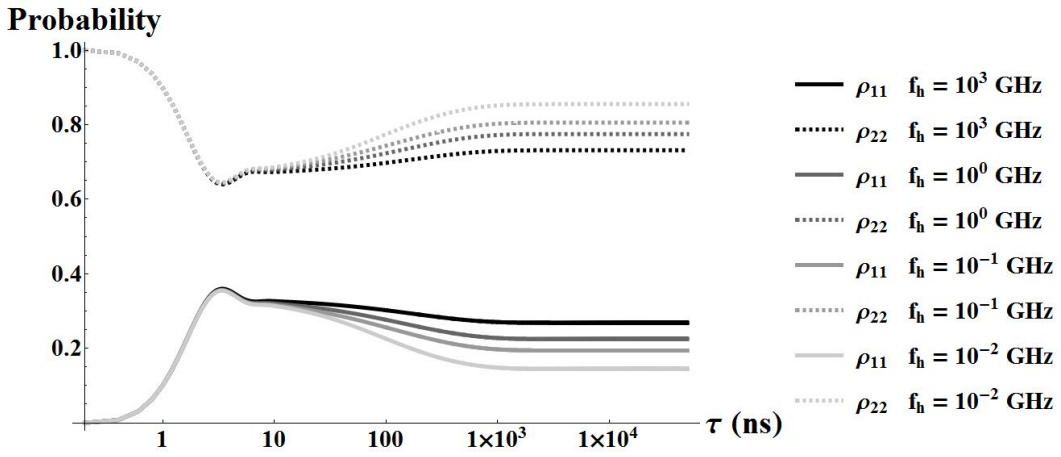

Figure 6.12: Graph showing the excited and ground state probabilities of the quantum dot as a function of f_l. The spontaneous decay rate of the qubit (γ_i) as well as the Rabi frequency (Ω_i) is set to 1 GHz, f_h is set to 10^3 GHz and the noise strength Δ^2 is set to 0.01 GHz.

We note that Figs. 6.11 and 6.12 show that f_h affects the height of the correlation peak and as with f_l, the smaller the maximum frequency, the larger the height of the peak. This may at first glance appear odd, since making the maximum frequency smaller means that there are fewer frequencies between it and the minimum, which one might think would mean that there would be less of a decohering effect. If we look at Eq. 6.31 (shown graphically in Fig. 6.13), we see that the denominator is minimised by making the maximum and minimum frequencies equal, thus lowering the maximum frequency in fact increases the rate of decoherence.

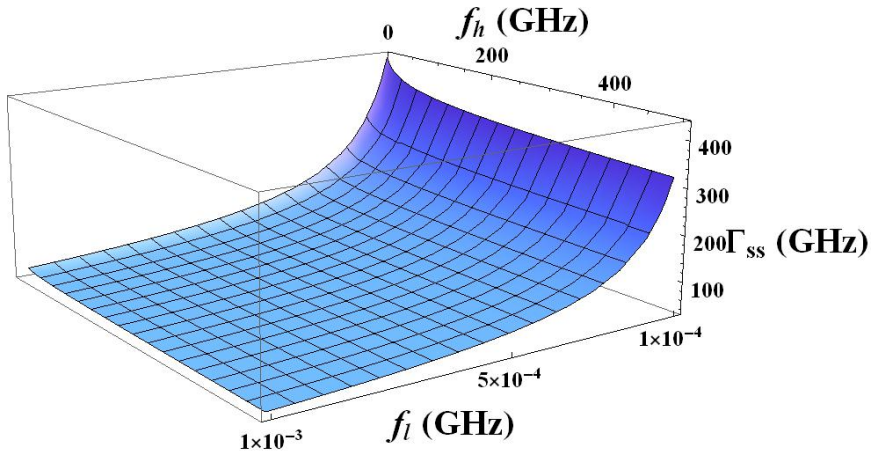

Figure 6.13: Graph showing the steady state dephasing rate as a function of the minimum (f_l) and maximum (f_h) frequencies of the spectral density

In the case of varying the minimum frequency, this is in competition with the density of states favouring lower frequencies, which is why the decoherence rate increases by lowering the minimum frequency and taking it further away from the maximum frequency. Comparing Figs 6.8 and 6.11, it should noted that f_h does not affect the time scale of the correlation decay, as can be seen on Fig. 6.11 by the convergence of all the curves on the order of 10^3 ns, which is the reciprocal of f_l set at 10^{-3} GHz. It is uncertain if there is anything contained within a specific curve that would indicate the value of f_h. It can be argued that with the knowledge that the minimum frequency determines the time scale of the decay, then the maximum frequency may be inferred from the height of the peak. This does, however, rely on knowing the value of Δ^2. In addition, were these parameter values to be known, the sample would have to exhibit only $1/f$ noise, which is unrealistic.

Next we examine the impact of varying the overall noise amplitude Δ^2. This is a multiplicative pre-factor to the decoherence rate and so changing it only results in a linear scaling, but it is useful to compare its effect on the auto-correlation function with that of f_l and f_h.

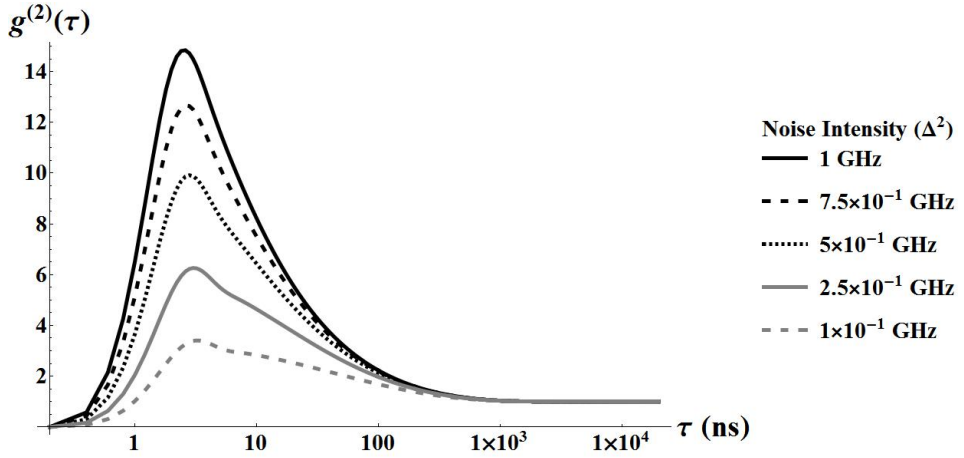

Figure 6.14: Graph showing $g^{(2)}(\tau)$ auto-correlation for different values of Δ^2. The spontaneous decay rate of the qubit (γ_i) as well as the Rabi frequency (Ω_i) is set to 1 GHz, f_l is set to 1 MHz and f_h is set to 1 THz.

Comparing Fig 6.14 with Figs 6.11 and 6.8, we see that changing Δ^2 does not preserve the shape of the peak below 10 ns. The initial peak is due to Rabi os-

cillations from the laser. $1/f$ noise builds to a maximum decoherence rate, but a large Δ^2 makes the build up multiplicatively larger and washes out the peak. This behaviour is also seen in Fig. 6.10, where increases the noise amplitude makes the distinguishing between the peak and the decohering tail increasingly difficult.

6.4.1 Limit of zero minimum frequency ($f_l \rightarrow 0$)

As discussed earlier, if we allow the minimum frequency to reach zero then the steady state of the system will be the ground state. This is bad for our calculations since if we recall Eq. 5.65 from chapter 5, this will give us a result of infinity for $g^{(2)}$ no matter the value of τ, because the denominator describes the excited state probability in the steady state, which is zero. However, we may get a non-infinite result by specifying the times for the two time auto-correlation $g^{(2)}(t_1, t_2)$. In other words, we don't allow the system to reach its steady state and therefore avoid an infinite result. Let us then perform a simulation where the total time is constant (2 μs), but the time at which the first photon is detected is varied. Varying the time at which the first photon is detected (t_1), we obtain Fig 6.15.

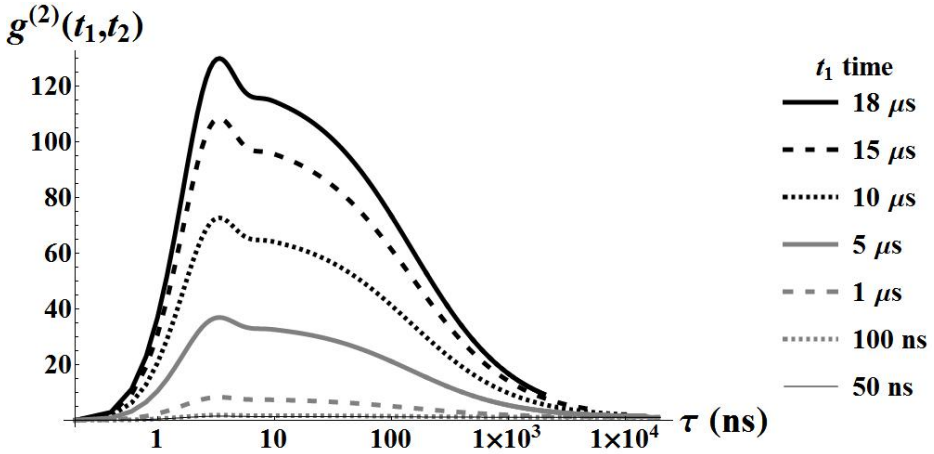

Figure 6.15: Graph showing $g^{(2)}(t_1, t_2)$ auto-correlation for different values of t_1. The spontaneous decay rate of the qubit (γ_i) as well as the Rabi frequency (Ω_i) is set to 1 GHz and f_l is set to zero, which makes f_h irrelevant.

There are two main results from this graph. We see that in the case where we specify the two times of the auto-correlation function and that the steady state is the ground state; that since we don't allow the system to reach the steady state, the correlation function does not fall to unity. The second result is that the longer the t_1 time, the higher the peak of the curve. This curve is determined by the difference

between the two times. To understand this, we begin with Eq.5.41 for a single qubit where the system is initially in the ground state.

$$g^{(2)}(t_1, t_1+\tau) = \frac{\langle \sigma_+(t_1)\sigma_+(t_1+\tau)\sigma_-(t_1+\tau)\sigma_-(t_1)\rangle_{gr}}{\langle \sigma_+(t_1)\sigma_-(t_1)\rangle_{gr}\langle \sigma_+(t_1+\tau)\sigma_-(t_1+\tau)\rangle_{gr}}, \tag{6.32}$$

where the subscript gr shows that the system was initialised in the ground state. After time t the first photon is observed, and by necessity the system is returned to the ground state

$$\sigma_-\rho_{gr}(t)\sigma_+ = \langle \sigma_+(t)\sigma_-(t)\rangle_{gr}\rho(0)_{gr}. \tag{6.33}$$

This means that the second set of operators in the numerator of Eq. 6.32 is effectively shifted backwards in time by t_1,

$$g^{(2)}(t_1, t_1+\tau) = \frac{\langle \sigma_+(t_1)\sigma_-(t_1)\rangle_{gr}\langle \sigma_+(\tau)\sigma_-(\tau)\rangle_{gr}}{\langle \sigma_+(t_1)\sigma_-(t_1)\rangle_{gr}\langle \sigma_+(t_1+\tau)\sigma_-(t_1+\tau)\rangle_{gr}}, \tag{6.34}$$

and we are left with

$$\frac{\langle \sigma^+(\tau)\sigma^-(\tau)\rangle_{gr}}{\langle \sigma^+(t_1+\tau)\sigma^-(t_1+\tau)\rangle_{gr}}. \tag{6.35}$$

The result shown in Eq. 6.35 is true only in the case where the QD is initialised in the ground state, which means that after the first photon is observed, the system returns to the initial state, effectively resetting the time for the numerator of Eq. 6.35. We can see this graphically in Figs. 6.16 and 6.17 for a t_1 time of 50 ns.

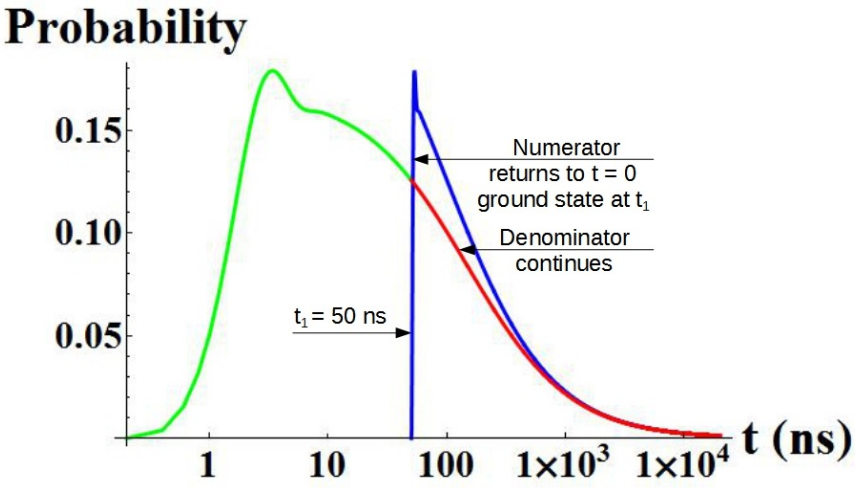

Figure 6.16: Graph showing the numerator (green and blue) and denominator (red) of Eq. 6.35 starting from $t = 0$ for a system initialised in the ground state. There is a photon detection event at 50 ns after which the numerator returns to ground state, effectively shifting the function by t_1.

The experiment begins at $(t = 0)$ and progresses to $(t = t_1)$ as shown in green, where the excited state probability returns to zero, since we have detected a photon and know for certain that the system is in the ground state. We then see the same system behaviour again as shown in blue, though due to the logarithmic scale of Fig. 6.16 it looks squashed. If we showed this on a linear scale, the blue and green curves would look identical, as we see in Fig. 6.17. The denominator of Eq. 6.35 is shown in red, which corresponds to the same function shifted by t_1. Showing only the relevant parts of Fig. 6.16 for the calculation (red and blue) and starting at $(\tau = t - t_1 = 0)$ we see the numerator (blue) and denominator (red) are parts of the same function, but shifted by (t_1). Zooming in on Fig. 6.16 and setting the time to zero at what was 50 ns we get Fig. 6.17.

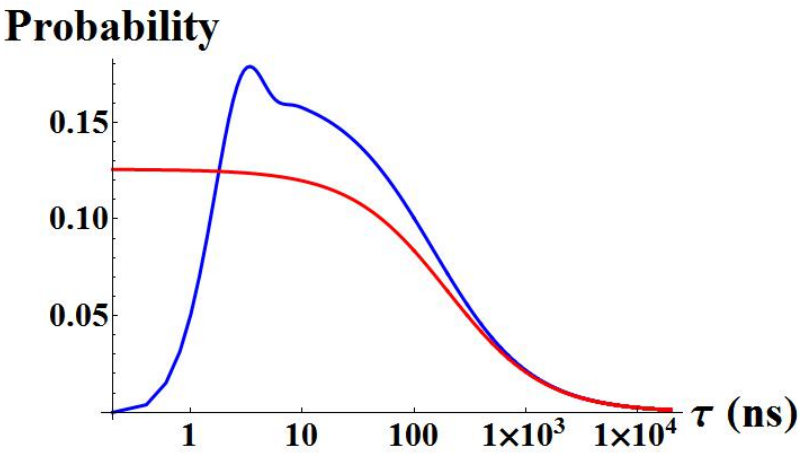

Figure 6.17: Graph showing the numerator (blue) and denominator (red) of Eq. 6.35 starting from $\tau = t_1 = 0$ for a system initialised in the ground state.

We can show that the green and blue curves are the same, by using a linear scale

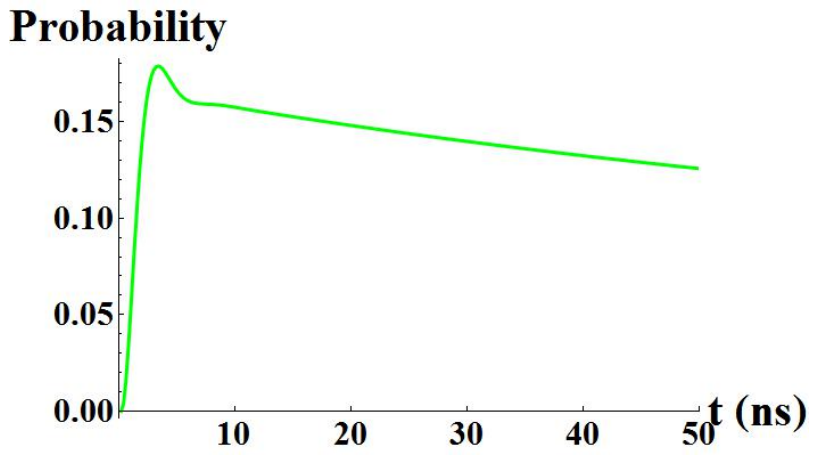

Figure 6.18: Graph showing the numerator (green) of Eq. 6.35 starting from $t = 0$ for a system initialised in the ground state.

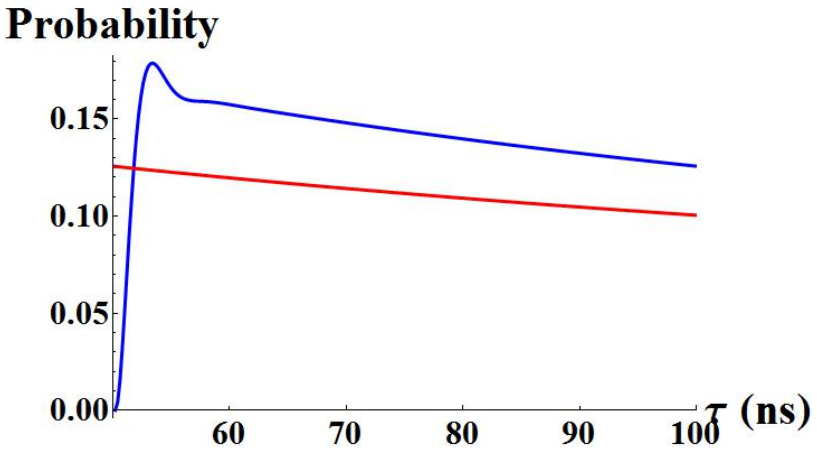

Figure 6.19: Graph showing the numerator (blue) and denominator (red) of Eq. 6.35 starting from $t = 50$ for a system initialised in the ground state.

Working with defined t_1 time provides an opportunity to investigate the frequencies that $1/f$ noise is comprised of. That is to say, if we return to the case where there is a minimum frequency (f_l), we can see how far the $1/f$ nature of the spectral density goes. The minimum frequency (f_l) can be determined from Fig 6.8 as the scale on which the correlation decays to unity and it was discussed that this was due to the nature of the density of states. This should allow us to perform a simulation where we may alter the time at which the first photon is observed (t_1) to make it appear after the reciprocal time of f_l. At this time, the system has progressed beyond the maximum correlation time (set by f_l) and so above this threshold there should be no observable effect of altering the t_1 time on the shape of the correlation function. The results of this simulation are presented in Fig 6.20.

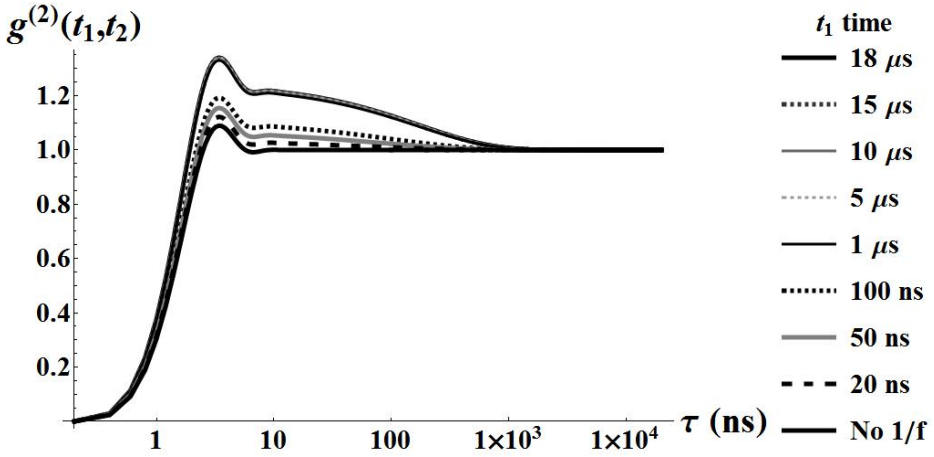

Figure 6.20: Graph showing $g^{(2)}(t_1, t_2)$ auto-correlation for different values of t_1. The spontaneous decay rate of the qubit (γ_i) as well as the Rabi frequency (Ω_i) is set to 1 GHz, f_l is set to 1 MHz and f_h is set to 1 THz.

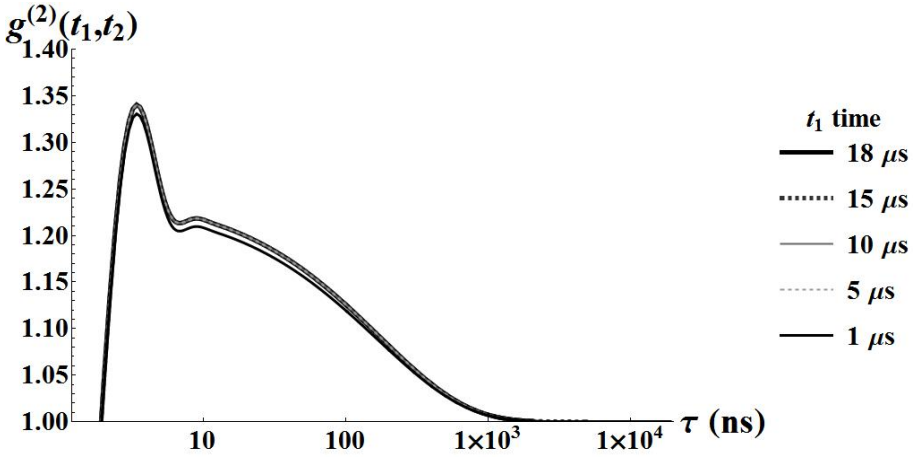

Figure 6.21: A zoomed in version of Fig. 6.20 showing $g^{(2)}(t_1, t_2)$ auto-correlation for different values of t_1. The spontaneous decay rate (γ_i) of the qubit as well as the Rabi frequency (Ω_i) is set to 1 GHz, f_l is set to 1 MHz and f_h is set to 1 THz.

The minimum frequency (f_l) has been set to 1 MHz and so our threshold time will be 1 μs. It is plain to see in Figs. 6.20 and 6.21 that as the t_1 time is shortened, there is no corresponding change in the correlation function, and thus the curves all lie on top of each other, until $t_1 < 1\mu$s ($1/f_l$) at which point the function decreases with t_1. This is difficult to see, but just visible in Fig. 6.21 is the curve representing a t_1 time of 1 μs as distinct from the others, which are all lying on top of one another. If we think of the system comprising of discrete frequencies then, their reciprocals determine the time scale in which they fluctuate. As t_1 is decreased

below the value of each of these fluctuation time scales, those frequencies cease to affect the correlation, since few, if any fluctuations at those frequencies. Thus the correlation decreases as more frequencies are cut out. There is an additional curve on in Fig 6.20 where there is no $1/f$ noise. This curve reaches a steady state very quickly, but does display Rabi oscillations to begin with. This limits the t_1 comparison between it and the other curves to 10 ns before the shape of no $1/f$ curve begins to change as well. The two regimes will still converge, but it becomes more difficult to compare when both curves are changing.

6.4.2 Adding a fluctuating charge

Using the same technique, it is also possible to discern $1/f$ noise when there is a fluctuating charge present.

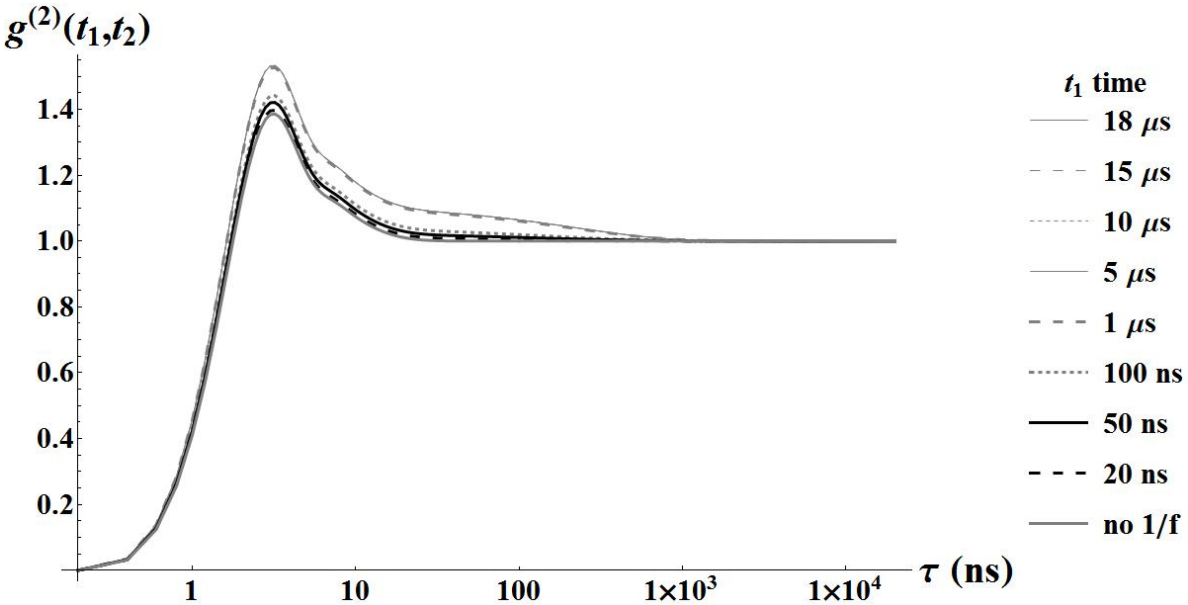

Figure 6.22: Graph showing $g^{(2)}(t_1, t_2)$ auto-correlation with a single fluctuating charge for different values of t_1. The spontaneous decay rate of the qubit (γ_i) as well as the Rabi frequency (Ω_i) is set to 1 GHz, f_l is set to 1 MHz and f_h is set to 1 THz. The fluctuation rate of the charge P is set to 0.1 GHz and the charge-qubit interaction strength is set to 1 GHz.

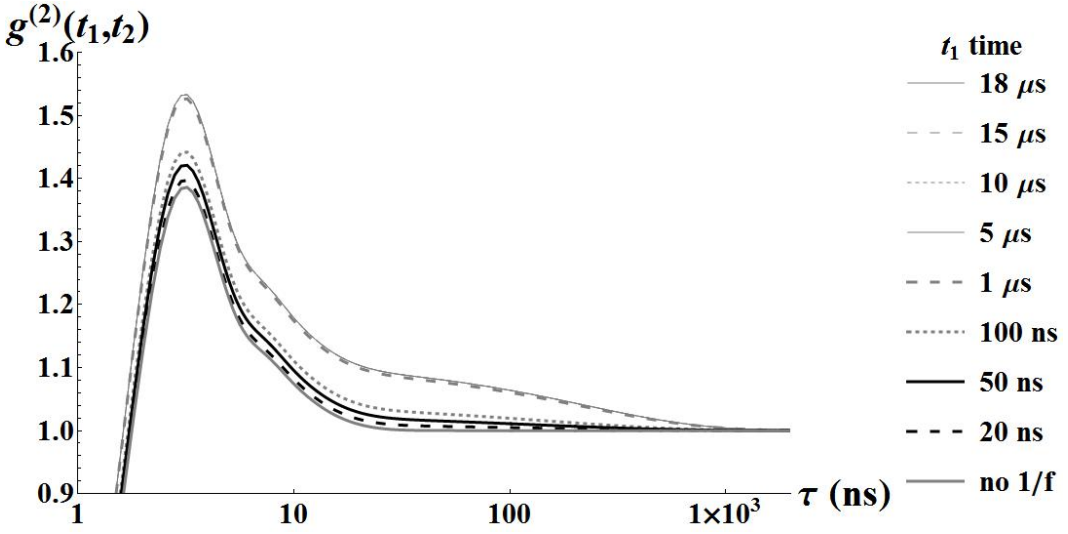

Figure 6.23: Graph showing $g^{(2)}(t_1, t_2)$ auto-correlation with a single fluctuating charge for different values of t_1. The spontaneous decay rate of the qubit (γ_i) as well as the Rabi frequency (Ω_i) is set to 1 GHz, f_l is set to 1 MHz and f_h is set to 1 THz. The fluctuation rate of the charge P is set to 0.1 GHz and the charge-qubit interaction strength is set to 1 GHz.

We see that there is a plateau and a shoulder in Fig 6.22, which we can zoom-in on in Fig. 6.23. This plateau and shoulder indicate that there are two time scales of decoherence. The term shoulder is used here, because the feature is not flat enough to be a plateau and the deviation is on the side of another feature i.e., the plateau. The charge is fluctuating with a frequency of 0.1 GHz and there is a shoulder near 10 ns and also the long decay reaching unity at 1 μs from f_l being set to 1 MHz. In addition, by altering t_1 we see that there is no change in the correlation function until $t_1 < 1/f_l$ at which point the curve peak decreases in height closer resembling the case where there is no $1/f$ noise present (for $t_1 > 10$ ns).

After 10 ns, as the time between the initialisation of the QD state and the detection of the first photon lengthens, the state of the QD closer approaches the ground state. As such the denominator of $g^{(2)}(t_1, t_2)$ closer approaches zero and so the peak of the curve becomes higher.

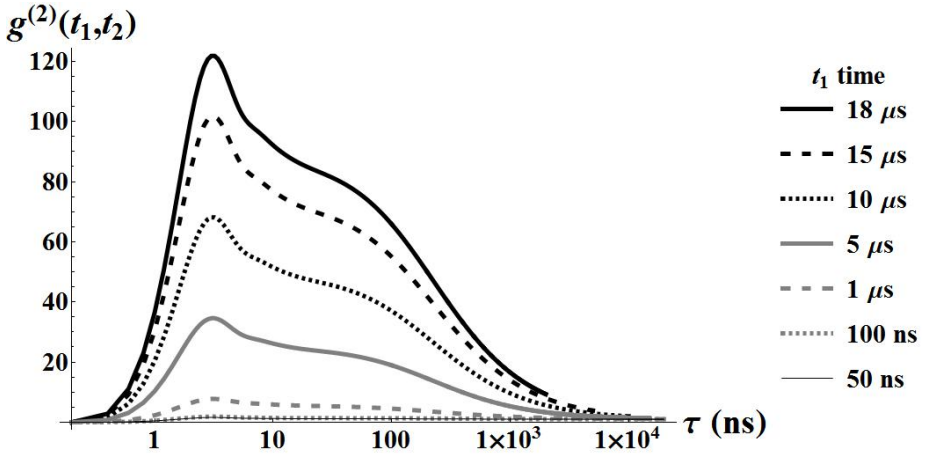

Figure 6.24: Graph showing $g^{(2)}(t_1, t_2)$ auto-correlation with a single fluctuating charge for different values of t_1. The spontaneous decay rate of the qubit (γ_i) as well as the Rabi frequency (Ω_i) is set to 1 GHz and f_l is set to zero, which makes f_h irrelevant. The fluctuation rate of the charge P is set to 0.1 GHz and the charge-qubit interaction strength is set to 1 GHz.

In the limiting case of a zero minimum frequency, we see in Fig. 6.24 the two time scales of decoherence, there is a shoulder at 10 ns and then a long decay which show that the peak height is a function of the t_1 time, but understandably, there is no change in the form of the curve showing cut-offs in different frequencies.

6.5 Summary

In this second research chapter, the system under study was a single quantum dot suffering from $1/f$ noise in addition to the charge noise explored in the first research chapter. We explained that the exact mechanism or indeed mechanisms of $1/f$ noise are currently unknown and debated and so the noise remains as a mathematical construct of the spectral density. As such we used a sum of Lorentzian functions to model the noise. The aim of this chapter was to detect signatures of $1/f$ noise within the correlation statistics of emitted photon. However, unlike in first research chapter, only one qubit was simulated. This aim was broken done into four questions, namely:

(i) What are the experimental signatures of $1/f$ noise? Alternatively, by observation of the auto-correlation function, how can it be known that the noise affecting our system is of the type $1/f$?

(ii) Can the effects of $1/f$ noise be determined when other noise sources are present? Just as in the first research chapter, we have a fluctuating charge and so we would like to distinguish between noise sources.

(iii) How can it experimentally observed if there is a low cut-off frequency? In this research chapter we explored the paradox of having a spectral density that is not integrable and made mention of the idea that there may exist some intrinsic low cut-off frequency. The question we would like to explore is how to check if one exists.

(iv) Can the cut-off frequency be determined? To put it another way, can the cut-off frequency be found via the observation of the auto-correlation function.

We believe that we have answered these questions and shown that the auto-correlation function is a useful tool in the acquisition of fundamental information regarding $1/f$ noise in quantum optical systems. We believe that we have found signatures of $1/f$ noise and are able to distinguish it from charge fluctuations of a limited number of charges. We must add this qualifier, since one of the mechanisms put forward of $1/f$ noise is that it is comprised of many charge fluctuators. We also used the notion of many fluctuators in our explanations. With regards to the questions we sought to answer, we have seen in Figs. 6.8, 6.11 and 6.14 that the auto-correlation displays a long decay, which is set by the reciprocal time; a quantity that we defined as $1/f_l$. We believe that this is a signature of $1/f$ noise since while all noise sources will cause the correlation to diminish to the un-correlated steady state, the minimum or low frequency which determines the decay time of the correlation function is clearly visible. This low frequency forms the lower limit of the $1/f$ behaviour in the model and since the frequency can be detected and determined we can say that this answers question (iii) and (iv). If such a low cut-off frequency did happen to exist and was intrinsic to the system, it would be detectable from the auto-correlation function as we have shown.

Since this work is theoretical, we are able to adjust parameters and, in so doing, are able to simulate situations that could only be arrived at experimentally by performing large numbers of experiments and sifting through each outcome, selecting those that fall within the regime that we are interested in. One such simulation is setting the t_1 time, the time at which the first photon is detected.

By sweeping across different t_1 times, we can see how the correlation behaves across the cut-off frequency boundary. Assuming that the $1/f$ noise has a low frequency cut-off, we have seen that both in the case of only $1/f$ noise (Fig. 6.20) and with an additional fluctuating charge interacting with the qubit (Fig. 6.22), that the forms of the curves do not change until the time that the initial photon was detected (t_1) has been reduced to below the reciprocal time of the minimum or low frequency cut-off. After comparing these two figures, we saw that the addition of a charge fluctuator was detectable as a feature on the graph, which is not quite a plateau, but could be described as a shoulder appears. Since the presence of the charge was detected we believe that we have answered question (*ii*) in the positive. With this set of simulations as with the those where we altered the cut-off frequencies, we were also able to answer question (*iii*), since we were able to detect the presence of a low cut-off frequency. Question (*iv*) was also answered since, by sweeping through the t_1 times, we were able to find the cut-off frequency. In a physical experiment, one would have to repeat the experiment many times to get the t_1 times by chance, but while being more difficult to get the data, the findings will be the same.

This set of simulations was also repeated for $1/f$, where we modelled the noise as not having a cut-off frequency. Again, as before, we have seen that both in the case of only $1/f$ noise (Fig. 6.15) and with an additional fluctuating charge interacting with the qubit (Fig. 6.24), that the form of the curves are a quick rise to a peak set by the noise amplitude and a long decay, which is limited by the length of the experiment. The forms of the curves are quite distinctive and it is possible to distinguish $1/f$ noise from the noise caused by fluctuating charges as can be seen by comparing Fig. 6.15 and Fig. 6.24 as well as Fig. 6.20 and Fig. 6.22. As such we believe that we have answered question (*i*) and (*ii*). Naturally, questions (*iii*) and (*iv*) not able to be answered by this simulation since there is no cut-off frequency.

The validity of the results in this section deserve to be discussed since it is an area of active debate as to the applicability of the quantum regression theorem (QRT) to a system that has a time dependent master equation. The concern is that one of the requirements of the QRT is that the system should be wholly Markovian, hence the time independence of the master equation. However, in the inclusion of $1/f$ noise into our model makes it partially non-Markovian and so there exists the possibility that the QRT may not be valid and yield un-physical results.

Let us examine this in further detail. Markovianity is the condition that environment has a sufficiently small correlation time, in comparison to the subsystem

to which the environment is attached, that we may say that the future evolution of the subsystem is dependent only on its current state. In addition, when we talk about a Markovian master equation we have also performed the Born approximation, where the density matrix of the subsystem and environment must be separable. It is shown in a paper by McCutcheon [99] that in fact it must be factorisable at all times. Let us follow the reasoning in the paper by using, as it is done there, a two-time correlation function

$$G(t,\tau) = \langle A(t+\tau) B(t) \rangle = Tr_{s+E} \left[A(t+\tau) B(t) \chi(0) \right], \tag{6.36}$$

where A and B are system operators and χ is the combined system and environment density matrix. Assuming a time independent Hamiltonian we can use the time evolution operators $A(t) = U^{\dagger}(t) A U(t)$, where $U(t) = e^{-iHt}$ and where we have used $U(t)$ as shorthand for $U(0,t)$ going from $t_1 = 0$ to $t_2 = t$. We can then define an operator that is similar to the reduced system density operator, which is called the reduced *effective* density operator

$$\Lambda(t,\tau) = Tr_E \left[U(\tau) B \chi(t) U^{\dagger}(\tau) \right]. \tag{6.37}$$

We can see that this is only slightly different from the reduced system density operator, which we shall refer to as the reduced *physical* density operator, defined as

$$\rho(t) = Tr_E \left[U(t) \chi(0) U^{\dagger}(t) \right]. \tag{6.38}$$

The QRT states that since these two operators are defined so similarly, they should have the same equations of motion, but with different initial conditions, i.e. $\Lambda(t,0) = B\rho(t)$.

However, this statement only makes sense if $U(0,t) = U(t,t+\tau)$, which in general in not true. If we have a time dependent Hamiltonian, the time evolution operator between times t_1 and t_2 is given by the expression,

$$U(t_1,t_2) = T e^{-i \int_{t_1}^{t_2} ds H(s)}, \tag{6.39}$$

where T is the time ordering operator. So for the QRT to hold true, the integral $\int_{t_1}^{t_2} ds H(s)$ must equal for all intervals between t_1 and t_2. That is to say, the Hamiltonian must be time independent for the QRT to be true. In our treatment of $1/f$ noise we used a stochastic Hamiltonian. The second order correlation function gives us the equation $\langle \sigma_+(0,t+\tau) \sigma_+(0,t) \sigma_-(0,t) \sigma_-(0,t+\tau) \rangle$, which

is the same as saying $Tr[\sigma_{-}U(t,t+\tau)\sigma_{-}\rho(t)\sigma_{+}U^{\dagger}(t,t+\tau)\sigma_{+}]$. We know that $\sigma_{-}\rho(t)\sigma_{+} = \rho_{gr} \times \langle\sigma_{-}(0,t)\sigma_{+}(0,t)\rangle$, this is the projection of the density matrix into the ground state multiplied by the probability of being in the excited state. The initial state of the system was also in the ground state. The issue here is that this is not necessarily the same state as $t = 0$ since the Hamiltonian has evolved in time, hence the relation $U(0,t) = U(t,t+\tau)$ may not hold. In general it does not hold. We have, in our model, implicitly assumed that the bath randomises itself instantaneously after the photon detection event. The system evolves in a non-Markovian way, but is always reset to a Markovian one, since the randomisation of the bath means that there is no memory of the previous state of the system. If we assume that the assumption is valid, then the system has no dependence on detection at time (t) and the QRT can be used. This is due to $U(t,t+\tau) \to U(0,\tau)$ so we have the situation that we start again from $t = 0$ and $U(0,t) = U(0,\tau)$. In the case that the assumption is invalid, this requires a re-thinking of the model to include a memory term in the master equation that extends over photon detection events.

Using the time-convolutionless projection operator method[9], the paper goes on to define a super operator that projects from the total density matrix to the density matrix of the subsystem, thus allowing us to encapsulate all the relevant parts of the combined system dynamics into the subsystem part.

$$\mathcal{P}\Upsilon(t,\tau) = Tr_E[\Upsilon(t,\tau)] \otimes \rho_R = \Lambda(t,\tau) \otimes \rho_R, \tag{6.40}$$

where $\Upsilon(t,\tau) = U(\tau)B\chi(t)U^{\dagger}(\tau)$ for the effective density matrix and

$$\mathcal{P}\upsilon(t) = Tr_E[\upsilon(t)] \otimes \rho_R = \rho(t) \otimes \rho_R, \tag{6.41}$$

where $\upsilon(t) = U(t)\chi(0)U^{\dagger}(t)$ for the physical density matrix. It is for this reason that $\mathcal{P}\rho$ often called the relevant part of the density matrix in contrast to the other super operator $\mathcal{Q}$, which projects onto the irrelevant part of the density matrix.

$$\mathcal{Q} = \mathbb{1} - \mathcal{P}$$

These super operators also follow the relationships

$$\begin{aligned} \mathcal{P}^2 &= \mathcal{P} \\ \mathcal{Q}^2 &= \mathcal{Q} \\ \mathcal{Q}\mathcal{P} = \mathcal{P}\mathcal{Q} &= 0. \end{aligned} \tag{6.42}$$

Using this approach the paper goes on to derive in great mathematical detail the equations of motion for the system, which consist of a homogeneous term and inhomogeneous term. The homogeneous term is a function of $\mathcal{P}$, while the inhomogeneous term is a function of $\mathcal{P}$ and $\mathcal{Q}$. This inhomogeneous term is zero in the case that the physical density operator factorises from the environment (Born approximation) at all times. This means that the equations of motion for the effective density operator and the physical density operator become identical i.e. $U(0,t) = U(t,t+\tau)$. It is therefore this inhomogeneous term that dictates whether the QRT can be made. The case that the Born approximation is only made at $t = 0$ is considered and it is found that by making the Markov approximation, the inhomogeneous term is zero and we get the same result as if the Born approximation was made for all times. The Markov approximation implicitly applies the Born approximation for all times. Therefore a Markovian system allows the QRT to be made. The question is then asked, 'Is the converse true?'. If we have a non-Markovian system, are we by using the QRT, implicitly imposing the Markovianity condition onto the system?

The paper then considers the case that if the QRT is used on a non-Markovian system, can it be shown that some of the results of a theoretical work are un-physical. The system under consideration in the paper is a driven quantum dot with a non-Markovian phonon environment. The system dynamics are solved in the three cases of explicitly using the Markov approximation, using the fully non-Markovian theory and lastly using the QRT, which sets the inhomogeneous term to zero without using the Markov approximation. When calculating the first order correlation function with the three cases, the QRT method peforms well against the fully Markovian method, showing features in common with the fully non-Markovian theory. However, while the real part of the solution is in good agreement with the fully non-Markovian theory, there occurs a sign error in the imaginary part. This leads to an emission spectrum with incorrect sidebands.

This is precisely the problem in this chapter. No Markov approximation was made in the derivation of the master equation for the $1/f$ noise, but the QRT was used. It is possible then, that the results may be un-physical. This un-physicality is unfortunately difficult to detect as the results make intuitive sense. This is in contrast to the case discussed in the paper, where the side bands in the emission spectrum were clearly on the wrong side. In the paper, the time-convolutionless projection operator method yielded the correct results and so this would seem a good starting point to verify or correct the results presented in this chapter.

CHAPTER 7

Entanglement in the face of correlated noise

7.1 Introduction

In chapters 5 and 6 we have discussed the effect of charge fluctuators and $1/f$ noise on qubits. We have used the quantum dots as probes of correlated noisy environments. Now we are going to switch to investigating how this charge noise affects correlated qubits. That is to say, how charge noise affects the amount of entanglement held between two qubits. The motivation behind this is as follows. In section 4.4, we discuss the circuit model of quantum algorithms and alluded to there being another way. In the early days of the development of quantum computing as an idea, it was thought that to have a set of universal quantum gates, entanglement would need to be generated in a deterministic way. However, there are some techniques that allow entanglement to be generated stochastically. One such technique is measurement-based quantum computing [8, 100]. Also known as one-way quantum computing, it allows entanglement to be generated before-hand and stored until needed, thus avoiding the need to create entanglement during the quantum algorithm that is being performed, and lowers failure rate of the procedure as any problems with the entanglement process can be corrected before it is needed as a resource.

Generating entanglement in this way, as the name of the method suggests, is achieved via a measurement. The qubits do not need to interact directly as they would in other system architectures or indeed be in close proximity to each other. We have said a lot very quickly just now, so let's slow down and ask some questions. The first question to ask and answer is, what is entanglement?

Entanglement is the property of two or more particle being able to be described

by a single wavefunction that cannot be re-written as a product of states [71]. An example of such a state is

$$\frac{|0\rangle_A|0\rangle_B + |1\rangle_A|1\rangle_B}{\sqrt{2},} \tag{7.1}$$

where A and B represent the two qubits. It can be seen that the two qubit states cannot be separated into two single particle states in the way that the following bipartite state can

$$\frac{|0\rangle_A|0\rangle_B + |0\rangle_A|1\rangle_B}{\sqrt{2}} = \frac{1}{\sqrt{2}}\left(|0\rangle_A \otimes (|0\rangle_B + |1\rangle_B)\right). \tag{7.2}$$

7.1.1 Path Erasure

Another question to ask is, how can measuring a photon generate entanglement? Let us consider a thought experiment showing the steps needed to achieve entanglement between two qubits. It is best to begin with a structure for our qubits.

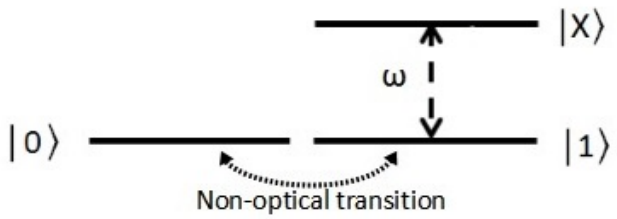

Figure 7.1: 'L' shaped electronic configuration [101, 102]

The qubits have an 'L' shape energy structure and it is proposed that the system is perfect such that no photon may be lost. Both qubits are prepared in the initial superposition of the ground states ($|0\rangle$ and $|1\rangle$).

If we stimulate the qubits simultaneously by a laser, as they de-excite it is possible to learn the state of the overall system without learning the states of the individual qubits. To be clearer, the experimental set up is such that if a qubit should decay and emit a photon, then the this may be detected, without the knowledge of which

qubit has decayed, thus giving us an entangled state in a superposition of having and not having decayed.

One possible way in which this may be achieved is via a Hong Ou Mandel style set up [103, 104] allowing, what is known as path erasure. A typical set up is shown in Fig. 7.2. The two qubits are separated from the two detector by a 50:50 beam splitter. The rationale behind this design is that should one of the two qubits decays and emit a photon, then there is a 50 % chance that the photon will pass through the beam splitter and be detected by the first detector and a 50 % chance of it being reflected and detected by the other. In doing so, there is no way that the detected photon can be known to have emitted from the first or second qubit.

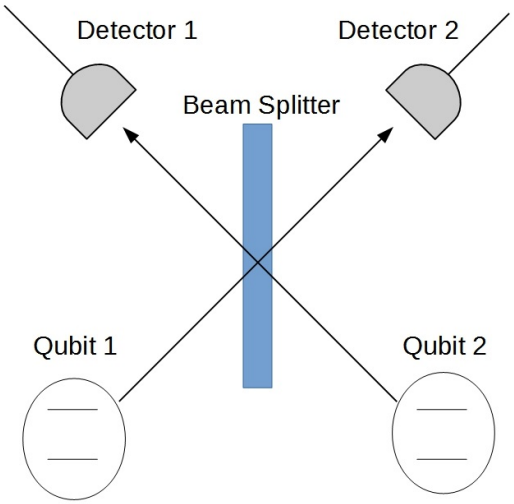

Figure 7.2: A typical set up for path erasure

The procedure then is to resonantly excite both qubits with a π pulse. This means that a laser pulse is given so that it performs half a Rabi cycle. As a result, each of the qubits is now in a superposition of the ground and excited state $(\frac{1}{\sqrt{2}}(|0\rangle + |X\rangle))$ and the overall state is given by [12, 16, 101, 102]:

$$1/2\left(|00\rangle + |0X\rangle + |X0\rangle + |XX\rangle\right). \tag{7.3}$$

Now all that is left to do is to wait for a detection event to occur. In order for the entangled state to be generated it is required that one and only one photon be detected. The reason for this is as follows. Looking at the overall state of the system it can be seen that the first term contains no excitations and so in order for

the system to be known to be in this state, no photons at all should be detected. Conversely, the last term contains two excitations and for the system to be known to be in this state, two photons must be seen. In both of these scenarios, there can be no doubt as to the final state of the system. However, if one and only one photon is observed, then due to path erasure it is not possible to know which of the two qubits emitted the photon.

It must be taken into account that the beam splitter will give a reflected photon a phase shift and so the detection creation operators before the beam splitter ($a_L^\dagger$ and $a_R^\dagger$) must be decomposed into post-beam splitter left ($b_L^\dagger$) and right ($b_R^\dagger$) detector creation operators with an i phase shift for a reflected photon.Let's take the case that only one photon is emitted. Only the $|X0\rangle$ and $|0X\rangle$ are necessary for treatment. Once the photon has been emitted, but before the beam splitter we have

$$\left(|0X\rangle + |X0\rangle\right)|vac\rangle \rightarrow \left(|01\rangle a_R^\dagger + |10\rangle a_L^\dagger\right)|vac\rangle, \tag{7.4}$$

where $|vac\rangle$ is the electromagnetic vacuum state. After the beam splitter, we must redefine our operators,

$$a_L^\dagger \rightarrow 1/\sqrt{2}\left(ib_L^\dagger + b_R^\dagger\right), a_R^\dagger \rightarrow 1/\sqrt{2}\left(b_L^\dagger + ib_R^\dagger\right). \tag{7.5}$$

Thus after the beams splitter, the overall state of the system becomes

$$\begin{aligned} & |01\rangle\left(b^\dagger{}_L + ib^\dagger{}_R\right)|vac\rangle + |10\rangle\left(ib^\dagger{}_L + b^\dagger{}_R\right)|vac\rangle \\ = \; & \left(|01\rangle + i|10\rangle\right)b^\dagger{}_L|vac\rangle + \left(i|01\rangle + |10\rangle\right)b^\dagger{}_R|vac\rangle. \end{aligned} \tag{7.6}$$

It can be seen from this that there are in fact two maximally entangled states arising from the detection of a photon in the left detector ($(|01\rangle + i|10\rangle)$) and in the right detector ($(i|01\rangle + |10\rangle)$).

Such generation of entangled pairs of qubits is the building block for the creation of much larger and more complex entangled blocks of qubits. These are known as graph and cluster states, which can be used up as the algorithm propagates, through a series of measurements. Though this method is only 50% successful, it is heralded and this is enough to build graphs.

7.1.2 Graph states

A graph is a mathematical diagram that consists of points/vertices connected by lines/edges [8, 12, 16, 105]. This tool has been used in the theory of quantum computing by stating that each of the points/vertices is representative of a qubit in the $|+\rangle = \frac{1}{\sqrt{2}}(|0\rangle + |1\rangle)$ state and the lines/edges joining then is a CPHASE operation, which was defined in section 4.4.1. It is not then a far logical leap to say that the state of the system that corresponds to the graph in question is called a graph state.

A pedagogical example of graphs states is given with the simplest of graph states, two qubits. Two qubits prepared in the plus state and the CPHASE operation between them, which would flip the sign on the $|11\rangle$ component of the state. If one of these two qubits was not in the $|+\rangle$ state, but instead was in some other arbitrary state, then this would not be a graph state, for the simple reason that we defined such a state to have vertices in the $|+\rangle$ state. The overall state of this system is given by:

$$|G^{'}\rangle = 1/\sqrt{2}\,(\alpha|00\rangle + \alpha|01\rangle + \beta|10\rangle - \beta|11\rangle) \tag{7.7}$$

Let us now measure out the first qubit, which was prepared in the arbitrary state. If we measure it in the X basis, then the two possible outcomes are the $|+\rangle$ and $|-\rangle$ states (if we recall the Bloch sphere, these would correspond the antipodean of the X axis). The second qubit that was initially prepared in the $|+\rangle$ state has now become a rotated version of the arbitrary state that the first qubit was prepared in. This is important, since as we discussed in section 4.4, quantum gates are rotations around the Bloch sphere, where the Z-Y decomposition shows that any single qubit quantum gate may be represented by three rotations in the Bloch Sphere [71].

7.2 Measures of entanglement

As stated previously, entanglement is an extremely important resource in quantum computing and quantum information processing in general. It is quite useful therefore to be able to measure and quantify it. The four most common methods and techniques for doing so are the partial-transpose criterion, the Von Neumann entropy, the concurrence and the entanglement of formation. Entanglement is more difficult to determine for mixed states than for pure states. The reason for this is that it becomes more difficult to define a separability condition. For pure states, we can say that a multiparite state is separable if the it can be written as a tensor product of subsystem states i.e. a separable state is a product state. How-

ever, for a mixed state this cannot be the case since, by definition, a mixed state is a sum of pure states, so a separable state is no longer a product state. Instead we must make a new definition. Since a mixed state is mixture of pure states, a mixed state that is not entangled should be a mixture of product states. We can then say that a mixed state is entangled if it is not able to be written as a sum of product states

$$\rho = \sum_k p_k \left(\rho_k^{(1)} \otimes \rho_k^{(2)} \right), \tag{7.8}$$

where the superscripts (1) and (2) correspond to qubit one and two and p_k must sum to 1. Each of ρ_k are pure states [12, 106]. An entangled mixed state must then be defined as the case where this condition is not met. The negative statement makes it difficult to be certain that a solution cannot be constructed. In addition, pure state entanglement means that the individual subsystems are in mixed states. This implies that a mixed state could be a subsystem of an entangled, larger system like the environment. Determining the entanglement of a mixed state, then is determining the entanglement of a subsystem within an entangled system, which should intuitively be more complicated than just determining the entanglement of a system.

7.2.1 Partial-transpose criterion

The partial-transpose criterion does not yield a numerical result and so isn't really a measure of entanglement, but useful as an indicator of it. We know that a two qubit density matrix can be written as a tensor product of the individual systems

$$\rho = \sum_k p_k \left(\rho_k^{(1)} \otimes \rho_k^{(2)} \right). \tag{7.9}$$

We can transpose one of the qubit density matrices, i.e. perform a partial transpose of the system

$$\rho' = \sum_k p_k \left(\left(\rho_k^{(1)} \right)^T \otimes \rho_k^{(2)} \right) \tag{7.10}$$

and if ρ' has any negative eigenvalues, then it shows that ρ must have been entangled, since a separable system must have positive eigenvalues. As an example, let $\rho^{(1)} = A|1\rangle\langle 1| + B|1\rangle\langle 0| + C|0\rangle\langle 1| + D|0\rangle\langle 0|$ and $\rho^{(2)} = E|1\rangle\langle 1| + F|1\rangle\langle 0| + G|0\rangle\langle 1| + H|0\rangle\langle 0|$.

In the computational basis, we can write this as a matrix

$$\left(\rho_k^{(1)} \otimes \rho_k^{(2)}\right) = \begin{pmatrix} AE & AF & BE & BF \\ AG & AH & BG & BH \\ CE & CF & DE & DF \\ CG & CH & DG & DH \end{pmatrix} \tag{7.11}$$

and

$$\left(\left(\rho_k^{(1)}\right)^{(T)} \otimes \rho_k^{(2)}\right) = \begin{pmatrix} AE & AF & CE & CF \\ AG & AH & CG & CH \\ BE & BF & DE & DF \\ BG & BH & DG & DH \end{pmatrix}. \tag{7.12}$$

A maximally entangled density matrix looks like $\frac{1}{2}|10\rangle\langle 10| + \frac{1}{2}|01\rangle\langle 01| \pm \frac{1}{2}|10\rangle\langle 01| \pm \frac{1}{2}|01\rangle\langle 10|$, which means we can write

$$\left(\rho_k^{(1)} \otimes \rho_k^{(2)}\right) = \begin{pmatrix} 0 & 0 & 0 & 0 \\ 0 & 1/2 & \pm 1/2 & 0 \\ 0 & \pm 1/2 & 1/2 & 0 \\ 0 & 0 & 0 & 0 \end{pmatrix}, \tag{7.13}$$

which has eigenvalues $(1, 0, 0, 0)$ and

$$\left(\left(\rho_k^{(1)}\right)^{(T)} \otimes \rho_k^{(2)}\right) = \begin{pmatrix} 0 & 0 & 0 & \pm 1/2 \\ 0 & 1/2 & 0 & 0 \\ 0 & 0 & 1/2 & 0 \\ \pm 1/2 & 0 & 0 & 0 \end{pmatrix}, \tag{7.14}$$

which has eigenvalues $(-\frac{1}{2}, \frac{1}{2}, \frac{1}{2}, \frac{1}{2})$. The negative eigenvalue shows that the state was entangled. We can see from Eq. 7.11 and 7.12 that, assuming all elements are real, the only elements that change during the partial transpose lie on the anti-diagonal. This makes perfect sense, since the four maximally entangled states, also known as Bell states, have elements on the anti-diagonal in the computational basis:

$$\begin{aligned} |\,\Psi^{\pm}\rangle &= \frac{1}{\sqrt{2}}\left(|\,10\rangle \pm |\,01\rangle\right) \\ |\,\Phi^{\pm}\rangle &= \frac{1}{\sqrt{2}}\left(|\,11\rangle \pm |\,00\rangle\right) \end{aligned} \tag{7.15}$$

and so for each of the Bell states, the partial transpose criterion will give negative eigenvalues.

7.2.2 Von Neumann entropy

Entropy is a way of measuring the amount of disorder in a system, but it can also tell us about the amount of information we have. In a pure state, we know that there is no uncertainty about the state, but there is in a mixed state. The way that classical entropy is measured is by the Boltzmann equation, which tells us that the amount of entropy in a system in related to the number of microstates that form a particular macrostate. When dealing with a classical bit, there are two possible states and so information theorists developed the Shannon entropy,

$$S(A) = -\sum_{A} \kappa_A log_2 \kappa_A, \tag{7.16}$$

where κ_i are the probabilities of the system. For a quantum system, the probabilities are described by the density matrix [12, 107],

$$S(\rho) = -\mathrm{Tr}\left(\rho log_2 \rho\right) = -\sum_{i} \lambda_i log_2 \lambda_i, \tag{7.17}$$

where λ_i are the eigenvalues of the system. Taking the partial trace of a two qubit system, we know that if the state was maximally entangled that we will get a mixed state. Taking the example of the maximally entangled state: $\frac{1}{2}|10\rangle\langle 10| + \frac{1}{2}|01\rangle\langle 01| \pm \frac{1}{2}|10\rangle\langle 01| \pm \frac{1}{2}|01\rangle\langle 10|$, which equivalent to the matrix

$$\left(\rho_k^{(1)} \otimes \rho_k^{(2)}\right) = \begin{pmatrix} 0 & 0 & 0 & 0 \\ 0 & 1/2 & \pm 1/2 & 0 \\ 0 & \pm 1/2 & 1/2 & 0 \\ 0 & 0 & 0 & 0 \end{pmatrix}. \tag{7.18}$$

Performing the partial trace over $\rho^{(2)}$ we get

$$\left(\rho_k^{(1)} \otimes \rho_k^{(2)}\right) = \begin{pmatrix} 1/2 & 0 \\ 0 & 1/2 \end{pmatrix}, \tag{7.19}$$

which has eigenvalues $(\frac{1}{2}, \frac{1}{2})$ and so $\mathrm{S}(\rho^{(1)}) = 1$. This is the maximum value that the entropy can take and any pure state, will give a result of zero. While measuring the entropy isn't really a measure of entanglement itself, it does give a result for a related quantity and is good in the case of pure states.

7.2.3 Concurrence and the entanglement of formation

The Von Neumann entropy requires pure states, but our first true measure called the concurrence does not. Instead of taking the partial trace, we now consider the full density matrix. To find it, we must find the eigenvalues, but we must prepare the density matrix as

$$\rho\tilde{\rho} = \rho\sigma_{y_{(1)}} \otimes \sigma_{y_{(2)}}\rho^*\sigma_{y_{(1)}} \otimes \sigma_{y_{(2)}}, \tag{7.20}$$

where $\sigma_{y_{(i)}}$ are the Pauli Y matrices for qubits 1 and 2. The concurrence is then found by taking the eigenvalues and square rooting them. The concurrence is then

$$C = \beta_1 - \beta_2 - \beta_3 - \beta_4, \tag{7.21}$$

where β_i are the square rooted eigenvalues in descending order. This doesn't reduce to the von Neumann entropy, but the two are related by

$$S(\rho) = -Clog_2(C) - (1-C)log_2(1-C). \tag{7.22}$$

Systems that have noise processes, dephase them and so the entanglement generated may not be maximal. If we make many partially entangled pairs, it is possible to increase the entanglement of a single pair by cannibalising the entanglement of the others. This process is called distillation.

A related measure to the concurrence is the entanglement of formation, which reduces to the von Neumann entropy in the case of pure two qubit states [108]. It was first shown by Bennett *et al.* [109] that it is possible to take many pairs of mixed entangled states and distil them into a smaller number of pairs with a greater entanglement using only local operations and classical communication (LOCC). The ratio of the number of distilled states (n) to the number of undistilled states (m), which we started with can be calculated in the case that the undistilled states are pure and is limited by the entanglement of formation. That is to say that the ratio or yield of distilled states depends on the protocol used and that the maximum number of states or the maximum distillable entanglement is given by the entanglement of formation. In the case of mixed entangled states, the calculation for the ratio is not known, but is still bounded by the entanglement of formation [109, 110]. The concurrence and entanglement of formation are related through

$$E_F = -\tilde{C}Log_2(\tilde{C}) - (1-\tilde{C})Log_2(1-\tilde{C}), \tag{7.23}$$

where $\tilde{C} = \frac{1+\sqrt{1-C^2}}{2}$. These are the two measures that we will be using.

7.3 Model

THE SYSTEM we shall study here consists of two qubits, where each qubit consists of three levels arranged in an 'L' shape as shown in Fig. 7.3.

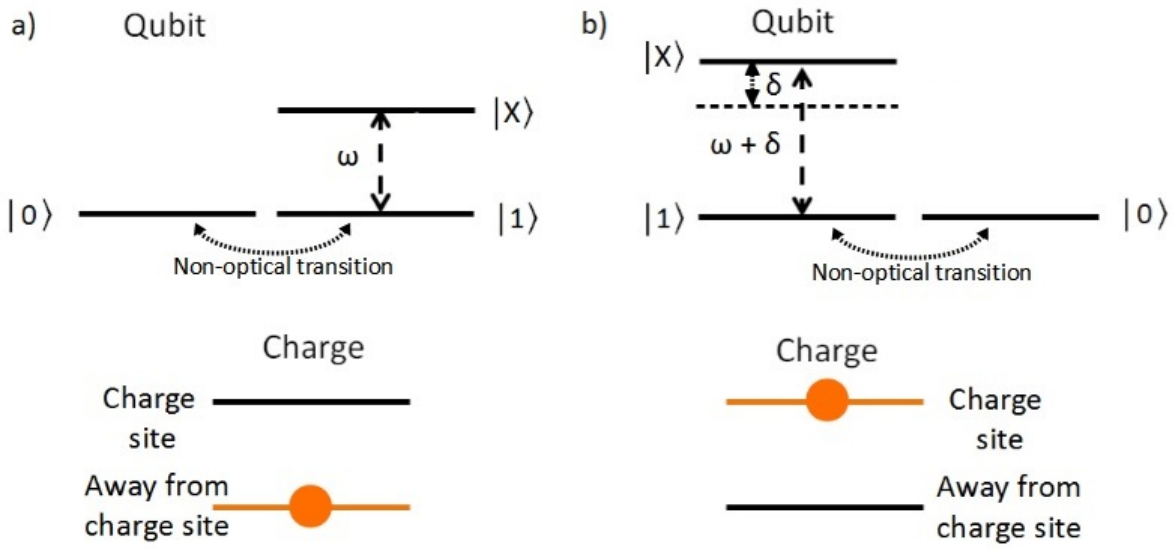

Figure 7.3: The qubit energy shift for an unoccupied (left) and charged (right) trap. The exciton creation energy is denoted by ω and the charge-qubit interaction strength is δ.

A possible physical realisation of this system is based on the exciton system described in Chapter 4, shown in Fig. 4.3 and again in Fig. 7.4.

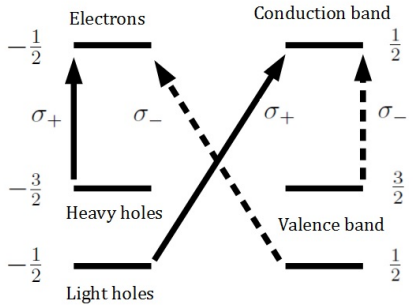

Figure 7.4: The direction of the polarised light add or take away a spin of 1 from the ground states unless there is heavy hole light hole mixing.

We see that there are six possible states, two electronics conduction band states,

two heavy hole valence band states and two light hole valence band states, the two types of holes being separated by an energy gap. In self assembled quantum dots heavy holes and light holes are separated significantly and so we can in this instance ignore the formation of light holes. We then have four levels, two in the conduction band with spin $\pm\frac{1}{2}$ and two in the valence band of $\pm\frac{3}{2}$. We have discussed in section 4.2, that circularly polarised light can impart/take away a spin of 1 to/from the system. If we use a single polarisation, σ_+ for example, we can only create an exciton from the $-\frac{3}{2}$ state to the $-\frac{1}{2}$ state. If we dope the conduction band with an electron, then if it is in the $-\frac{1}{2}$ spin state, then we cannot create an exciton, but we can if it is in the $\frac{1}{2}$ spin state. This phenomenon is called Pauli blocking and is the basis of the L-shaped or trion system. We define the $-\frac{1}{2}$ spin state of the conduction electron as $|0\rangle$ and the $\frac{1}{2}$ spin state as $|1\rangle$. Only from the $|1\rangle$ state is the excited (trion) state accessible. The dephasing between the two ground states is ignored since it is a spin transition, which in general has a much longer dephasing time (micro seconds)[111] than the 50 ns of the experimental duration and excitonic dephasing times (nanosecond)[112]. The three orders of magnitude difference between the time scales should mean there should be little dephasing between the ground states. The generalised Hamiltonian is almost the same as in Eq. 6.6, but requires redefining some of the operators, has no laser driving and the charges are no no longer classical

$$\begin{aligned} H &= \sum_i \frac{\omega_i}{2}\theta_i + \sum_j \frac{\epsilon_j}{2}\xi_j \\ &\quad + \sum_{\mathbf{k},i} \beta_{i,\mathbf{k}}(a^\dagger_{\mathbf{k}}\sigma_{-,i} + a_{\mathbf{k}}\sigma_{+,i}) \\ &\quad + \sum_{i,j} \frac{\delta_{ji}}{2}\mu_{ji} \end{aligned} \tag{7.24}$$

With the new definitions of operators, the first term describes the energy levels ω_i of the QDs and θ_i is the operator for the ith QD, which in the computational basis for two qubits and a charge is given by

$$\theta \equiv \begin{pmatrix} 1 & 0 & 0 \\ 0 & 0 & 0 \\ 0 & 0 & 0 \end{pmatrix} \ , \ \theta_1 \equiv \mathbb{1}_2 \otimes \mathbb{1}_3 \otimes \theta \ , \ \theta_2 \equiv \mathbb{1}_2 \otimes \theta \otimes \mathbb{1}_3 \tag{7.25}$$

The second term represents the energy levels ϵ_i of the charges and the ξ_i are the states which the charges can take. The third term describes the interaction of the QD TLSs with a photonic bath with wave vectors $\mathbf{k}$ with creation and annihilation

operators $a_{\mathbf{k}}^{\dagger}$ and $a_{\mathbf{k}}$ that interact with a strength $\beta_{i,\mathbf{k}}$. The operator σ_- is given by

$$\sigma_- \equiv \begin{pmatrix} 0 & 0 & 0 \\ 1 & 0 & 0 \\ 0 & 0 & 0 \end{pmatrix} \ , \ \sigma_{-,1} \equiv \mathbb{1}_2 \otimes \mathbb{1}_3 \otimes \sigma_- \ , \ \sigma_{-,2} \equiv \mathbb{1}_2 \otimes \sigma_- \otimes \mathbb{1}_3 \tag{7.26}$$

and σ_+ is given by

$$\sigma_+ \equiv \begin{pmatrix} 0 & 1 & 0 \\ 0 & 0 & 0 \\ 0 & 0 & 0 \end{pmatrix} \ , \ \sigma_{+,1} \equiv\equiv \mathbb{1}_2 \otimes \mathbb{1}_3 \otimes \sigma_+ \ , \ \sigma_{+,2} \equiv\equiv \mathbb{1}_2 \otimes \sigma_+ \otimes \mathbb{1}_3 \tag{7.27}$$

The fourth term describes the interaction δ_{ji} between the jth charge and the ith QD, where μ_{ji} is of the form $\mu_{11} = \delta_{11}\left(\frac{1}{2}\left(\mathbb{1}_2 + \sigma_z\right) \otimes \mathbb{1}_3 \otimes \theta_i\right)$, $\mu_{12} = \delta_{12}\left(\frac{1}{2}\left(\mathbb{1}_2 + \sigma_z\right) \otimes \theta_i \otimes \mathbb{1}_3\right)$. To build the master equation, we begin from Eq. 2.51. We have previously used the secular approximation, where terms having different frequencies ω and $\omega^{'}$ were neglected. This was done, because $\omega - \omega^{'}$ much faster than the dynamics of the system. We will perform a partial secularisation, where terms that are twice the frequencies of ω_i, i.e. when $\omega_i = -\omega_i^{'}$, will be neglected. Terms where the frequencies come from different qubits will be kept if $\omega_i - \omega_i^{'}$ does not oscillate faster than the system dynamics. In this way there will be cross terms, which were not present in chapter 5, the dissipator will be given by

$$\begin{aligned} D\left(\rho\right) &= \gamma_1 \left(\sigma_{1,-} \rho\left(t\right) \sigma_{1,+} - \frac{1}{2} \sigma_{1,+} \sigma_{1,-} \rho\left(t\right) - \frac{1}{2} \rho\left(t\right) \sigma_{1,+} \sigma_{1,-} \right) \\ &+ \gamma_2 \left(\sigma_{2,-} \rho\left(t\right) \sigma_{2,+} - \frac{1}{2} \sigma_{2,+} \sigma_{2,-} \rho\left(t\right) - \frac{1}{2} \rho\left(t\right) \sigma_{2,+} \sigma_{2,-} \right) \\ &+ e^{i\omega t} \sqrt{\gamma_1 \gamma_2} \left(\sigma_{1,-} \rho\left(t\right) \sigma_{2,+} - \frac{1}{2} \sigma_{2,+} \sigma_{1,-} \rho\left(t\right) - \frac{1}{2} \rho\left(t\right) \sigma_{2,+} \sigma_{1,-} \right) \\ &+ e^{-i\omega t} \sqrt{\gamma_1 \gamma_2} \left(\sigma_{2,-} \rho\left(t\right) \sigma_{1,+} - \frac{1}{2} \sigma_{1,+} \sigma_{2,-} \rho\left(t\right) - \frac{1}{2} \rho\left(t\right) \sigma_{1,+} \sigma_{2,-} \right) \end{aligned} \tag{7.28}$$

where $\omega = \omega_2 - \omega_1$ and ω_i are the energy differences between the ground states and the excited state X. In the case where there is no charge interaction and the qubits are identical, these energies are the same. Using the procedure that we outlined in chapter 3 for the construction of the unconditional master equation, we have a jump

operator that is time dependent and given by

$$\begin{aligned} J^{-}\rho = \gamma_1 \left(\sigma_{1,-}\rho\left(t\right)\sigma_{1,+}\right) \\ +\gamma_2 \left(\sigma_{2,-}\rho\left(t\right)\sigma_{2,+}\right) \\ +e^{i(\omega)t}\sqrt{\gamma_1\gamma_2}\left(\sigma_{1,-}\rho\left(t\right)\sigma_{2,+}\right) \\ +e^{-i(\omega)t}\sqrt{\gamma_1\gamma_2}\left(\sigma_{2,-}\rho\left(t\right)\sigma_{1,+}\right) \end{aligned} \tag{7.29}$$

Remembering that the exponentials came from Eq. 2.32, we can remove this time dependence by switching back into Schrödinger picture.

$$\begin{aligned} J^{-}\rho = \gamma_1 \left(\sigma_{1,-}\rho\left(t\right)\sigma_{1,+}\right) \\ +\gamma_2 \left(\sigma_{2,-}\rho\left(t\right)\sigma_{2,+}\right) \\ +\sqrt{\gamma_1\gamma_2}\left(\sigma_{1,-}\rho\left(t\right)\sigma_{2,+}\right) \\ +\sqrt{\gamma_1\gamma_2}\left(\sigma_{2,-}\rho\left(t\right)\sigma_{1,+}\right) \end{aligned} \tag{7.30}$$

At this point we could do the path erasure procedure and we would generate data, calculate the concurrence and entanglement of formation for each run and then average a large number of these runs to obtain an average concurrence and entanglement of formation for a given set of parameters. However, we realised that doing single trajectories was in fact unnecessary due to the post selection procedure. In our path erasure experiment, we discard all trajectories where there has been two photons detected or none at all. Our initial conditions for these simulations is always

$$\begin{aligned} \rho(0) &= |xx\rangle\langle xx| + |xx\rangle\langle x0| + |x0\rangle\langle xx| + |x0\rangle\langle x0| \\ &+ |0x\rangle\langle 0x| + |0x\rangle\langle 00| + |00\rangle\langle 0x| + |00\rangle\langle 00|, \end{aligned} \tag{7.31}$$

where $|x\rangle$ is the optically excited state and $|0\rangle$ is the down state. In the event that there are no photons detected, then we end up in the state $|00\rangle\langle 00|$, because that is the only state without an excitation. In the event that there are two photons detected, then we must have been in the doubly excited state and so we fall into doubly up state $|11\rangle\langle 11|$. If we see exactly one photon detected, then we end up in the entangled state $(|10\rangle\langle 10| + |10\rangle\langle 01| + |01\rangle\langle 10| + |01\rangle\langle 01|)$. These three results have no overlapping elements. As a result we can use the unconditional master equation, we get the outcomes of all three results, but we can subtract the $|00\rangle\langle 00|$ and the $|11\rangle\langle 11|$ elements out of the density, since we know for sure that they do not contain information about the one detection case. The density matrix must be renormalised, but now we have the average result for obtaining a single detection

event.

7.4 Results

In order for the concurrence to show a non-zero result, there must be a single photon detected, which we know will project our system into an entangled state. The impact of a charge fluctuating near our qubits will be detrimental to the amount of entanglement generated and we shall investigate the degree to which does this. Let us begin by thinking of a charge that does not fluctuate, but is always in the vicinity of the qubits. In order to differentiate the photons coming from the two qubits and therefore degrading the generated entanglement by allowing us to say that it was more likely that the photon came from one rather than the other, we shall have a charge interact with the first qubit, but not the second. What we expect to happen in this case is that as the Stark shift from the charge will alter the frequency of the emitted photon from one qubit thus allowing the emitted photons form this system to be more distinguishable. As the charge interaction strength or Stark shift increases, which would correspond to moving the charge closer to the qubit, we should see that the system should become more distinguishable and the concurrence should decrease.

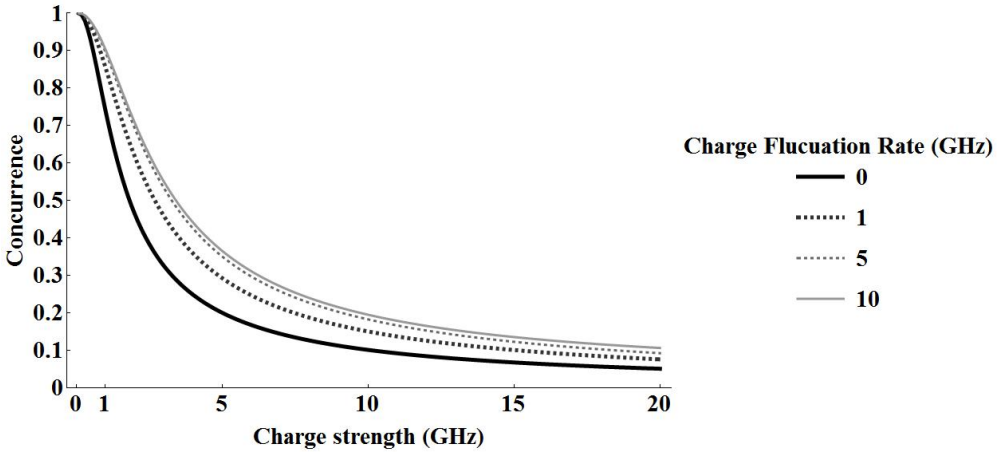

Figure 7.5: Graph showing the concurrence between two qubits subject to charge noise. The charge interaction strength is varied within each curve. The fluctuation rate is also varied, but a single fluctuation rate is used per curve. The decay rates for the qubits are both 1 GHz. The charge interaction strength in each curve is swept between 0 and 20 GHz. The graph shows four curves for 0, 1, 5 and 10 GHz.

Indeed, Fig. 7.5 shows that as we increase the charge interaction strength, we see

that the concurrence decreases as expected. From the graph, it seems that as the charge strength reaches infinity, the concurrence will reach zero. This is again an expected result, as this would make the emitted photons from the two qubit at increasingly different frequencies and so we could say with an increasingly high degree of certainty that the photon came from the other qubit. We also see that as we increase the charge fluctuation rate, the concurrence increases. We first came across this effect in Chapter 5, where we saw that as the charge fluctuation rate was increased, the effect of the charge was lessened or averaged out to half the detuning given by the Stark shift. Due to the way that we defined the operator θ, this will be $\frac{1}{2}\delta_{ij}$

7.4.1 Mixed charge state

Let us now change the initial conditions of our system. Since we don't know whether the charge is present or not at the initial time of the experiment, we will begin in a mixed state for the charge with a probability of 0.5 for each state.

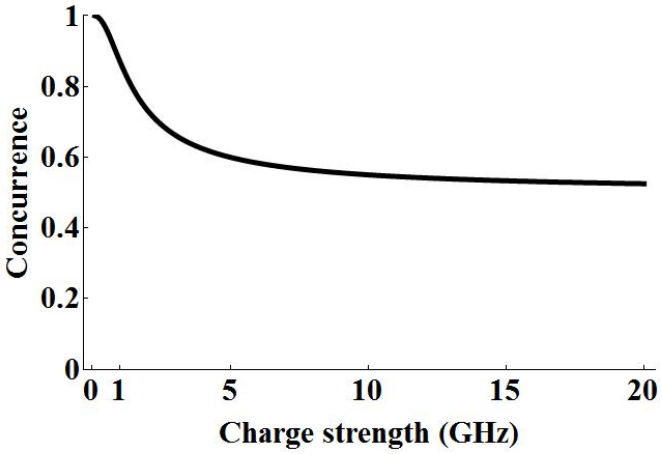

Figure 7.6: Graph showing the concurrence between two qubits with a charge interacting with only the first qubit. The varying quantity is the charge interaction strength. The decay rates for the qubits are both 1 GHz and the charge fluctuation rate is 0 GHz. The interaction strength is swept between 0 and 20 GHz.

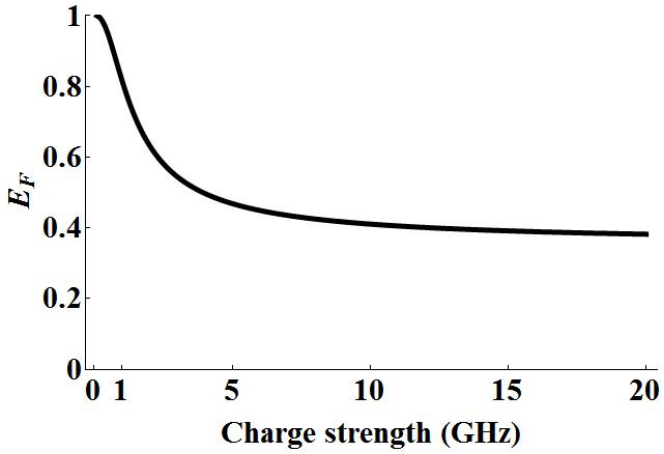

Figure 7.7: Graph showing the entanglement of formation between two qubits with a charge interacting with only the first qubit. The varying quantity is the charge interaction strength. The decay rates for the qubits are both 1 GHz and the charge fluctuation rate is 0 GHz. The interaction strength is swept between 0 and 20 GHz.

As was suspected, the concurrence asymptotically reaches 0.5. Since the charge only interacts with one qubit, the point at which the qubits are indistinguishable in Figs. 7.6 and 7.7 is at zero charge strength, where we see the peak. Now that we have seen how the charge interaction strength affect the entanglement, let us make the charge fluctuate and explore how the rate of fluctuation affects it.

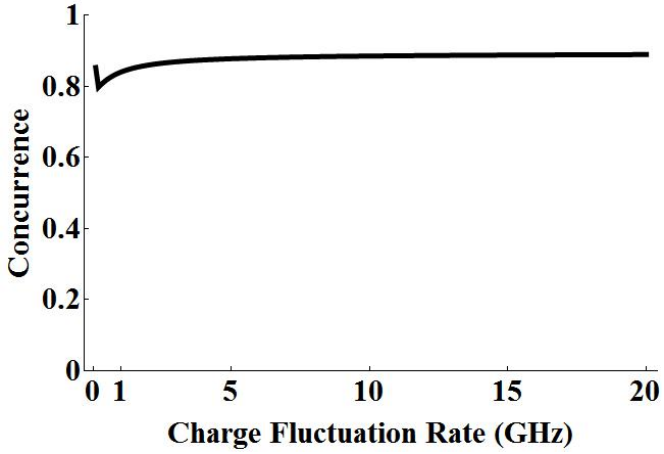

Figure 7.8: Graph showing the concurrence between two qubits with a charge interacting with only the first qubit. The varying quantity is the charge fluctuation rate. The decay rates for the qubits are both 1 GHz and the charge interaction strength is 1 GHz. The fluctuation rate is swept between 0 and 20 GHz.

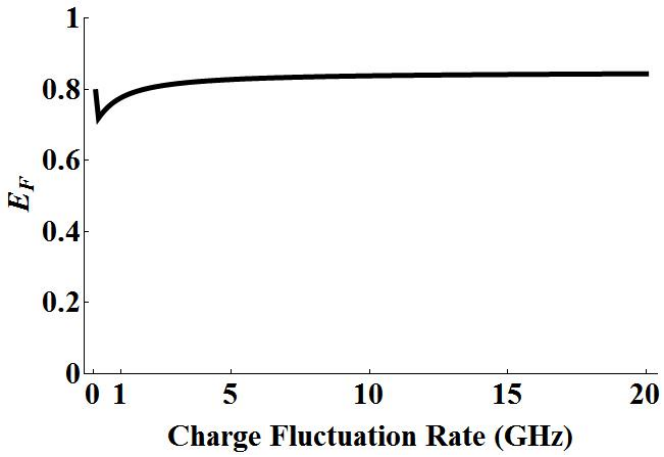

Figure 7.9: Graph showing the concurrence between two qubits with a charge interacting with only the first qubit. The varying quantity is the charge fluctuation rate. The decay rates for the qubits are both 1 GHz and the charge interaction strength is 1 GHz. The fluctuation rate is swept between 0 and 20 GHz.

As we saw in Figs. 7.5, Figs. 7.8 and 7.9 show us that as we increase the charge fluctuation rate, the concurrence and entanglement of formation increase. We do, however, have a new feature, which is an initial decrease in the concurrence and entanglement of formation. When the fluctuation rate is zero, the two charge states are independent, so in the case that the charge is far away, once the system has emitted a photon, the system density matrix does not vary with time. As such, in the case where the charge is far away is always maximally entangled. As soon as we turn the fluctuations on, the system dynamics for the two charge states are not independent and the entanglement is degraded. We also got the qualitative result that as we increase the fluctuation rate, the gradient of the graph decreases, converging to steady value. If the charge fluctuation rate is very fast, the charge interacts as if it were always present, but at half strength. This half strength come from an averaging of the charge on and off interactions. We see from Fig. 7.8 that this is about 0.9.

We know that it is the case that the concurrence is unity if and only if the photons from both qubits are indistinguishable. As we saw in Fig. 7.5, by allowing a charge to interact with one of the qubits and not the other, we were able to get some information about how likely it was that a photon detected came from a particular qubit. If we now allow the charge to interact with both qubits, without fluctuating, but with dissimilar interaction strength, we should observe a similar effect. We ex-

pect that, when the charge interacts equally with both qubits, the concurrence is at its maximum (unity) and that as the charge interactions for each qubit become increasingly different, the concurrence should decrease to the limit of 0.5 at infinite charge strength difference, since the initial state of the system was in a mixed state of charge present or not. Naturally, if the charge is not present, then there is no interaction with either qubit and the photons from the qubits are indistinguishable. If the charge is present and the interaction is very strong then the qubits are very distinguishable, so the limit is 0.5.

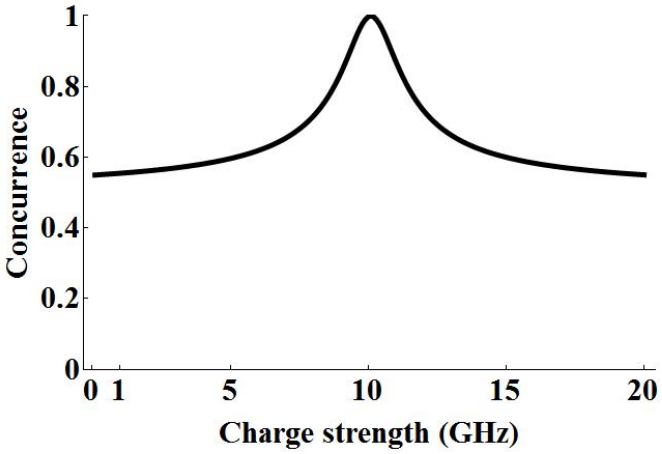

Figure 7.10: Graph showing the concurrence between two qubits interacting with a single charge. The interaction strength of the charge with the second qubit is fixed at 10 GHz while the interaction with the first qubit is swept between 0 and 20 GHz. The decay rates for the qubits are both 1 GHz.

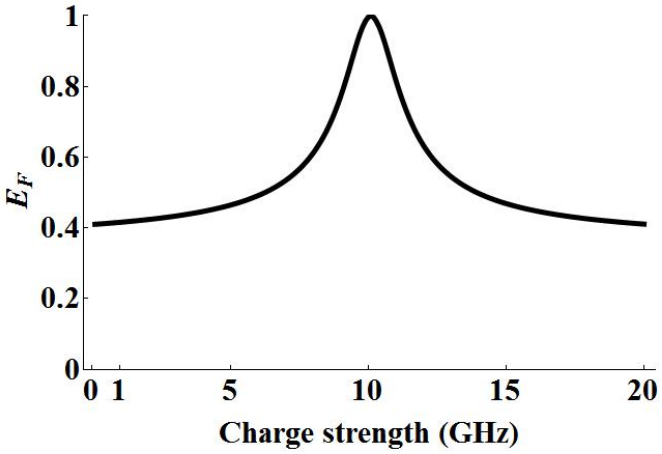

Figure 7.11: Graph showing the entanglement of formation between two qubits interacting with a single charge. The interaction strength of the charge with the second qubit is fixed at 10 GHz while the interaction with the first qubit is swept between 0 and 20 GHz. The decay rates for the qubits are both 1 GHz.

Just as we expected, Figs. 7.10 and 7.11 show a peak at 10 GHz which the charge interaction strength with respect to the second qubit was set. The peak height is unity showing that when the interaction strengths of the charge with both qubits is equal, then the decays from the two qubits has once again become indistinguishable. The curve is symmetric about the peak and if the behaviour of the curve over the range plotted continues, then the curve should reach a concurrence of 0.5 as the charge strength reaches infinity.

7.4.2 Symmetric interactions

If we change the two charge state so that the interaction detunes the qubit positively in one state and negatively in the other, $\sigma_z \otimes \theta$, rather than $\mathbb{1}_2 \otimes \theta$ as we have had until now, then as the fluctuation rate of the charge increases this interaction should average to zero and the concurrence should become unity. All real negative detunings are introduced by the lasers. However, we could make a negative detuning using the z-direction geometry we discussed in section 5.2.2. If the dipoles of the two qubits are both facing in the same direction and charge is in between them, then one dipole will be facing the charge and one will be facing away. The stark shifts should then have opposite signs, since we would in effect be changing the sign of the field for one the the dipoles.

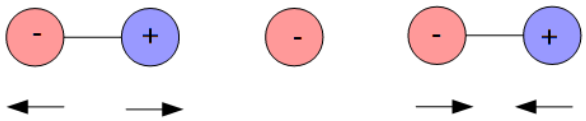

Figure 7.12: Dipoles in the z-direction, facing in the same direction

The symmetric interactions here are, however, a rescaling of the shifts. Initially we modelled the dots as having a zero energy shift when the charge was at a far away site and then a positive shift when at the trap site. In the symmetric case, we model the dots as having a negative detuning of half the shift when the charge was at the far away site and positive detuning of half the shift when at the trap site. The reason for doing this is to show that very fast fluctuation rates lead to an effective shift equal to the average of the shift energies. In the case of the shifts being 0 and 1, the average is $\frac{1}{2}$ and in the case of $-\frac{1}{2}$ and $\frac{1}{2}$ the average is 0 and the limiting system behaviour is as if there is no charge present.

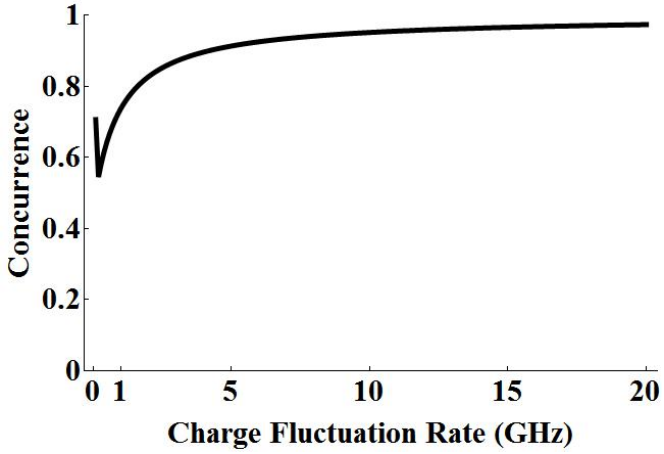

Figure 7.13: Graph showing the concurrence between two qubits with a charge interacting with only the first qubit, where the interaction is symmetric. The varying quantity is the charge fluctuation rate. The decay rates for the qubits are both 1 GHz and the charge interaction strength is 1 GHz. The fluctuation rate is swept between 0 and 20 GHz.

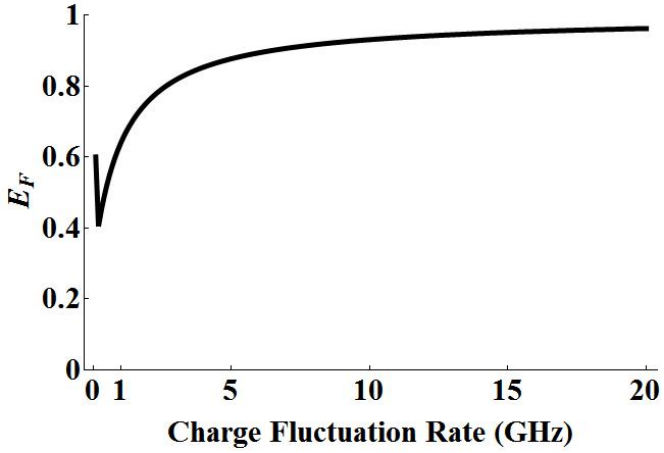

Figure 7.14: Graph showing the concurrence between two qubits with a charge interacting with only the first qubit, where the interaction is symmetric. The varying quantity is the charge fluctuation rate. The decay rates for the qubits are both 1 GHz and the charge interaction strength is 1 GHz. The fluctuation rate is swept between 0 and 20 GHz.

As we see in Figs. 7.13 and 7.14, the concurrence seems to display the limiting behaviour at large fluctuation rates by tending toward unity. We see that when the charge is not fluctuating, then there is a higher concurrence than when the charge fluctuates at small frequencies. Unlike the case of asymmetric charge interaction, where the charge could be far away and so the entanglement would be maximal, the charge corrupts the entanglement in either state. This highlights the idea of time scales and relative values. There are three factor in this problem. The qubit

decay rates, the charge interaction strength and the charge fluctuation rate. If the charge interaction strength is set to 1 GHz, the qubit decay rates both set to 1 GHz and the charge fluctuation rate is set to 0.1 GHz, then the resulting concurrence is 0.545. If the charge interaction strength is set to 10 GHz, the qubit decay rates both set to 10 GHz and the charge fluctuation rate is set to 1 GHz, then the resulting concurrence is also 0.545. Clearly then, it is not the absolute values of the parameters that matters, but the relative ones. The regime where the charge fluctuation rate in slower than the qubit decay rate, but non-zero, seems to be particularly bad for this entanglement scheme. For the non-fluctuation case, since we know that both charge states corrupt the entanglement the concurrence should be lower than that of the asymmetric case. We see when comparing it to Fig. 7.8 that this is indeed the case.

7.4.3 Differing decay rates

In addition to the charge interaction, the entanglement of the qubits is affected by a difference in the decay rate of the two qubits. The reason is straight forward; if one qubit decays faster than the other, on average, then when a photon is detected it is more likely to have come from that qubit.

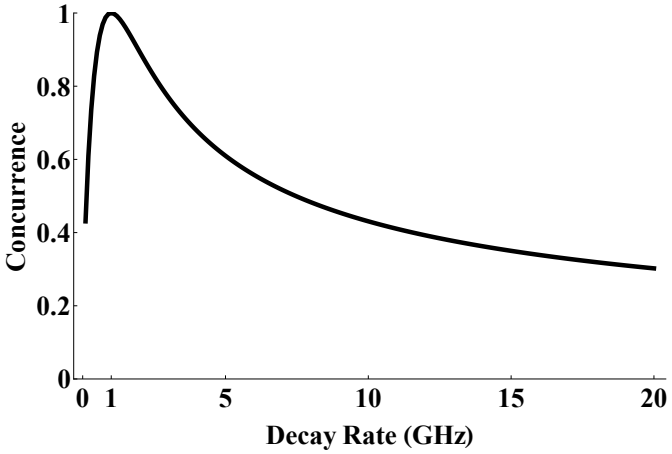

Figure 7.15: Graph showing the concurrence between two qubits with differing decay rates. The decay rate of the second qubit is fixed at 1 GHz while the first is swept between 0 and 20 GHz.

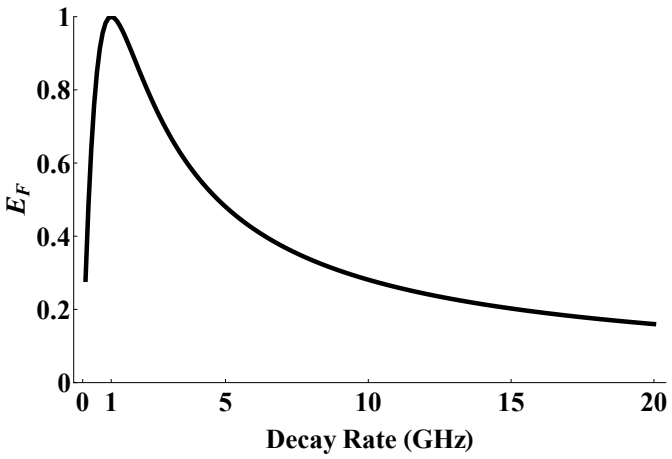

Figure 7.16: Graph showing the entanglement of formation between two qubits with differing decay rates. The decay rate of the second qubit is fixed at 1 GHz while the first is swept between 0 and 20 GHz.

As we see in Fig. 7.15 and 7.16, there is a peak at 1 GHz, which is to be expected since at this point the two qubits have the same decay rate.

Since all the other parameters are set to zero and the qubits are identical, the graph will have an underlying symmetry. If the first qubit has a decay rate of 10 and the other 1, then if we observed a photon coming from the pair, we know that it is ten times as likely that the photon came from the fist qubit. A question to think about, is what if the decay rates were reduced proportionally? If the decay rate for the first qubit becomes 1 and the other becomes 0.1, it is still ten times as likely that an emitted photon came from the first qubit. To see this, we need to plot the same data on a different scale.

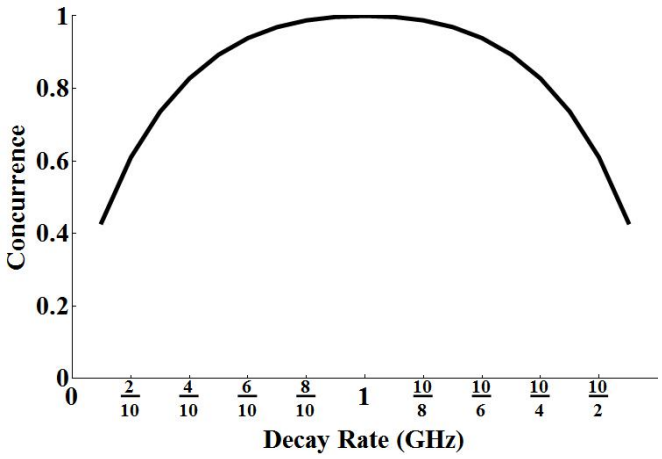

Figure 7.17: Graph showing the concurrence between two qubits with differing decay rates on a modified scale. The decay rate of the second qubit is fixed at 1 GHz while the first is swept between 0.1 and 10 GHz.

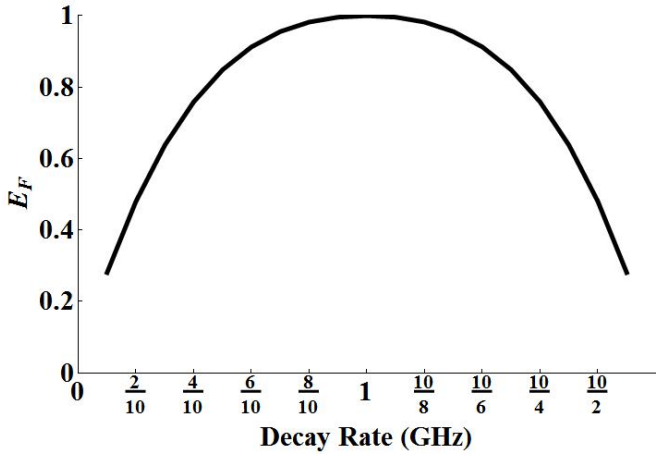

Figure 7.18: Graph showing the entanglement of formation between two qubits with differing decay rates on a modified scale. The decay rate of the second qubit is fixed at 1 GHz while the first is swept between 0.1 and 10 GHz.

As can be seen in Figs. 7.17 and 7.18, on this scale, the graph is symmetric about a decay rate of 1 GHz. Naturally, the symmetry is only there if there parameters. If we introduce a charge, then then the symmetry between the qubits is destroyed. As can be seen in Figs. 7.19 and 7.20.

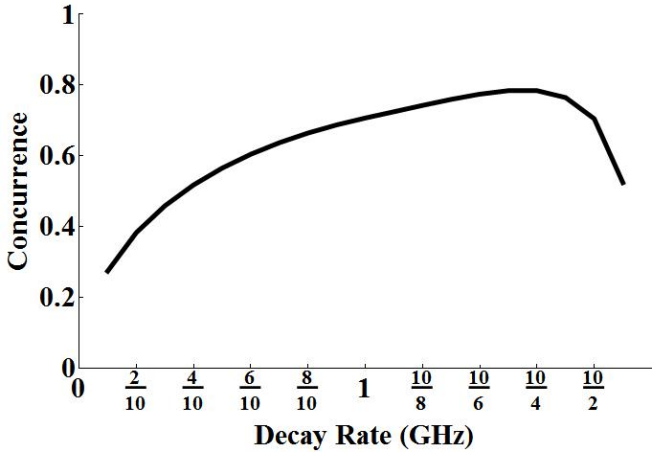

Figure 7.19: Graph showing the concurrence between two qubits with differing decay rates on a modified scale. The charge now interacts with the first qubit only with a strength of 1 GHz. The decay rate of the second qubit is fixed at 1 GHz while the first is swept between 0.1 and 10 GHz.

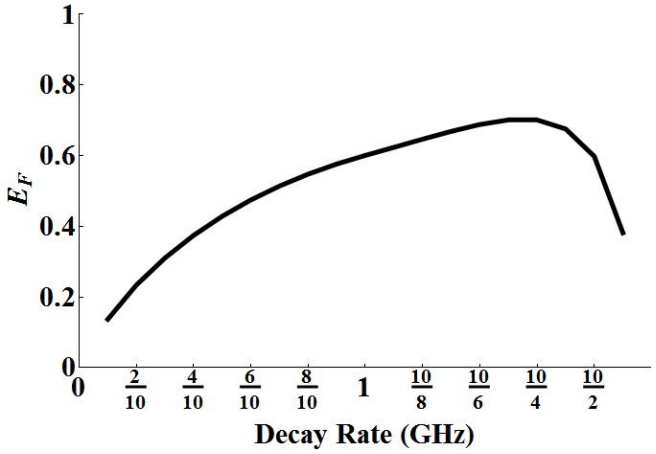

Figure 7.20: Graph showing the entanglement of formation between two qubits with differing decay rates on a modified scale. The charge now interacts with the first qubit only with a strength of 1 GHz. The decay rate of the second qubit is fixed at 1 GHz while the first is swept between 0.1 and 10 GHz.

To incorporate $1/f$ noise properly in this model as future work, it may be necessary to work with a microscopic model of the noise. Alternatively, since the noise is described as being Gaussian in nature and we know that the two time noise

correlation function is given by Eq. 6.20; we could then model the noise as a two site fluctuator giving a variable Stark shift, whose values replicate the two time correlation function.

7.5 Summary

In this final research chapter, we have dealt with a system of two qubits, we have an 'L' shaped electronic configuration and interact with a single charge. We have also performed a partial secularisation so that the qubits can have some interaction with each other. The aim of the research in this chapter was to determine the effect of the charge fluctuators seen in chapter 5 on entanglement generated between two qubits as well as having qubits with dissimilar decay rates. The larger picture was that entangled can be generated via a measurement, a pair of optically excited qubits decay and emit a photon, which when detected projects the qubits into an entangled state. This scheme for entanglement generation is shown to be useful in measurement-based quantum computing, in which clusters of entangled states are generated and then used up by measurements. The scheme works on the principle on path erasure, where the entanglement is dependent on the inability to determine which of the qubits emitted the photon. The introduction of a fluctuating charge, disrupts the scheme by making the photons more distinguishable. There are distillation techniques to 'repair' the entanglement by concentrating the entanglement from many pairs of mixed entangled qubits to created fewer pairs with greater entanglement. In the case of pure entangled states, the ratio of initial pairs to distilled pairs is given by the entanglement of formation. In the case of mixed entangled states, it is not known how this ratio may be calculated, but the upper bound is again given by the entanglement of formation.

We have seen the effect of the fluctuation rate of the charge in Figs. 7.5 and 7.8. We see that the faster the fluctuation, the better the concurrence and so the fewer entangled pairs we would need to have to distil more highly entangled pairs. It was only to be expected that the as the charge strength interaction with one qubit is increased away from the other, the concurrence would decrease and so we see in Figs. 7.10. Very important is the difference in the decay rates of the qubits. Naturally, if this path erasure scheme is to be used, the qubits should decay on the same time scale, or it becomes more and more likely that the faster decaying qubit has emitted at low times and the slower one has decayed at large times, thus making the qubits more distinguishable as shown by the decrease in concurrence in Fig. 7.15.

CHAPTER 8

Bibliography

[1] David Deutsch and Richard Jozsa. Rapid solution of problems by quantum computation. *Proceedings of the Royal Society of London A: Mathematical, Physical and Engineering Sciences*, 439:553–558, 1992.

[2] P. W. Shor. Polynomial-time algorithms for prime factorization and discrete logarithms on a quantum computer. *SIAM journal on computing*, 26:1484–1509, 1997.

[3] Lov K. Grover. A fast quantum mechanical algorithm for database search. In *Proceedings of the Twenty-eighth Annual ACM Symposium on Theory of Computing*, STOC '96, pages 212–219, New York, NY, USA, 1996. ACM.

[4] T. Itakura and Y. Tokura. Dephasing due to background charge fluctuations. *Phys. Rev. B*, 67:195320, 2003.

[5] B. Cheng, Q. Wang, and R. Joynt. Transfer matrix solution of a model of qubit decoherence due to telegraph noise. *Phys. Rev. A*, 78:022313, 2008.

[6] Y. M. Galperin, B. L. Altshuler, J. Bergli, and D. V. Shantsev. Non-gaussian low-frequency noise as a source of qubit decoherence. *Phys. Rev. Lett.*, 96:097009, 2006.

[7] H. J. Wold, H. Brox, Y. M. Galperin, and J. Bergli. Decoherence of a qubit due to either a quantum fluctuator, or classical telegraph noise. *Phys. Rev. B*, 86:205404, 2012.

[8] Sean D. Barrett and Pieter Kok. Efficient high-fidelity quantum computation using matter qubits and linear optics. *Phys. Rev. A*, 71:060310, 2005.

[9] H.P. Breuer and F. Petruccione. *The Theory of Open Quantum Systems*. OUP Oxford, 2007.

[10] M. Fox. *Quantum Optics : An Introduction: An Introduction*. Oxford Master Series in Physics. OUP Oxford, 2006.

[11] D.F. Walls and G.J. Milburn. *Quantum Optics*. Springer, 2008.

[12] P. Kok and B.W. Lovett. *Introduction to Optical Quantum Information Processing*. Cambridge University Press, 2010.

[13] I. Travěnec. Solvability of the two-photon rabi hamiltonian. *Phys. Rev. A*, 85:043805, 2012.

[14] R. Loudon. *The Quantum Theory of Light*. OUP Oxford, 2000.

[15] H.J. Carmichael. *Statistical Methods in Quantum Optics*. Number v. 1. Springer, 1999.

[16] S.C. Benjamin, B.W. Lovett, and J.M. Smith. Prospects for measurement-based quantum computing with solid state spins. *Laser & Photonics Reviews*, 3:556–574, 2009.

[17] G. D. Fuchs, G. Burkard, P. V. Klimov, and D. D. Awschalom. A quantum memory intrinsic to single nitrogen-vacancy centres in diamond. *Nature Physics*, 7:789–793, 2011.

[18] H. Bernien, B. Hensen, W. Pfaff, G. Koolstra, M. S. Blok, L. Robledo, T. H. Taminiau, M. Markham, D. J. Twitchen, L. Childress, and R. Hanson. Heralded entanglement between solid-state qubits separated by three metres. *Nature*, 497:86–90, 2013.

[19] M. Stern, G. Catelani, Y. Kubo, C. Grezes, A. Bienfait, D. Vion, D. Esteve, and P. Bertet. Flux qubits with long coherence times for hybrid quantum circuits. *Phys. Rev. Lett.*, 113:123601, 2014.

[20] Luca Chirolli and Guido Burkard. Full control of qubit rotations in a voltage-biased superconducting flux qubit. *Phys. Rev. B*, 74:174510, 2006.

[21] E. Il'ichev, N. Oukhanski, A. Izmalkov, Th. Wagner, M. Grajcar, H.-G. Meyer, A. Yu. Smirnov, Alec Maassen van den Brink, M. H. S. Amin, and A. M. Zagoskin. Continuous monitoring of rabi oscillations in a josephson flux qubit. *Phys. Rev. Lett.*, 91:097906, 2003.

[22] Carlo Ottaviani, David Vitali, Maurizio Artoni, Francesco Cataliotti, and Paolo Tombesi. Polarization qubit phase gate in driven atomic media. *Phys. Rev. Lett.*, 90:197902, 2003.

[23] Mustafa Gündoğan, Patrick M. Ledingham, Attaallah Almasi, Matteo Cristiani, and Hugues de Riedmatten. Quantum storage of a photonic polarization qubit in a solid. *Phys. Rev. Lett.*, 108:190504, 2012.

[24] S. Kocsis, G. Y. Xiang, T. C. Ralph, and G. J. Pryde. Heralded noiseless amplification of a photon polarization qubit. *Nature Physics*, 9:23–28, 2013.

[25] A. M. Tyryshkin, S. A. Lyon, A. V. Astashkin, and A. M. Raitsimring. Electron spin relaxation times of phosphorus donors in silicon. *Phys. Rev. B*, 68:193207, 2003.

[26] J. L. O'Brien, S. R. Schofield, M. Y. Simmons, R. G. Clark, A. S. Dzurak, N. J. Curson, B. E. Kane, N. S. McAlpine, M. E. Hawley, and G. W. Brown. Towards the fabrication of phosphorus qubits for a silicon quantum computer. *Phys. Rev. B*, 64:161401, 2001.

[27] R. Bratschitsch and A. Leitenstorfer. Quantum dots: Artificial atoms for quantum optics. *Nature Materials*, 5:855–856, 2006.

[28] S-S. Sun and N. S. Sariciftci. *Organic Photovoltaics: Mechanisms, Materials, and Devices*. Optical Science and Engineering. Taylor & Francis, 2005.

[29] A. Rogach. *Semiconductor Nanocrystal Quantum Dots: Synthesis, Assembly, Spectroscopy and Applications*. Springer ebook collection / Chemistry and Materials Science 2005-2008. Springer, 2008.

[30] T. H. Stievater, Xiaoqin Li, D. G. Steel, D. Gammon, D. S. Katzer, D. Park, C. Piermarocchi, and L. J. Sham. Rabi oscillations of excitons in single quantum dots. *Phys. Rev. Lett.*, 87:133603, 2001.

[31] T. Gentile, B. Hughey, D Kleppner, and T. Ducas. Experimental study of one- and two-photon rabi oscillations. *Phys. Rev. A*, 40:5103–5115, 1989.

[32] H. Kamada, H. Gotoh, J. Temmyo, T. Takagahara, and H. Ando. Exciton rabi oscillation in a single quantum dot. *Phys. Rev. Lett.*, 87:246401, 2001.

[33] A. J. Ramsay, A. V. Gopal, E. M. Gauger, A. Nazir, B. W. Lovett, A. M. Fox, and M. S. Skolnick. Damping of exciton rabi rotations by acoustic phonons in optically excited InGaAs/GaAs quantum dots. *Phys. Rev. Lett.*, 104:017402, 2010.

[34] B. Trauzettel, D.V. Bulaev, D. Loss, and G. Burkard. Spin qubits in graphene quantum dots. *Nat Phys*, 3:192–196, 2007.

[35] D.l Loss and D. P. DiVincenzo. Quantum computation with quantum dots. *Phys. Rev. A*, 57:120–126, 1998.

[36] J. J.L. Morton and B. W. Lovett. Hybrid solid-state qubits: The powerful role of electron spins. *Annual Review of Condensed Matter Physics*, 2:189–212, 2011.

[37] M. Atatre, J. Dreiser, A. Badolato, A. Hgele, K. Karrai, and A. Imamoglu. Quantum-dot spin-state preparation with near-unity fidelity. *Science*, 312:551–553, 2006.

[38] D. Brunner, B. D. Gerardot, P. A. Dalgarno, G. Wst, K. Karrai, N.k G. Stoltz, P. M. Petroff, and R. J. Warburton. A coherent single-hole spin in a semiconductor. *Science*, 325:70–72, 2009.

[39] S. Buckley, K. Rivoire, and J. Vučković. Engineered quantum dot single-photon sources. *Reports on Progress in Physics*, 75:126503, 2012.

[40] Y-M He, Y. He, J-Y. Wei, D. Wu, M. Atatüre, C. Schneider, S. Hoöfling, M. Kamp, C-Y Lu, and J-W. Pan. On-demand semiconductor single-photon source with near-unity indistinguishability. *Nat Nano*, 8:213–217, 2013.

[41] T. Volz, A. Reinhard, M. Winger, A. Badolato, K. J. Hennessy, E. L. Hu, and A. Imamoglu. Ultrafast all-optical switching by single photons. *Nature Photonics*, 6:605–609, 2012.

[42] N. Akopian, N. H. Lindner, E. Poem, Y. Berlatzky, J. Avron, D. Gershoni, B. D. Gerardot, and P. M. Petroff. Entangled photon pairs from semiconductor quantum dots. *Phys. Rev. Lett.*, 96:130501, 2006.

[43] Oliver Benson, Charles Santori, Matthew Pelton, and Yoshihisa Yamamoto. Regulated and entangled photons from a single quantum dot. *Phys. Rev. Lett.*, 84:2513–2516, 2000.

[44] X. Li and G. Yang. Modification of stranskikrastanov growth on the surface of nanowires. *Nanotechnology*, 25:435605, 2014.

[45] P. Micher. *Single Semiconductor Quantum Dots*. Springer-Verlag Berlin Heidelberg, 2009.

[46] G. S. Solomon, J. A. Trezza, A. F. Marshall, and J. S. Harris, Jr. Vertically aligned and electronically coupled growth induced inas islands in gaas. *Phys. Rev. Lett.*, 76:952–955, 1996.

[47] A.A. Golovin and A.A. Nepomnyashchy. *Self-Assembly, Pattern Formation and Growth Phenomena in Nano-Systems: Proceedings of the NATO Advanced Study Institute, held in St. Etienne de Tinee, France, August 28 - September 11, 2004*. Nato Science Series II:. Springer Netherlands, 2006.

[48] Arvind Baskaran and Peter Smereka. Mechanisms of stranski-krastanov growth. *Journal of Applied Physics*, 111:–, 2012.

[49] A. J. Ramsay. A review of the coherent optical control of the exciton and spin states of semiconductor quantum dots. *Semiconductor Science and Technology*, 25:103001, 2010.

[50] Pablo Alonso-Gonzlez, Luisa Gonzlez, Yolanda Gonzlez, David Fuster, Ivn Fernndez-Martnez, Javier Martn-Snchez, and Leon Abelmann. New process for high optical quality inas quantum dots grown on patterned gaas(001) substrates. *Nanotechnology*, 18:355302, 2007.

[51] R. Notzel, Z. Niu, M. Ramsteiner, H. Schonherr, A. Tranpert, L. Daweritz, and K. H. Ploog. Uniform quantum-dot arrays formed by natural self-faceting on patterned substrates. *Nature*, 392:56–59, 1998.

[52] J. M. MacLeod, C. V. Cojocaru, F. Ratto, C. Harnagea, A. Bernardi, M. I. Alonso, and F. Rosei. Modified stranskikrastanov growth in ge/si heterostructures via nanostenciled pulsed laser deposition. *Nanotechnology*, 23:065603, 2012.

[53] Alex Zunger. Pseudopotential theory of semiconductor quantum dots. *physica status solidi (b)*, 224:727–734, 2001.

[54] P.A. Ling. *Quantum Dots: Research Developments*. Horizons in world physics. Nova Science Publishers, 2005.

[55] C. Hamaguchi. *Basic Semiconductor Physics*. Springer Berlin Heidelberg, 2013.

[56] P. YU and M. Cardona. *Fundamentals of Semiconductors: Physics and Materials Properties*. Springer Berlin Heidelberg, 2013.

[57] H.S. Nalwa. *Deposition and Processing*. Elsevier Science & Technology Books, 2001.

[58] H. Haug and S.W. Koch. *Quantum Theory of the Optical and Electronic Properties of Semiconductors*. World Scientific, 2009.

[59] B. W. Lovett, J. H. Reina, A. Nazir, and G. Andrew D. Briggs. Optical schemes for quantum computation in quantum dot molecules. *Phys. Rev. B*, 68:205319, 2003.

[60] N.W. Ashcroft and N.D. Mermin. *Solid State Physics*. HRW international editions. Holt, Rinehart and Winston, 1976.

[61] C. Kittel. *Introduction to Solid State Physics*. Wiley, 2004.

[62] B. W. Lovett, A. Nazir, E. Pazy, S. D. Barrett, T. P. Spiller, and G. Andrew D. Briggs. Quantum computing with spin qubits interacting through delocalized excitons: Overcoming hole mixing. *Phys. Rev. B*, 72:115324, 2005.

[63] K. Kuroda, T. Kuroda, K. Watanabe, T. Mano, K. Sakoda, G. Kido, and N. Koguchi. Final-state readout of exciton qubits by observing resonantly excited photoluminescence in quantum dots. *Applied Physics Letters*, 90:–, 2007.

[64] A. Vasanelli, R. Ferreira, and G. Bastard. Continuous absorption background and decoherence in quantum dots. *Phys. Rev. Lett.*, 89:216804, 2002.

[65] Xiaoqin Li, Yanwen Wu, Duncan Steel, D. Gammon, T. H. Stievater, D. S. Katzer, D. Park, C. Piermarocchi, and L. J. Sham. An all-optical quantum gate in a semiconductor quantum dot. *Science*, 301:809–811, 2003.

[66] Eliana Biolatti, Rita C. Iotti, Paolo Zanardi, and Fausto Rossi. Optical quantum gates with semiconductor nanostructures. *International Journal of Circuit Theory and Applications*, 29:137–150, 2001.

[67] D.D. Solnyshkov, O. Bleu, and G. Malpuech. All optical controlled-not gate based on an excitonpolariton circuit. *Superlattices and Microstructures*, 83:466 – 475, 2015.

[68] A. J. Ramsay, R. S. Kolodka, F. Bello, P. W. Fry, W. K. Ng, A. Tahraoui, H. Y. Liu, M. Hopkinson, D. M. Whittaker, A. M. Fox, and M. S. Skolnick. Coherent response of a quantum dot exciton driven by a rectangular spectrum optical pulse. *Phys. Rev. B*, 75:113302, 2007.

[69] S. Stufler, P. Ester, A. Zrenner, and M. Bichler. Quantum optical properties of a single $in_xga_{1-x}As$-GaAs quantum dot two-level system. *Phys. Rev. B*, 72:121301, 2005.

[70] P. Borri, W. Langbein, S. Schneider, U. Woggon, R. L. Sellin, D. Ouyang, and D. Bimberg. Ultralong dephasing time in ingaas quantum dots. *Phys. Rev. Lett.*, 87:157401, 2001.

[71] M. A. Nielsen and I. L. Chuang. *Quantum Computation and Quantum Information*. Cambridge university press, 2010.

[72] A. A. Cordones and S. R. Leone. Mechanisms for charge trapping in single semiconductor nanocrystals probed by fluorescence blinking. *Chem. Soc. Rev.*, 42:3209–3221, 2013.

[73] M. B. Weissman. $\frac{1}{f}$ noise and other slow, nonexponential kinetics in condensed matter. *Rev. Mod. Phys.*, 60:537–571, 1988.

[74] R. J. Warburton, C. Schulhauser, D. Haft, C. Schäflein, K. Karrai, J. M. Garcia, W. Schoenfeld, and P. M. Petroff. Giant permanent dipole moments of excitons in semiconductor nanostructures. *Phys. Rev. B*, 65:113303, Feb 2002.

[75] J. J. Finley, M. Sabathil, P. Vogl, G. Abstreiter, R. Oulton, A. I. Tartakovskii, D. J. Mowbray, M. S. Skolnick, S. L. Liew, A. G. Cullis, and M. Hopkinson. Quantum-confined stark shifts of charged exciton complexes in quantum dots. *Phys. Rev. B*, 70:201308, 2004.

[76] R. Hanbury Brown and R. Q. Twiss. Correlation between photons in two coherent beams of light. *Nature*, 177:27–29, 1956.

[77] M.O. Scully and S. Zubairy. *Quantum Optics: XD-US. ...* Cambridge University Press, 1997.

[78] T. Aichele, M. Scholz, S. Ramelow, and O. Benson. Non-classical light from artificial atoms. volume 53 of *Advances In Atomic, Molecular, and Optical Physics*, pages 1 – 32. Academic Press, 2006.

[79] A. V. Kuhlmann, J. Houel, A. Ludwig, L. Greuter, D. Reuter, A.D. Wieck, M. Poggio, and R Warburton. Charge noise and spin noise in a semiconductor quantum device. *Nat Phys*, 9:570–575, 2013.

[80] C. Sobie, A. Babul, and R. de Sousa. Neuron dynamics in the presence of $1/f$ noise. *Phys. Rev. E*, 83:051912, 2011.

[81] I. Csabai. 1/f noise in computer network traffic. *Journal of Physics A: Mathematical and General*, 27:L417, 1994.

[82] X Zhang and G Hu. $1/f$ noise in a two-lane highway traffic model. *Phys. Rev. E*, 52:4664–4668, 1995.

[83] R Voss and J Clarke. $1/f$ noise in music and speech. *Nauture*, 258:317 – 318, 1975.

[84] P. Dutta and P. M. Horn. Low-frequency fluctuations in solids: $\frac{1}{f}$ noise. *Rev. Mod. Phys.*, 53:497–516, 1981.

[85] E. Paladino, L. Faoro, G. Falci, and Rosario Fazio. Decoherence and $1/f$ noise in josephson qubits. *Phys. Rev. Lett.*, 88:228304, 2002.

[86] M. Pelton, D. G. Grier, and P. Guyot-Sionnest. Characterizing quantum-dot blinking using noise power spectra. *Applied Physics Letters*, 85, 2004.

[87] Al. L. Efros and M. Rosen. Random telegraph signal in the photoluminescence intensity of a single quantum dot. *Phys. Rev. Lett.*, 78:1110–1113, 1997.

[88] P. Frantsuzov, M. Kuno, B. Jank, and R. A. Marcus. Universal emission intermittency in quantum dots, nanorods and nanwires. *Naure Physics*, 4:519, 2008.

[89] F.D. Stefani, J.P. Hoogenboom, and E. Barkai. Beyond quantum jumps: Blinking nanoscale light emitters. *Physics Today*, 62, 2009.

[90] Rogier Verberk, Antoine M. van Oijen, and Michel Orrit. Simple model for the power-law blinking of single semiconductor nanocrystals. *Phys. Rev. B*, 66:233202, 2002.

[91] R. F. Voss and J. Clarke. Flicker ($\frac{1}{f}$) noise: Equilibrium temperature and resistance fluctuations. *Phys. Rev. B*, 13:556–573, 1976.

[92] P. Reutler, A. Bensaid, F. Herbstritt, C. Höfener, A. Marx, and R. Gross. Local magnetic order in manganite thin films studied by $1/f$ noise measurements. *Phys. Rev. B*, 62:11619–11625, 2000.

[93] O. Cohen, Z. Ovadyahu, and M. Rokni. $1/f$ noise and incipient localization. *Phys. Rev. Lett.*, 69:3555–3558, 1992.

[94] M. Niemann, H. Kantz, and E. Barkai. Fluctuations of $1/f$ noise and the low-frequency cutoff paradox. *Phys. Rev. Lett.*, 110:140603, 2013.

[95] J.F Stephany. Frequency limits of 1/ f noise. *Journal of Physics: Condensed Matter*, 12:2469, 2000.

[96] Y. Matsuzaki and H. Tanaka. Quantum Zeno effect in an unstable system with NMR. *ArXiv e-prints*, 2012.

[97] P. Kuopanportti, M. Möttönen, V. Bergholm, O. Saira, J. Zhang, and K. B. Whaley. Suppression of $1/f^{\alpha}$ noise in one-qubit systems. *Phys. Rev. A*, 77:032334, 2008.

[98] B. Kaulakys, V. Gontis, and M. Alaburda. Point process model of $1f$ noise vs a sum of lorentzians. *Phys. Rev. E*, 71:051105, 2005.

[99] D. P. S. McCutcheon. Optical Signatures of Non-Markovian Behaviour in Open Quantum Systems. *ArXiv e-prints*, April 2015.

[100] S.C. Benjamin, B.W. Lovett, and J.M. Smith. Prospects for measurement-based quantum computing with solid state spins. *Laser & Photonics Reviews*, 3:556–574, 2009.

[101] A. Kolli, B. W. Lovett, S. C. Benjamin, and T. M. Stace. All-optical measurement-based quantum-information processing in quantum dots. *Phys. Rev. Lett.*, 97:250504, 2006.

[102] A. Kolli, B. W. Lovett, S. C. Benjamin, and T. M. Stace. Measurement-based approach to entanglement generation in coupled quantum dots. *Phys. Rev. B*, 79:035315, 2009.

[103] C. K. Hong, Z. Y. Ou, and L. Mandel. Measurement of subpicosecond time intervals between two photons by interference. *Phys. Rev. Lett.*, 59:2044–2046, 1987.

[104] S. Bose, P. L. Knight, M. B. Plenio, and V. Vedral. Proposal for teleportation of an atomic state via cavity decay. *Phys. Rev. Lett.*, 83:5158–5161, 1999.

[105] P Walther, K.J. Resch, T. Rudolph, E. Schenck, H. Weinfurter, V. Vedral, M. Aspelmeyer, and A. Zeilinger. Experimental one-way quantum computing. *Nature*, 434:169–176, 2005.

[106] G.W.F. Drake. *Springer Handbook of Atomic, Molecular, and Optical Physics*. Springer Handbook of Atomic, Molecular, and Optical Physics. Springer, 2006.

[107] John Von Neumann. *Mathematical Foundations of Quantum Mechanics*. Investigations in physics. Princeton University Press, 1955.

[108] Volodymyr Krasnoholovets and F.H. Columbus. *Trends in Quantum Physics*. Nova Science Publishers, 2004.

[109] Charles H. Bennett, Gilles Brassard, Sandu Popescu, Benjamin Schumacher, John A. Smolin, and William K. Wootters. Purification of noisy entanglement and faithful teleportation via noisy channels. *Phys. Rev. Lett.*, 76:722–725, 1996.

[110] Charles H. Bennett, Herbert J. Bernstein, Sandu Popescu, and Benjamin Schumacher. Concentrating partial entanglement by local operations. *Phys. Rev. A*, 53:2046–2052, 1996.

[111] J. R. Petta, A. C. Johnson, J. M. Taylor, E. A. Laird, A. Yacoby, M. D. Lukin, C. M. Marcus, M. P. Hanson, and A. C. Gossard. Coherent manipulation of coupled electron spins in semiconductor quantum dots. *Science*, 309(5744):2180–2184, 2005.

[112] P. Borri, W. Langbein, S. Schneider, U. Woggon, R. L. Sellin, D. Ouyang, and D. Bimberg. Ultralong dephasing time in ingaas quantum dots. *Phys. Rev. Lett.*, 87:157401, Sep 2001.